UNIVERSITY OF CALIFORNIA, SAN DIEGO

Structural Testing and Analysis of a Non-Traditional Pier

A thesis submitted in partial satisfaction of the requirements for the degree

Master of Science

in

Structural Engineering

by

Adam Bogage

Committee in Charge:

Professor P. Benson Shing, Chair
Professor Francesco Lanza di Scalea
Professor Chia-Ming Uang

2008

The Thesis of Adam Bogage is approved, and it is acceptable in quality and form for publication on microfilm and electronically:

_____

_____

_____

Chair

University of California, San Diego

2008

DEDICATION

For Beth, without whom it would all be meaningless.

EPIGRAPH

If one advances confidently in the direction of his dreams, and endeavors to live the life which he has imagined, he will meet with a success unexpected in common hours.

Henry David Thoreau

TABLE OF CONTENTS

LIST OF FIGURES

LIST OF TABLES

ACKNOWLEDGEMENTS

It has been a privilege to work with Professor Benson Shing. He is a talented teacher, a brilliant analyst, and his patience with me was endless. Professor Chia-Ming Uang is also a gifted individual and it was a pleasure to work with him as well.

The structural tests would not have been possible without the contributions of several people: The assistance of two graduate student research assistants, Jerry Lee and Elizabeth Schroth-Nichols, in the field work was invaluable; Jim Newell was responsible for the design of the testing apparatus; and Hussein Okail, who was able to bend Abacus to serve his will. I am also grateful to the hard work of Dr. Christopher Latham, Robert Parks, Andrew Gunthardt and the entire staff of the UCSD Charles Lee Powell Laboratory in helping to set up and conduct the field tests.

Dave Cunningham, of Marathon Construction, was able to understand my needs and make them a reality at an extremely challenging location. His professionalism and that of his crew, was something that could be counted on in an otherwise capricious situation.

This research was made possible by funding from the Naval Facilities Engineering Service Center (NFESC) through BERGER/ABAM Engineers, Inc. under Contract No. 2006-3979. The technical input from Dr. Markus Wernli and Michael LaNier of BERGER/ABAM Engineers and Preston Springston and Dr. Robert Zueck of NFESC is gratefully acknowledged.

ABSTRACT OF THE THESIS

Structural Testing and Analysis of a Non-Traditional Pier

by

Adam Bogage

Master of Science in Structural Engineering

University of California, San Diego, 2008

Professor P. Benson Shing, Chair

This thesis explores the structural performance of a non-traditional pier. The Modular Hybrid Pier (MHP) being investigated here is a structure that consists of two floating, reinforced-concrete, modular sections post-tensioned together. The three main objectives were: confirm that the operations deck could sustain a typical outrigger crane load without damage; verify the capacity of a bollard used to moor ships to the MHP; and model the behavior of the structure subjected to earthquake excitations.

During the deck test, the load was applied at a position perceived to be the most vulnerable. The operations deck behaved linearly up to the maximum applied load. The deck performed in a satisfactory manner without structural damage during the test.

Vessels are berthed at the MHP with mooring lines that are wrapped around a steel bollard which is fixed to the pier deck. The bollard performed according to the design requirements in terms of the load capacity and there was no observable damage in the deck of the MHP.

A multi-degree-of-freedom analytical model of the MHP was created to determine the effects of the dynamic loading of seismic events on the fenders and the structure as a whole. The model incorporates the load rate dependent nature of the fender material and change in axial force with deformation. Ten earthquakes were used to find the seismic response of the structure.

1 Introduction

1.1 Description of Modular Hybrid Pier

A floating reinforced concrete Modular Hybrid Pier (MHP) design has been developed by Berger/ABAM Engineers in conjunction with over 25 government agencies, private firms, and universities as an alternative to a traditional pier design. The MHP being investigated here is a test-bed structure that consists of two floating reinforced concrete modular sections which are post-tensioned together to form a pier. A view of the east end of the structure is shown in Figure 1.1. The test-bed structure has a length of 100 ft. (30.5 m), a width of 50 ft. (15.2 m), and a height of 29 ft. (8.8 m). It has been designed using full-size MHP components configured to represent elements of a full- size (1300 x 88 ft./400 x 27 m) MHP. The modules were constructed with post-tensioned concrete wall panels and prestressed concrete planks with overlying post-tensioned cast-in-place concrete slabs. The modules have three levels. The lowermost level is sealed and serves as a floatation compartment. The second internal level is referred to as the service deck and is designed to route utilities (hoteling) to moored ships through large openings in the exterior wall. The uppermost level is referred to as the operations deck and is designed for trucks and cranes to service moored ships and transfer cargo.

Figure 1.1 - Photograph of MHP - Southeast End

Because the concrete surfaces of the MHP could be in contact with salt water, there is a need for additional corrosion resistance. In the east module (module 2) of the MHP, stainless steel reinforcing bars are used in sections in which a concrete surface can be exposed to salt water. Epoxy coated reinforcement bars in combination with an enhanced durability post-tensioning system are used throughout the remainder of this structure. In the west module (module1) of the MHP, MMFX mild reinforcement is used in combination with conventional post-tensioning systems. The modules for the test structure were constructed in a dry dock facility in Washington State as shown in Figure 1.2. Afterwards, the dry dock was flooded and the modules were post tensioned to form a single structure. A tug boat was used to tow the structure in the open ocean to its current location in the U.S. Naval Base on the 32nd Street in San Diego.

This structure has numerous benefits over conventional pile-based pier structures by having the following features:

1. Seismic force isolation.
2. A low dependence on local soil conditions and tides.
3. The pier can be constructed off-site after which it can be towed to the desired location. This minimizes the construction impact on navy bases and allows for deployment of this structure to any location.
4. As the needs of a navy base changes over time, the pier modules can be relocated and/or reconfigured.
5. A utility deck with unique design features that allow economical revisions as ship technology and supporting utility requirements change over time.
6. Two deck levels separating utilities from deck operations.
7. 75-100 years of repair free service.

Figure 1.2 - MHP Test-Bed Structure in Dry Dock

1.2 Thesis Objective

. To ensure the targeted performance of the MHP, the Department of Structural Engineering at the University of California, San Diego was contracted to perform four types of tests on the structure. These include deck and bollard capacity tests, as well as long and short-term tests of the fender system at the primary mooring shaft. Figure 1.3 shows the plan view and Figure 1.4 shows the elevation view of the MHP test-bed investigated in this project including the test fixtures. This thesis addresses the operations deck test and the bollard capacity test. The deck test verifies the capacity of the operations deck, while the bollard test assesses its capacity and the resisting strength of the supporting concrete deck. Seismic behavior of the pier is also modeled and the results presented.

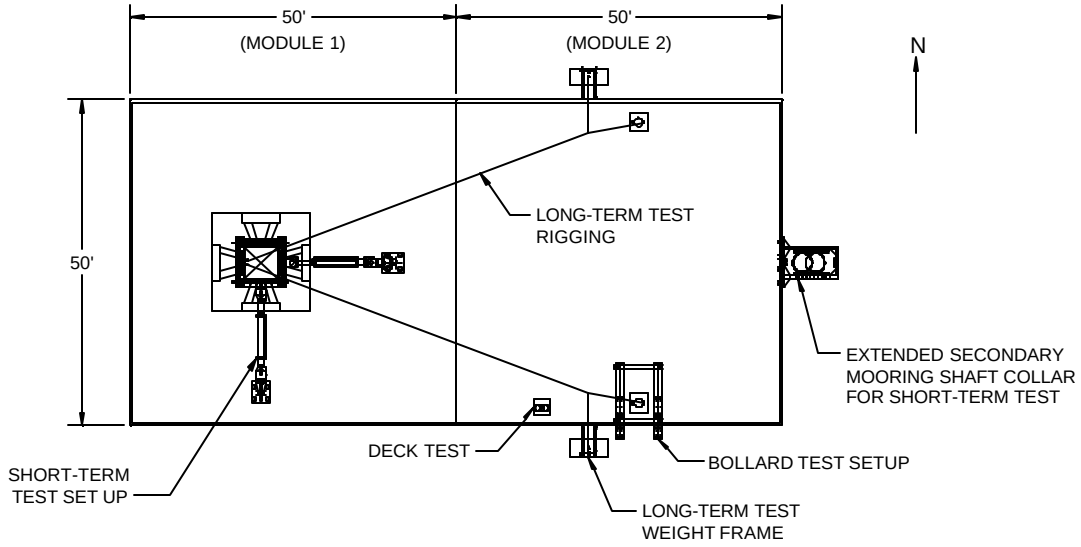

Figure 1.3 - MHP Test-Bed Structure - Plan View

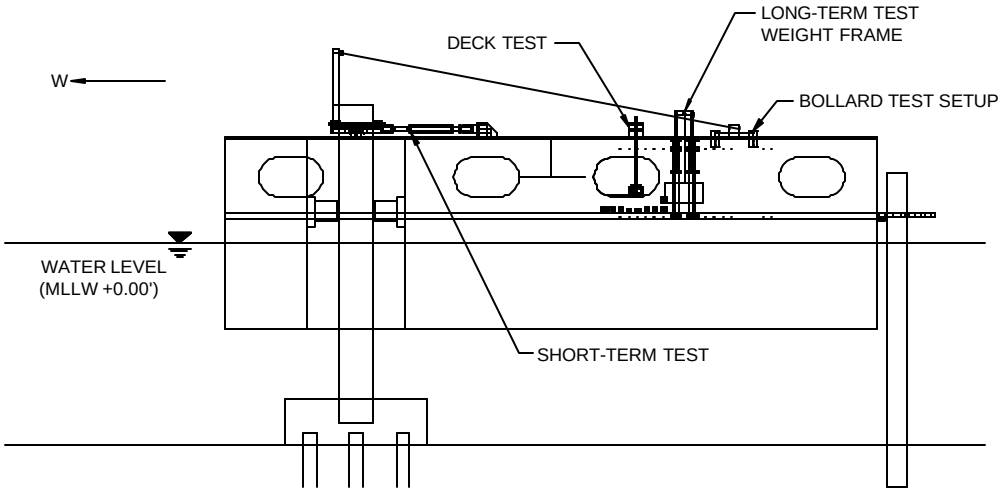

Figure 1.4 - MHP Test-Bed Structure - Elevation View

2 Operations Deck Capacity Structural Test

2.1 Introduction

2.1.1 Description of the Operations Deck

The uppermost deck of the MHP is the operations deck. The deck is designed to carry a maximum outrigger load of 250 kips, which corresponds to a factored design load of 400 kips. The deck design is shown in Figure 2.1 through Figure 2.2. The deck test was to be conducted at a location on the south side of Module 2. The deck consists of precast prestressed planks with a post-tensioned, cast-in-place, concrete slab on top. The reinforcement details of the cast-in-place slab are shown in Figure 2.1(b) and the design details of the precast planks are shown in Figure 2.3. The south side of the deck has the post-tensioning steel designed in the same way as that of the full-size MHP, while the north side does not. The deck has two continuous spans along the north-south direction. The planks in each span are supported by one exterior wall and one interior wall as shown in Figure 2.2 and Figure 2.4. The planks are haunched at the supported ends. The entire deck section is about 15-in. thick near the mid-span and over 20-in. thick near the supporting walls. A picture of the precast planks at the bottom of the operations deck in Module 2 is shown in Figure 2.4.

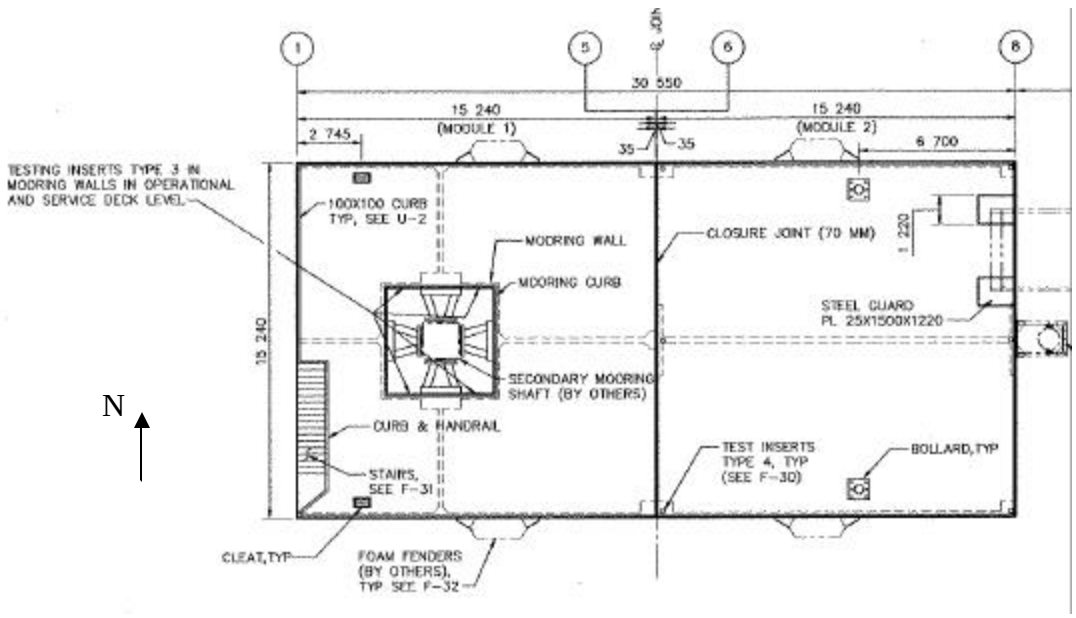

(a) Plan View of the Operations Deck

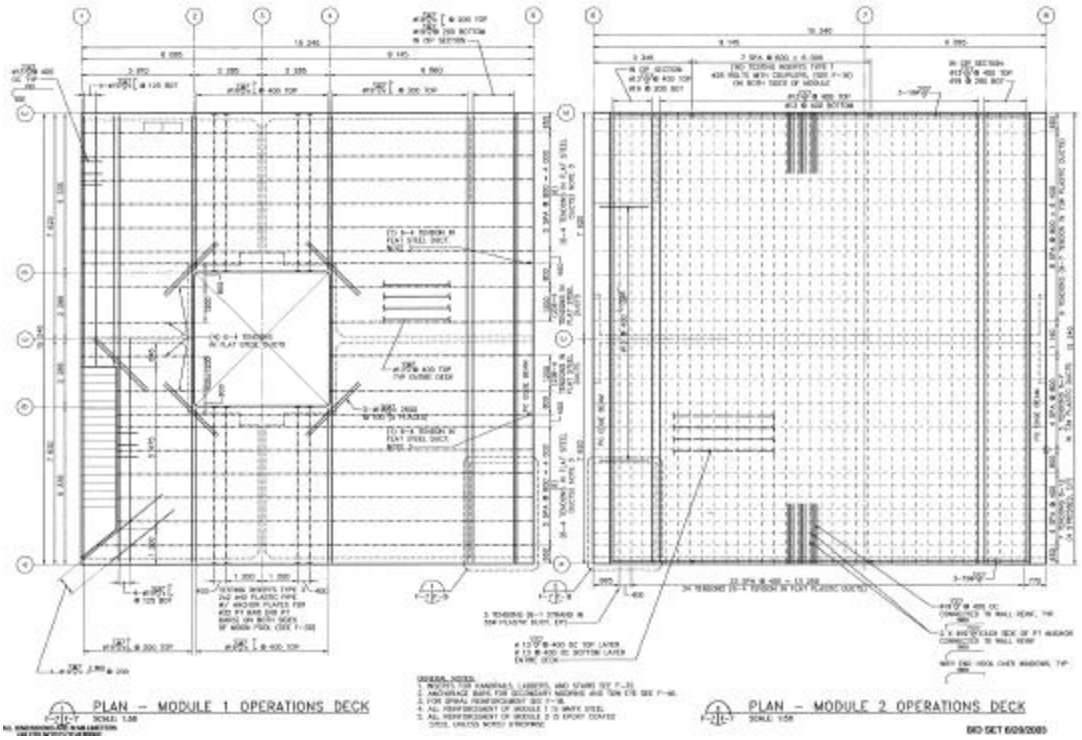

(b) Post-tensioning Details of the Operations Deck

Figure 2.1 - Design of the Operations Deck (in mm)

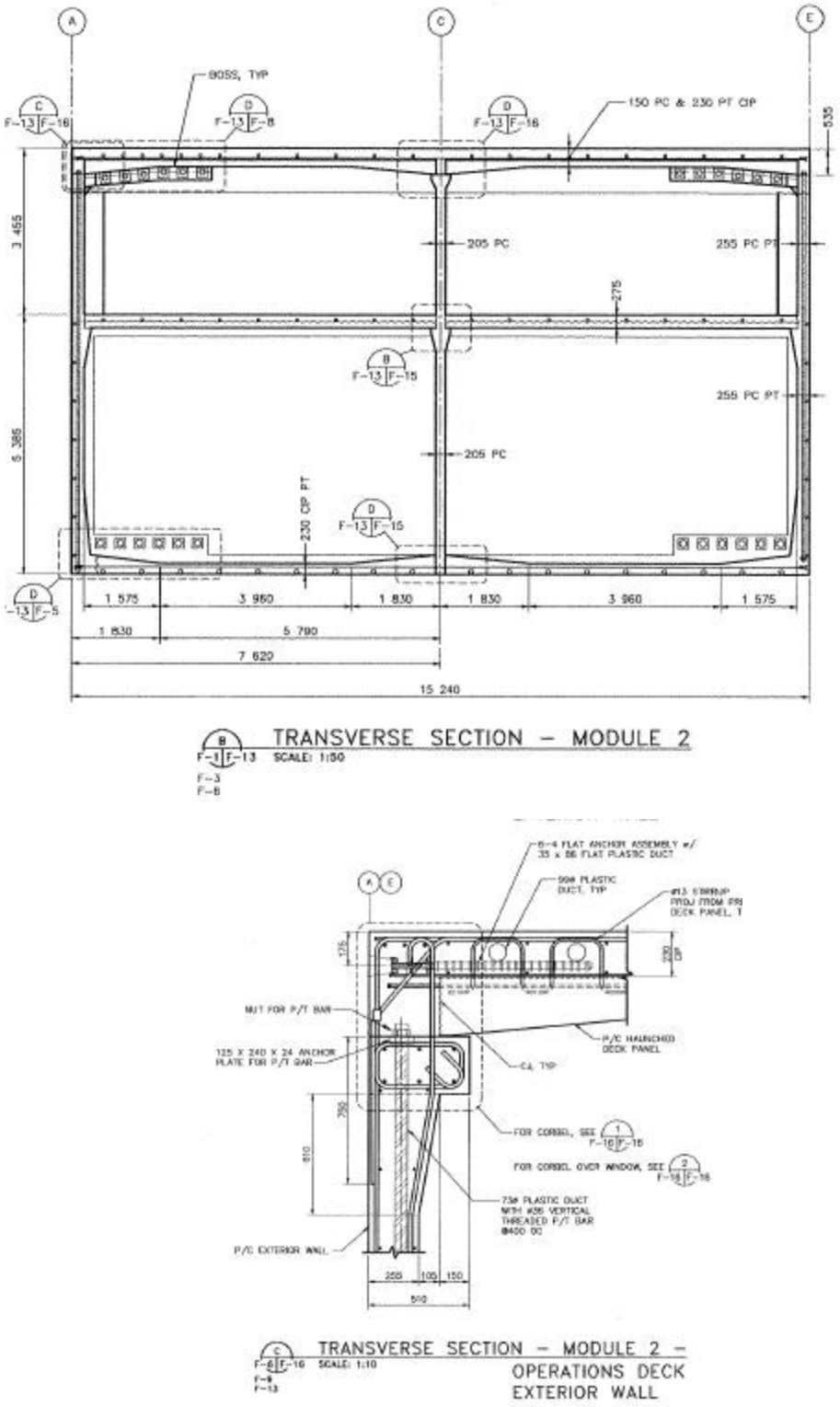

Figure 2.2 - Transverse Section View of the MHP - Module 2 (in mm)

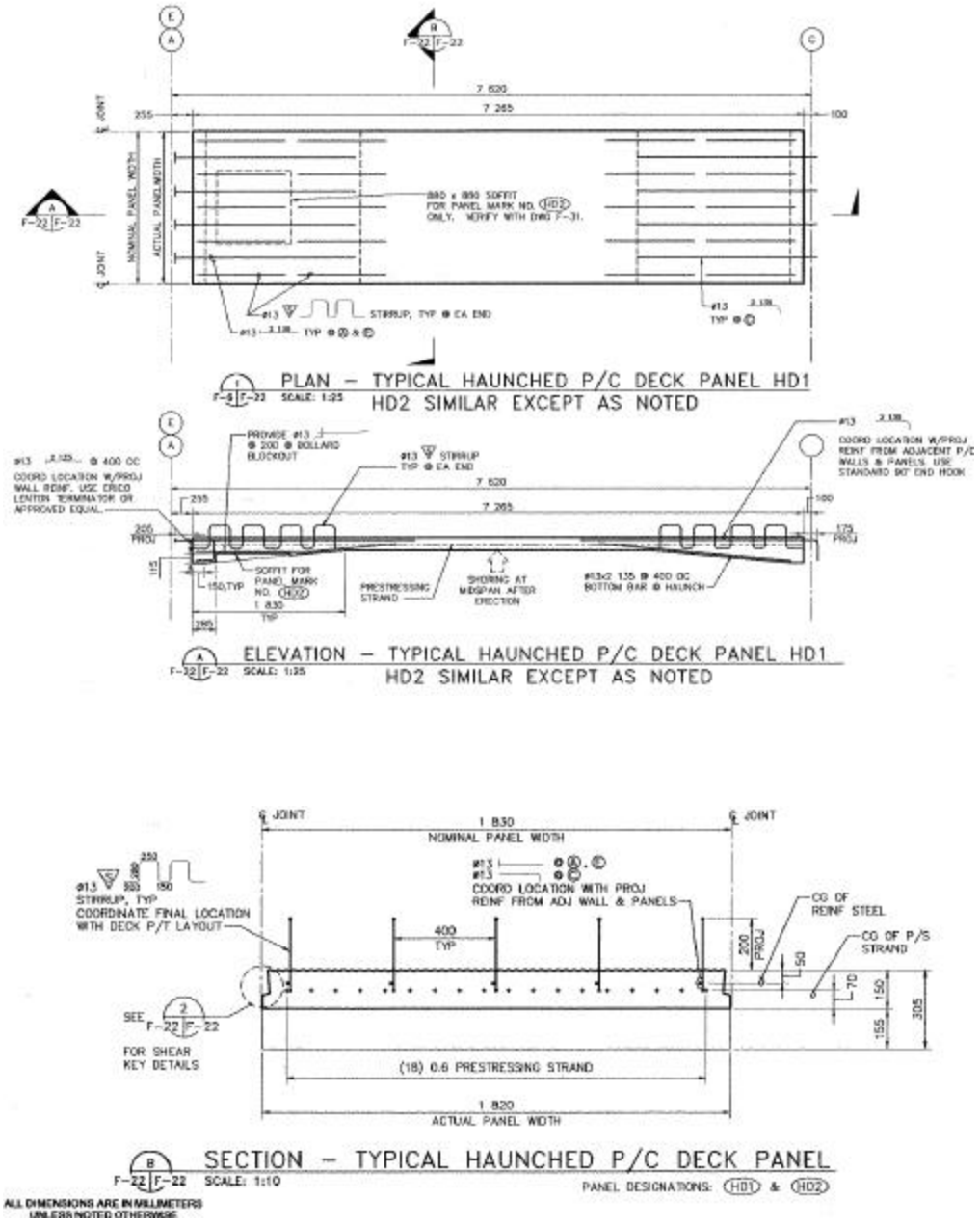

Figure 2.3 - Design of Precast Prestressed Planks (in mm)

Figure 2.4 - Bottom View of Prestressed Precast Planks

2.1.2 Test Objectives and Scope of Work

The main objective of the test reported here was to confirm that the operations deck can sustain the design service load of 250 kips without damage and to identify the reserve capacity of the deck by loading it to 400 kips or to a point at which noticeable but controlled damage might occur. For this purpose, it was decided that the test load would be applied on top of a drain hole on the south side of the operations deck near the second window from the east end, as shown in Figure 1.3, Figure 1.4 and Figure 2.4. This was perceived to be a position most vulnerable to damage because a significant portion of the load would be carried by the beam that supports the precast planks and spans across the window opening. The load was applied by a pair of hydraulic jacks and was distributed over the deck with a 30 x 30 x 3-in. steel plate. A 2-1/2-in-diameter Dywidag bar was passed through the drain hole to transfer

the load to a reaction beam secured against the walls at the service deck level of the modular pier. The test setup is described in detail later.

Pre-test analyses were conducted using simple design formulas and with a nonlinear finite element model was done by Hussein Okail using the commercial program ABAQUS (ABAQUS Manual 2006). Results of these analyses were used to determine the loading protocol and the instrumentation scheme. Once validated and fine tuned with the test data, the finite element model has been used to assess maximum load capacity of the deck. The test program and results are presented in the following sections.

2.2 Pre-Test Analyses

Pre-test analyses were conducted to predict the load capacity and the ultimate failure mechanism of the operations deck based on the loading condition to be used in the test. As mentioned in Section 1.3, the main objective of the test was to confirm that the deck can sustain the design service load of 250 kips without damage and to identify the reserve capacity of the deck by loading it to 400 kips or to a point at which noticeable but controlled damage might occur. The load was to be applied at a location close to a window in the south exterior wall of the modular hybrid pier. The applied load was to be distributed on the deck with a 30 x 30 x 3-in. steel plate. The capacity of the deck was expected to be governed by one of the two possible failure mechanisms. One is the punching shear failure of the deck and the other is the failure of the beam spanning across the window opening. Flexural failure of the deck was not likely because of the thick concrete slab, which could lead to a significant arching action. While the punching shear strength can be evaluated with simplified design formulas, the three-dimensional load resisting mechanism of the pier is best evaluated with a nonlinear finite element model. Hence, a 3-D finite element model was developed with the program ABAQUS. Results of these analyses were used to determine the loading protocol and instrumentation scheme. It had to be assured that the prescribed test load would not induce irreparable damage to the deck.

2.2.1 Punching Shear Strength

The punching shear capacity of the deck can be estimated with the ACI formula (ACI 2005), which for a two-way prestressed slab can be expressed as

$$V_c = \left(b_p \sqrt{f_c'} + 0.3 f_{pc} \right) b_o d \tag{2.1}$$

in which f_{pc} is the average of the compressive stresses at the centroids of the concrete sections in the two prestressed directions, b_o is the perimeter of the critical section for shear, d is the effective depth, and b_p is the smaller of 3.5 and $(a_s d / b_o + 1.5)$ with a_s equal to 40 for interior columns, 30 for edge columns, and 20 for corner columns. ACI also imposes the limits that f_{pc} be no greater than 500 psi and $\sqrt{f_c'}$ cannot exceed 70 psi due to the limited test data available for these situations. The above formula is based on an assumption that a punching shear failure is initiated by diagonal tensile cracking at the defined critical section. The critical shear stress that induces diagonal tensile cracks can be estimated with the following equation based on stress transformation.

$$t_n = \sqrt{\left(f_t' + \frac{f_{pc}}{2} \right)^2 - \left(\frac{f_{pc}}{2} \right)^2} \tag{2.2}$$

in which f_t' is the tensile strength of concrete that can be considered to be proportional to $\sqrt{f_c'}$ according to the ACI provisions. Hence, Equation (2.2) can be used to estimate the punching shear capacity. Equation (2.1) is an empirical equation

that leads to similar results as Equation (2.2). Since punching shear failure is not expected to occur when the maximum principal stress is less than the tensile strength of concrete, the limit imposed on f_{pc} by ACI seems very conservative when f_{pc} is sufficiently large to suppress a diagonal tensile crack. This was taken into consideration in the assessment of the punching shear capacity of the deck.

The deck considered here is made of lightweight concrete. According to ACI, for lightweight concrete, $\sqrt{f_c'}$ in Equation (2.1) should be replaced by $f_{ct}/6.7$ when the splitting tensile strength f_{ct} is specified and by $0.85\sqrt{f_c'}$ when f_{ct} is not specified. However, $f_{ct}/6.7$ should not be greater than $\sqrt{f_c'}$. With these considerations, Equation (2.1) was used to assess the punching shear capacity of the deck.

Based on the jacking force specified for the prestressing tendons in the design drawings, the concrete properties obtained from the quality control tests, and the 30 x 30-in. loading area that was to be used in the test, the following values were determined for the parameters in Equation (2.1): f_c' = 8,500 psi, f_{ct} = 580 psi, f_{pc} = 1,220 psi (assuming an effective prestress level of 135 ksi), b_p = 3.5, d = 12.25 in. (the deck was conservatively assumed to be 15-in. thick, which is the thickness of the shallowest portion of the deck around the mid-span), and b_o = 169 in.

To estimate the punching shear capacity with Equation (2.1), three cases with different levels of conservatism were considered: (1) the ACI formula without the stress and strength limits for f_{pc} and $\sqrt{f_c'}$ and without the consideration of lightweight concrete; (2) the ACI formula with the stress and strength limits but

without the consideration of lightweight concrete; and (3) the ACI formula with the stress and strength limits and with $\sqrt{f_c'}$ replaced by $f_{ct}/6.7$ but not exceeding $\sqrt{f_c'}$. The results are shown in Table 2.1.

Table 2.1 - Punching Shear Strength

	ACI – Case 1	ACI – Case 2	ACI – Case 3
V_c	1,430 kips	820 kips	820 kips

As the table shows, the capacity of the deck should be between 820 and 1,430 kips based on the ACI formula. Furthermore, it should be mentioned that the deck is haunched at the supported ends as shown in Figure 2.2, and at the load application location, the deck is over 20-in. thick. Hence, the actual punching shear capacity of the deck at that location would most likely be higher than that estimated here. This will be further confirmed by the finite element analysis presented next.

2.3 Experimental Setup

The design of the operations deck has been described in Section 2.1. The deck is designed to carry an outrigger load of 250 kips. This corresponds to a factored live load of 400 kips. The deck consists of precast prestressed planks with a post-tensioned, cast-in-place, concrete slab on top. It has no bottom reinforcement continuous in the east-west direction and the gravity load is essentially resisted by one-way bending. The test load was to be applied on top of a drain hole on the south side of the operations deck near the second window from the east end. This was perceived to be a position most vulnerable to damage because a significant portion of the load would be carried by the beam that supports the precast planks and spans across the window opening. The test was to validate the load capacity of the deck but not to induce irreparable damage. The testing apparatus was designed to apply a maximum load of 400 kips with a factor of safety of 1.5. According to the pre-test analyses, no damage could be induced on the deck at this load level. The testing apparatus, loading protocol, and instrumentation scheme are described below.

2.3.1 Test Setup

In the test, a load was introduced to the deck through a 30 x 30 x 3-in. steel plate and two 300-kip hydraulic jacks. A 2-1/2-in. diameter high-strength (Dywidag) bar was used to transfer the load to a reaction beam secured to the walls at the service deck level of the pier. The test setup and apparatus are shown in Figure 2.5 through Figure 2.7. The loading location took advantage of an existing drain hole, which is

located at the adjoining edges of two precast planks. The drain hole is 6 in. in diameter and is close to a window in the south exterior wall. The south end of the reaction beam was restrained from movement by inserting it into a rectangular hole in a 2-in.-thick steel plate that was post-tensioned to the exterior wall with nine high-strength rods. The south exterior wall is post-tensioned in the vertical direction and is able to resist the load transmitted by the reaction beam.

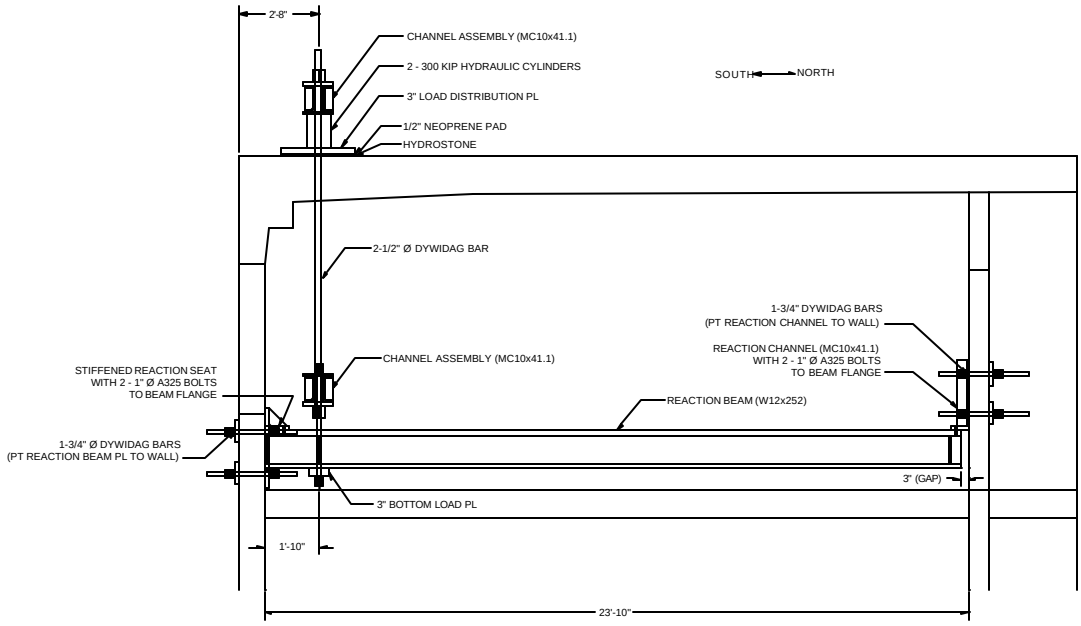

Figure 2.5 - Setup for Deck Test - Elevation View from the East

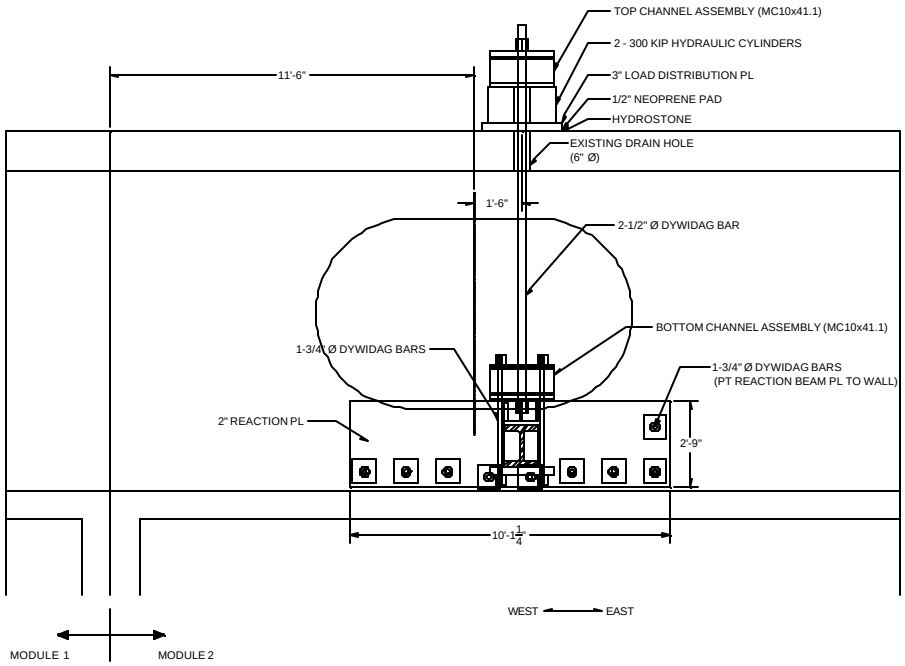

Figure 2.6 - Setup for Deck Test - Elevation View from the South

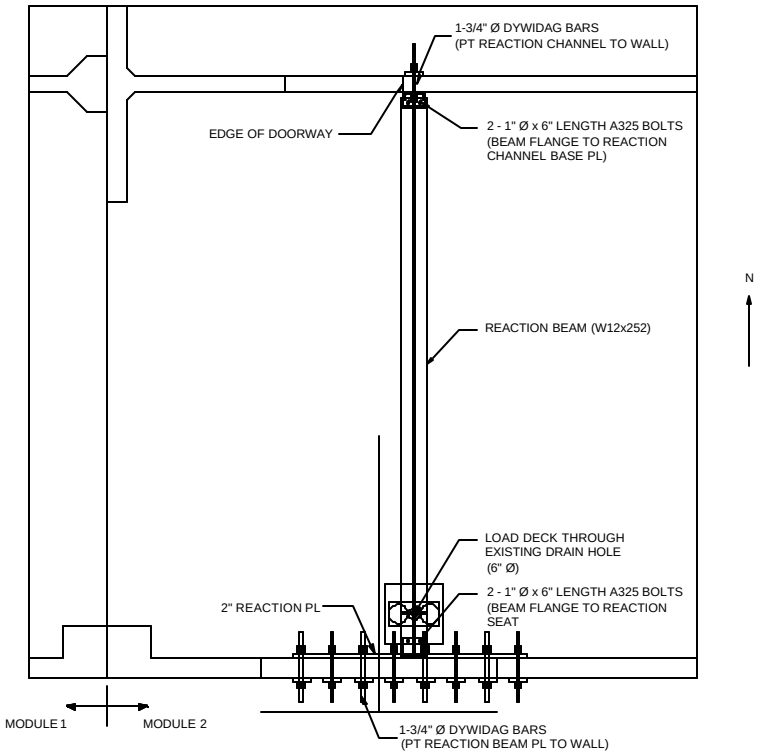

Figure 2.7 - Setup for Deck Test - Plan View at Service Deck Level

2.3.2 Instrumentation

Four types of instruments were used in the test: displacement transducers to measure deck deflection, strain gages to measure concrete deformation, inclinometers to record rotation of the beam above the window opening, and pressure transducers to monitor the hydraulic pressure in the jacks. The instrumentation scheme is illustrated in Figure 2.8 and Figure 2.9. Photographs of the instrumentation and test setup are shown in Figure 2.10. The strain was measured on the top and the bottom of the operations deck and in the north-south direction by gages SC-01 through SC-22 and SC-26 through SC-29. At each location, the gage with the lower number was at the top. SC-23 through SC-25 measured strain in the east-west direction on the outside of the south wall. These three gages were located two inches below the deck-beam interface. Deflections were measured from the service deck to the bottom of the operations deck by transducers DT-01 through DT-14. The window deformation was measured by DT-15 through DT-17 attached to the top and bottom of the window opening. The displacement of the reaction system was measured with respect to the service deck by DT-18 through DT-20. DT-21 through DT-23 measured the possible separation of the deck slab from the exterior face of the south wall. Additionally, a camera system with remote control was used to observe the condition of the concrete and to watch for cracking. During the testing, the deflection of the deck at the load point and of the beam above the window opening, and the strain at SC-18 were monitored and plotted against the load.

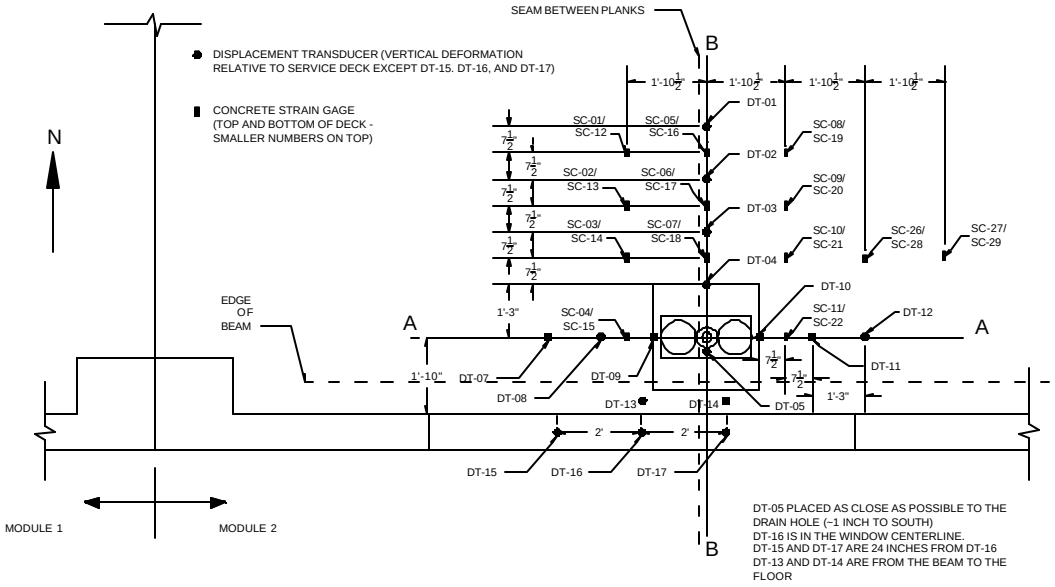

Figure 2.8 - Instrumentation Plan - Plan View

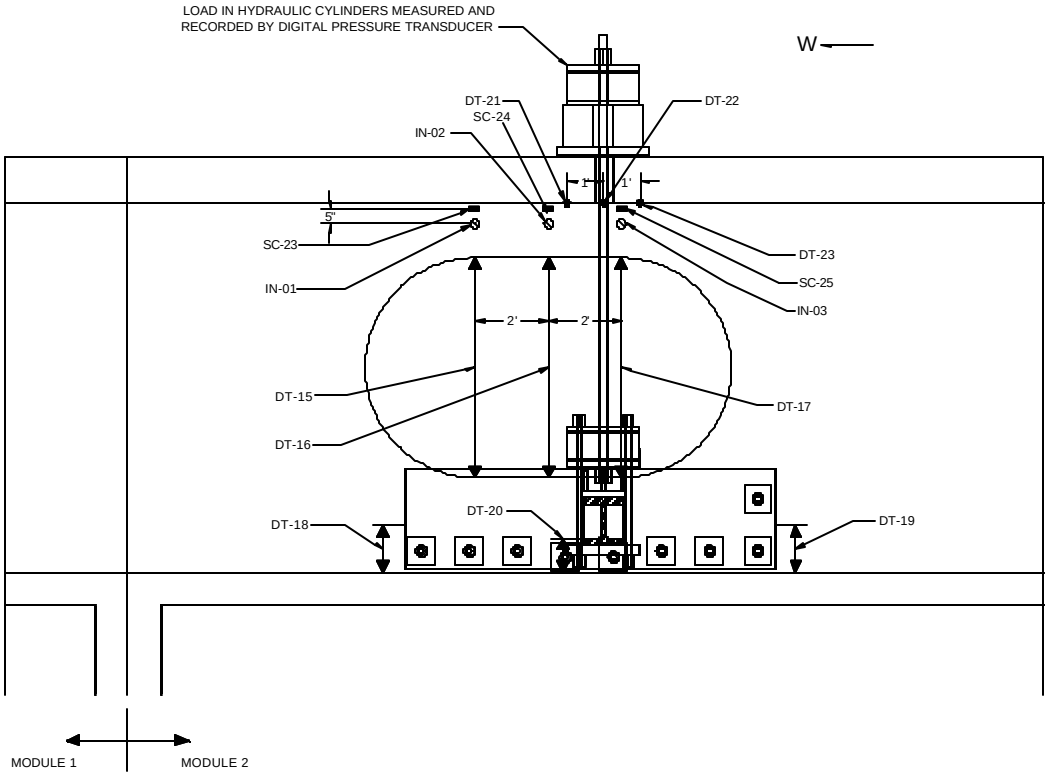

Figure 2.9 - Instrumentation Plan - Elevation View

(a) Looking up from the Service Deck

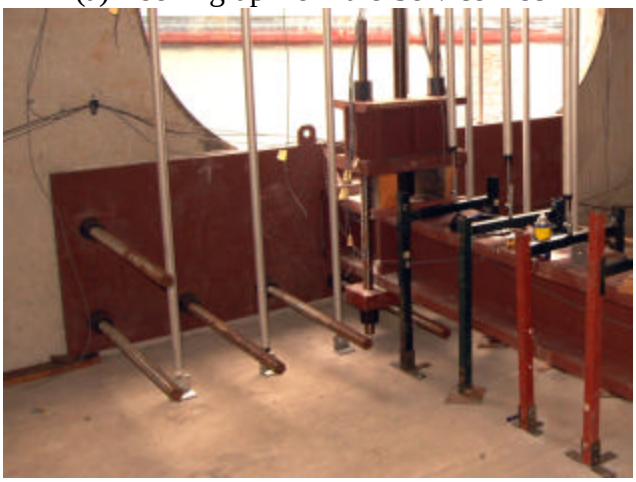

(b) Reaction Plate and Beam - Service Deck

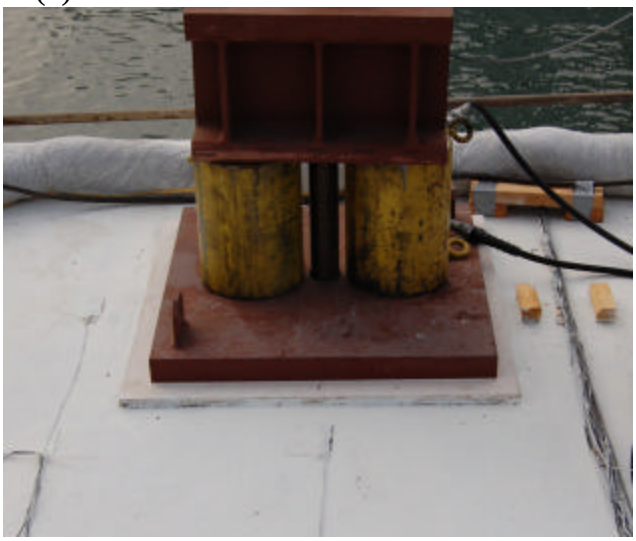

(c) Hydraulic Cylinders on Loading Plate - Operations Deck

Figure 2.10 - Deck Test Loading Apparatus and Instrumentation

2.3.3 Loading Protocol

The loading history applied is plotted in Figure 2.11. On the test day, the loading began at 10:30 am. The load was gradually increased to 250 kips over the next four minutes. This is the service load the deck is designed to carry. The load was then gradually unloaded to 30 kips at approximately the same rate. This pattern was repeated two more times. The deck was then loaded to 250 kips a fourth time and the load was held at this level for five minutes. The load was then increased to 400 kips without unloading and held for five minutes. The deck was then fully unloaded and this portion of the test concluded at 11:11 am.

After the deck was loaded to 400 kips, there was no discernible damage, and the decision was made to load the structure to 500 kips. At 2:22 pm, the deck was loaded to a maximum load of 495.5 kips and held for five minutes. The load was reduced to 400 kips and held for an additional five minutes. The deck was unloaded at 2:41 pm.

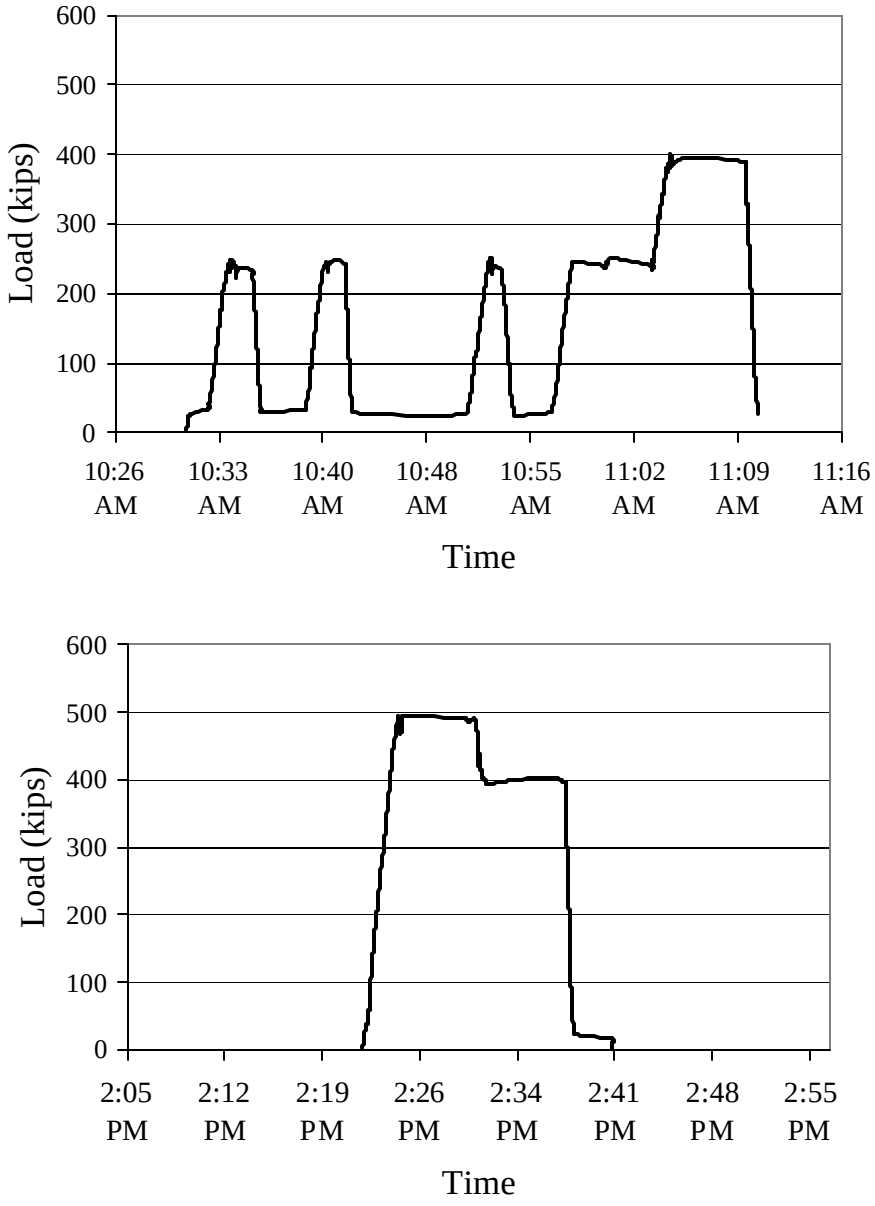

Figure 2.11 - Loading History on August 14th, 2007

2.4 Experimental Results

2.4.1 Observed Performance

There were few visible effects of the loading on the operations deck and the rest of the pier. There were hairline cracks radiating from the drain hole where the loading was applied, as seen in Figure 2.12. These cracks were on the west side of the hole and closed upon the release of the load. They were observed at a load of 500 kips but they could have occurred earlier. Furthermore, cracks were observed in the wall right below the window. They were caused by the load transferred from the reaction plate bolted to the wall. These cracks did not close fully after unloading and are discussed later.

2.4.2 Recorded Deck Performance

Figure 2.13 illustrates the maximum deck deflections recorded at the load levels of 250, 400, and 500 kips during the test. Figure 2.13a shows the vertical deflections recorded by displacement transducers DT-01 through DT-05 and DT-14, which were located along line B-B oriented in the north-south direction as shown in Figure 2.8. The deflected shape shows the tipping of the loading plate, whose south end was above the beam on the south wall that restrained the deflection of the deck. The edges of the plate are 15 in. from the center of the load. Figure 2.13b plots the deflection data obtained from DT-07 through DT-12, which were located along line A-A in the east-west direction as shown in Figure 2.8. It can be seen that the deck deflection is most significant at the center of the load and that the west side of the deck

deflects more than the east. It should be noted that the load was applied at the joint of two adjacent precast planks where the drain hole is located and that transducer DT-05 was located at the edge of the east plank as shown in Figure 2.10a. The relatively large difference between the readings from transducers DT-05 and DT-10 implies a relatively large deformation of the plank on the east side. This is difficult to explain. Displacement transducer DT-09, which was 15 in. west of the center of the load along line A-A, did not function properly, and its reading is, therefore, not shown.

Figure 2.14 shows the deflections of the beam spanning the window opening recorded by DT-13 and DT-14. It can be seen that the entire beam over the window opening deflected horizontally. Figure 2.15 plots the load against the deflection recorded directly under the center of the load by transducer DT-05. The curve shows that the load-deflection response is essentially linear with some small hysteresis loops under loading and unloading. The hysteresis loops appear to be more severe with the increase of the displacement amplitude. This could be due to friction in the load application system.

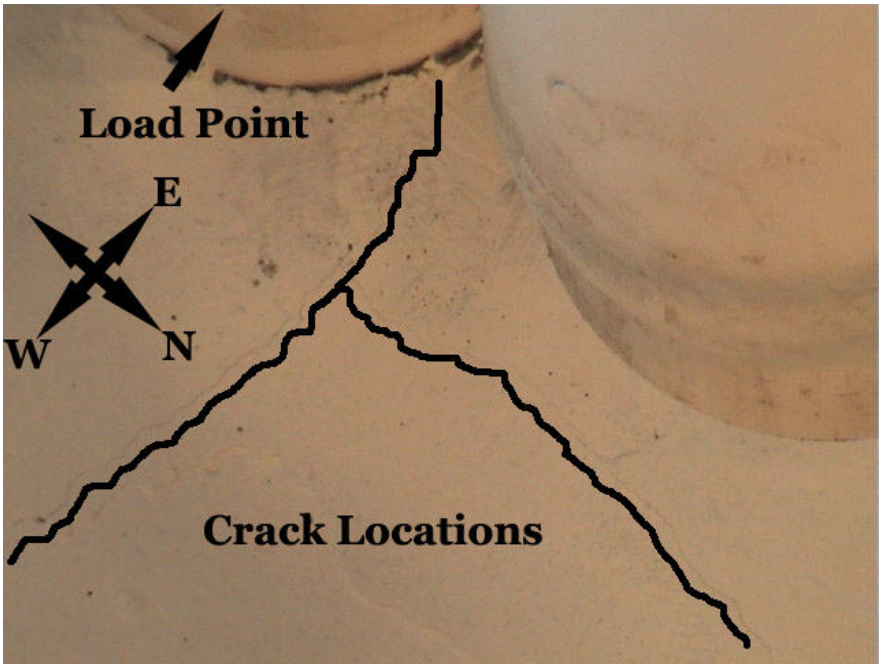

(a) Cracks Radiating from Drain Hole
(Cracks have been outlined with black to enhance visibility)

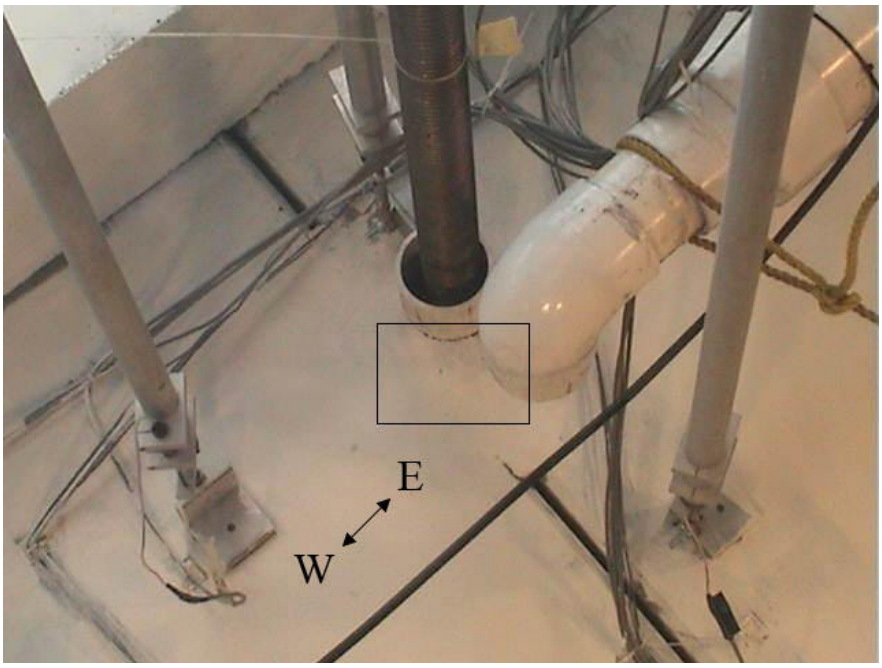

(b) Crack Location

Figure 2.12 - Hairline Cracks at 500-Kip Loading

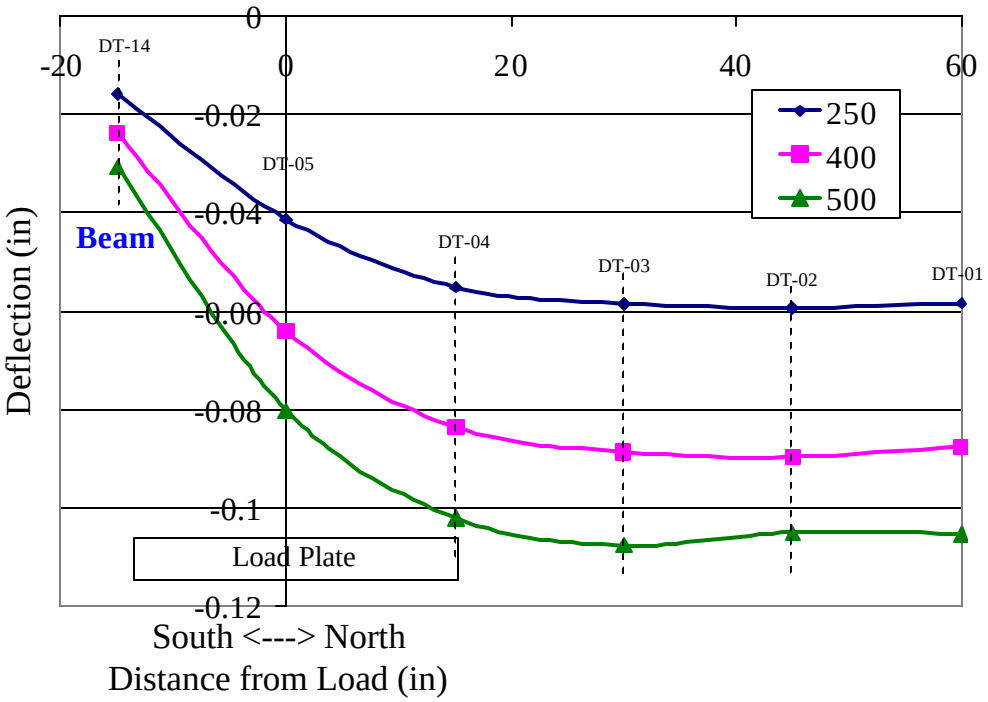

(a) Deflections Along North-South Direction (line B-B in Figure 2.8)

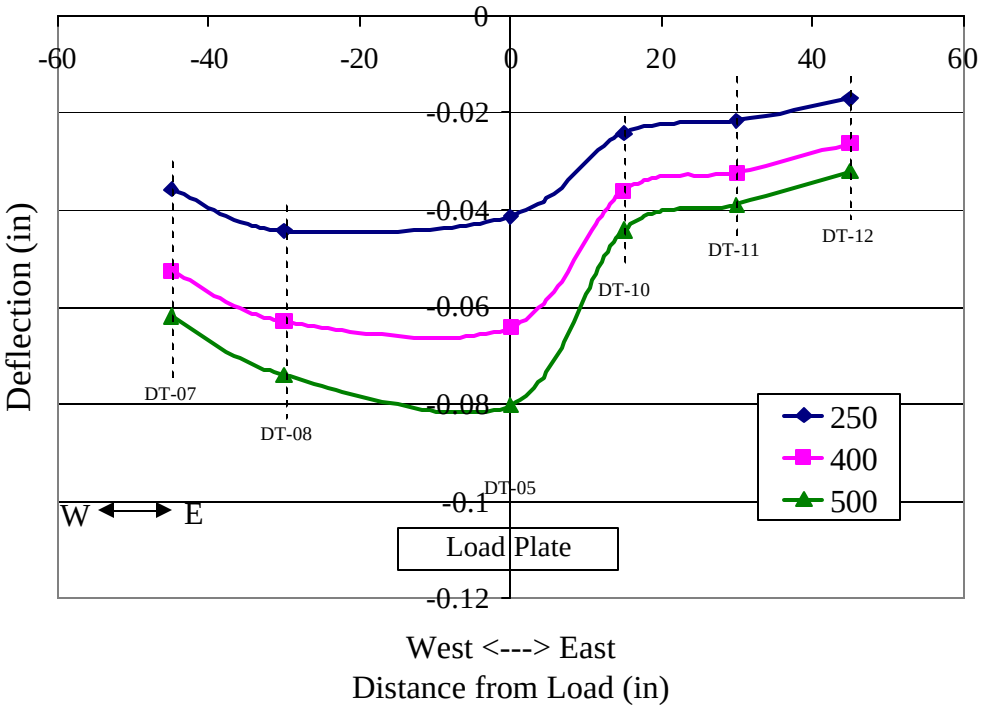

(b) Deflections Along East-West Direction (line A-A in Figure 2.8)

Figure 2.13 - Deck Deflections at Different Load Levels

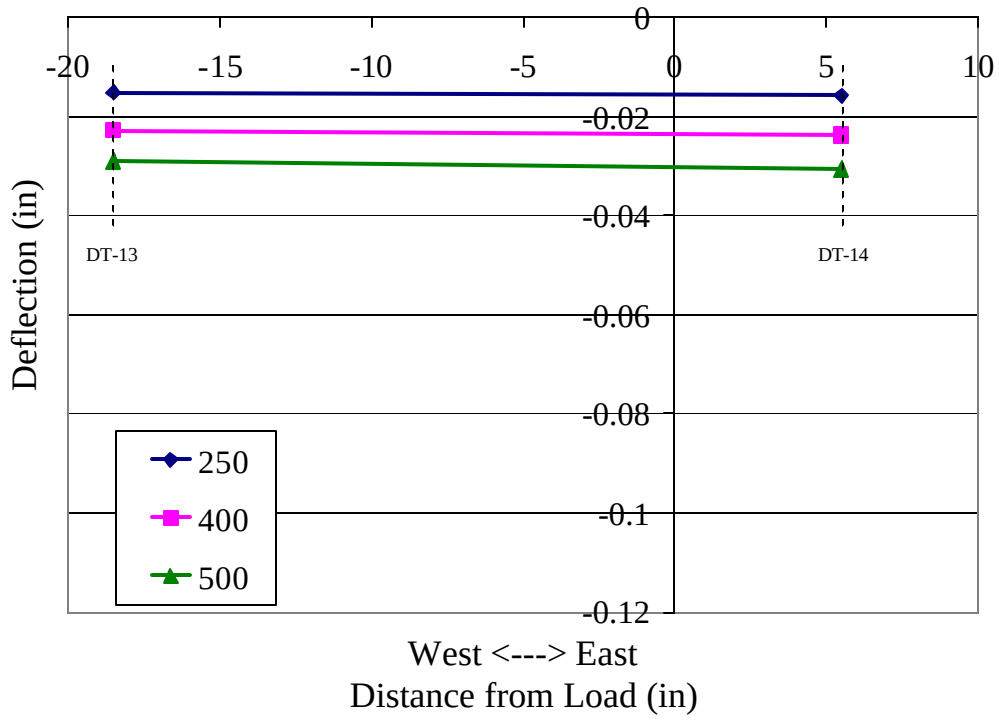

Figure 2.14 - Beam Displacements

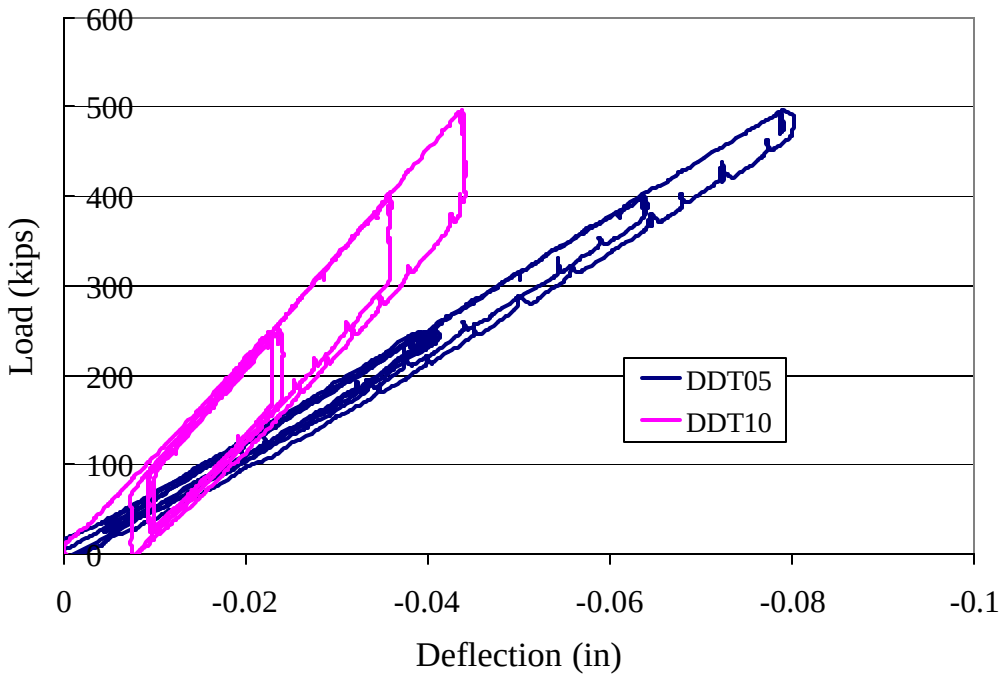

Figure 2.15 - Deck Deflection at Point of Loading (DT-05) & Edge of Load Plate (DT-10)

Figure 2.16 through Figure 2.19 plot the strains in the north-south direction against the distance from the center of the load in the east-west direction at each load level. Large differences in the strains measured at the top and bottom of the deck can be observed. At sections farther (52.5 and 37.5 inches) north of the loading point, the compressive strains at the top of the deck are consistently higher than the tensile strains at the bottom. This indicates that in-plane membrane strains were developed in the deck. These compressive member strains were produced by the arching action of the deck. The compressive membrane strains were less severe on the west side of the load. This could be due to the fact that the wall on the west side above the window might not provide enough support for the arching action to develop.

Figure 2.20 through Figure 2.23 show the membrane strains calculated by averaging the top and bottom strains at each location. Furthermore, as shown in Figure 2.22 and Figure 2.23, tensile membrane strains were found on the west side at sections close to the loading (0 and 22.5 inches north of the loading). The mechanism that created these tensile in-plane strains is not entirely clear. However, the membrane strains are calculated based on the assumption of an uncracked section. The tensile membrane strains could be an artifact of deck cracking near the drain hole. Even though such cracking was first observed at a 500-kip load, it could have occurred much earlier due to two reasons. First, the effective prestress in the precast planks in regions near the loading plate could be much lower than that in other areas because of the prestress loss in the stress transfer zone. The precompression at the bottom of the planks could be further reduced by the post-tensioning applied to the top cast-in-place

layer of the deck. Second, the drain hole would introduce stress concentration. These explain why cracks were observed in the test near the drain hole, while the pre-test finite element analysis indicated that these cracks would not occur till a load of 1100 kips.

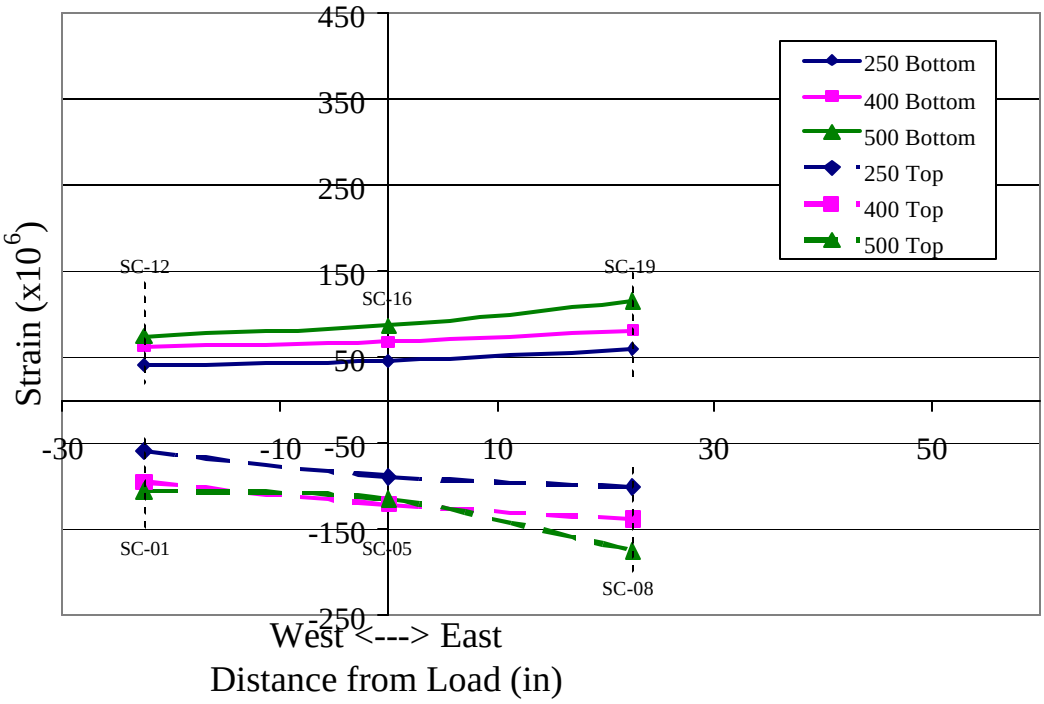

Figure 2.16 - Strains Measured at 52.5 inches North of Load

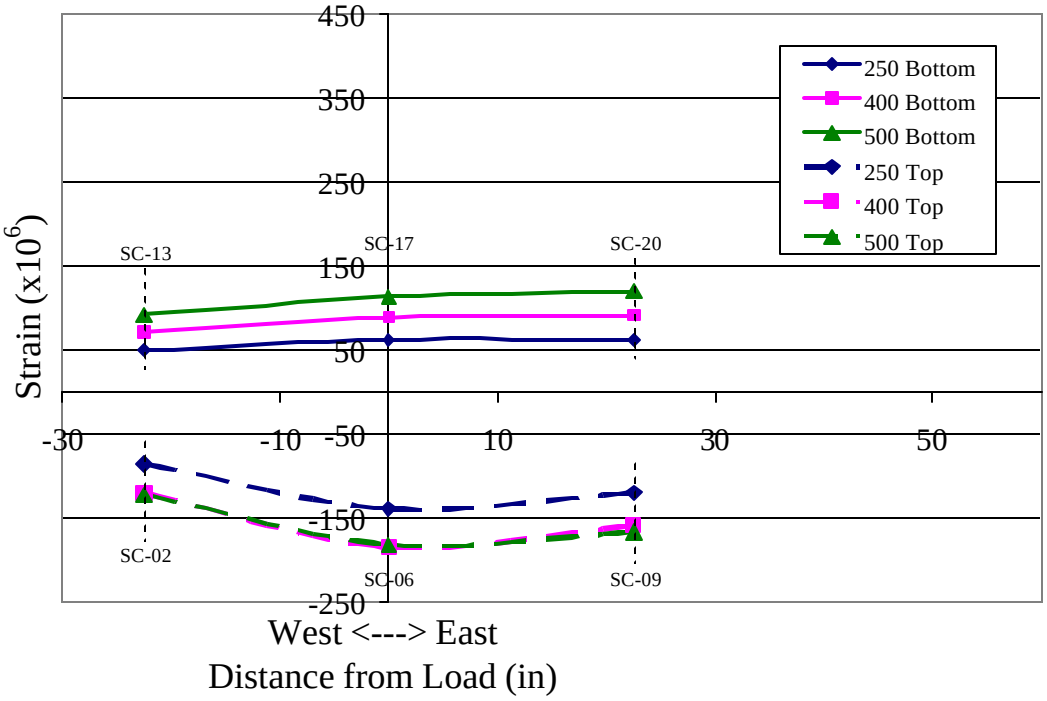

Figure 2.17 - Strains Measured at 37.5 inches North of Load

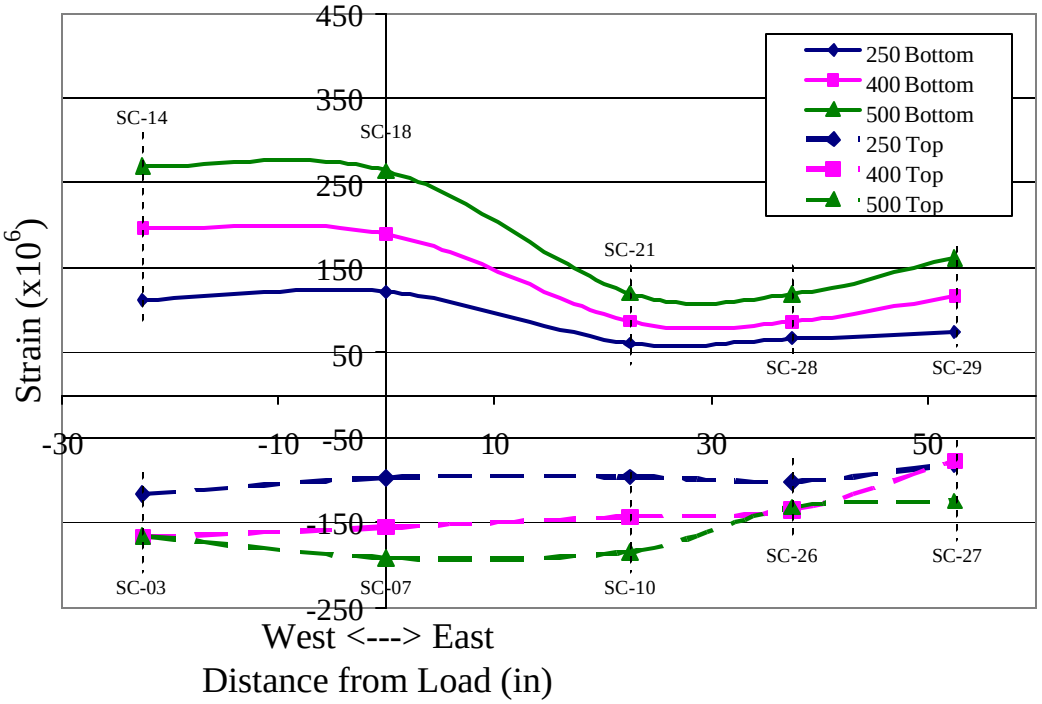

Figure 2.18 - Strains Measured at 22.5 inches North of Load

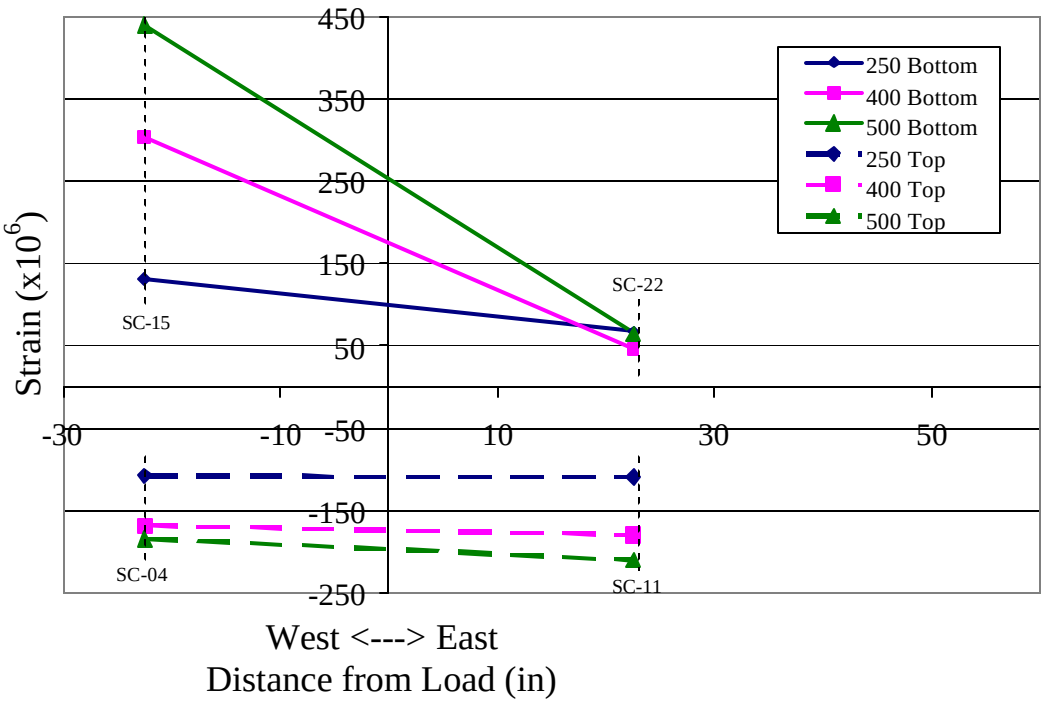

Figure 2.19 - Strains Measured at Load (line A-A)

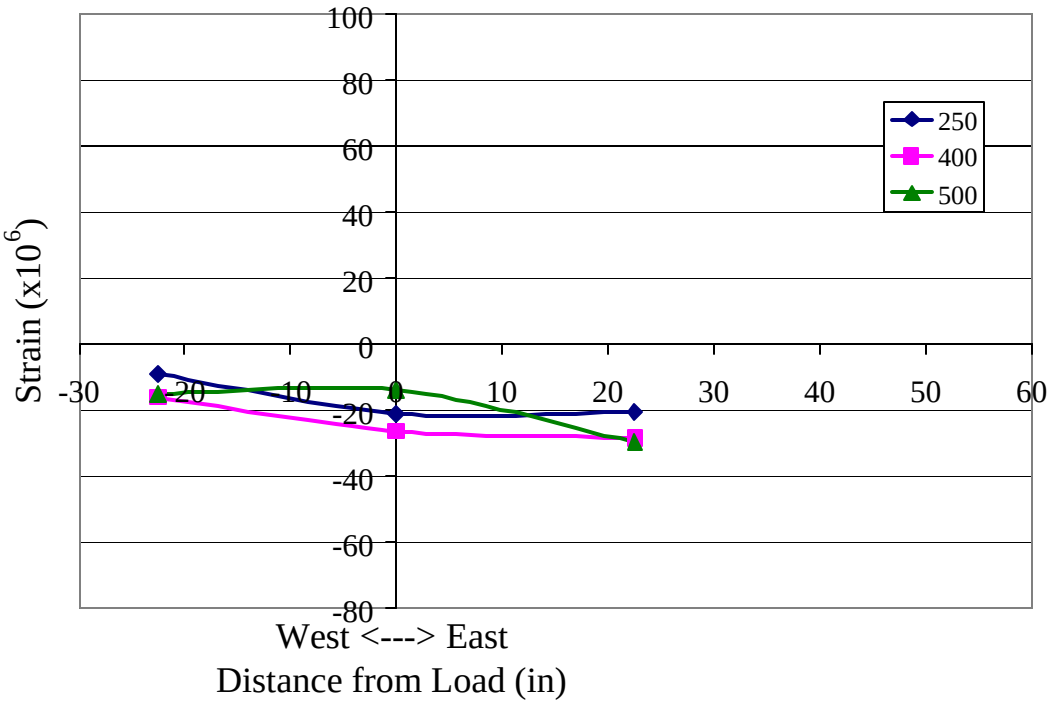

Figure 2.20 - Calculated Membrane Strains at 52.5 inches North of Load

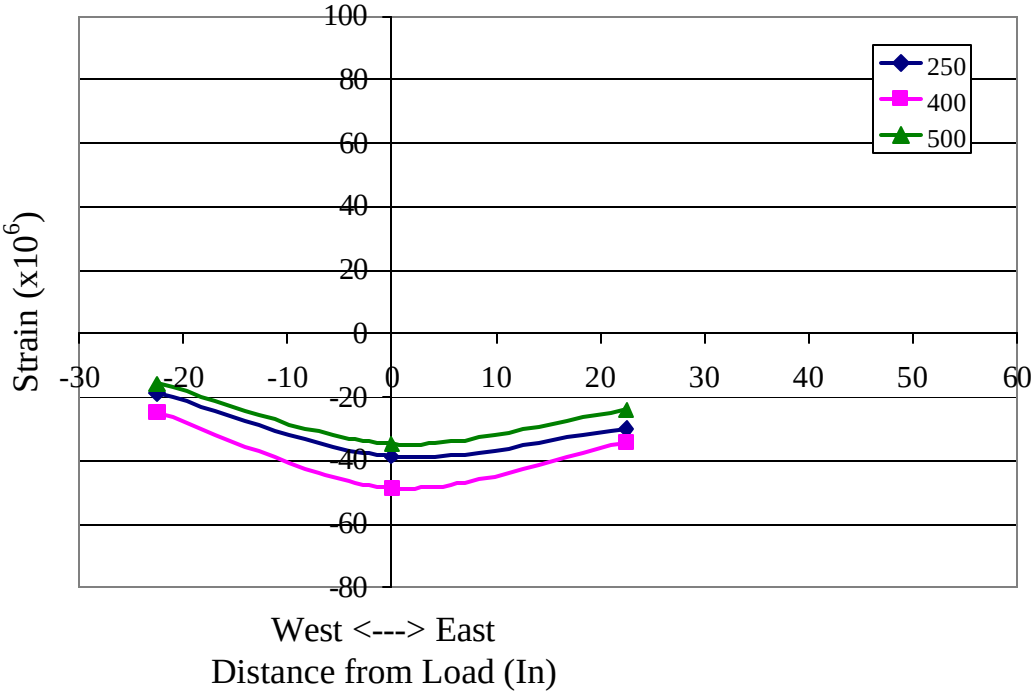

Figure 2.21 - Calculated Membrane Strains at 37.5 inches North of Load

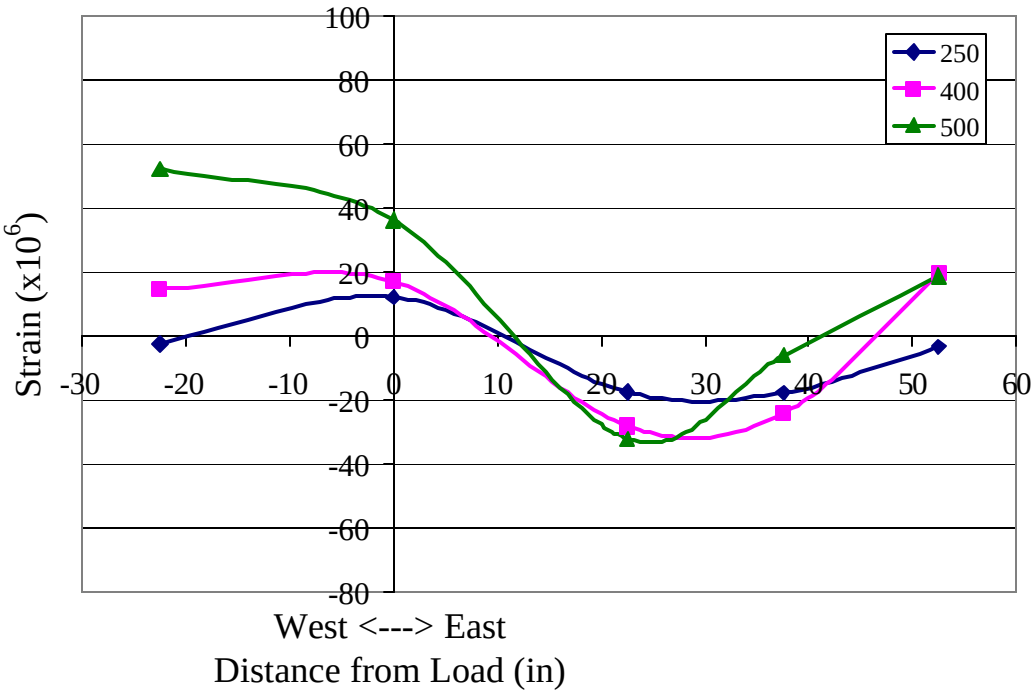

Figure 2.22 - Calculated Membrane Strains at 22.5 inches North of Load

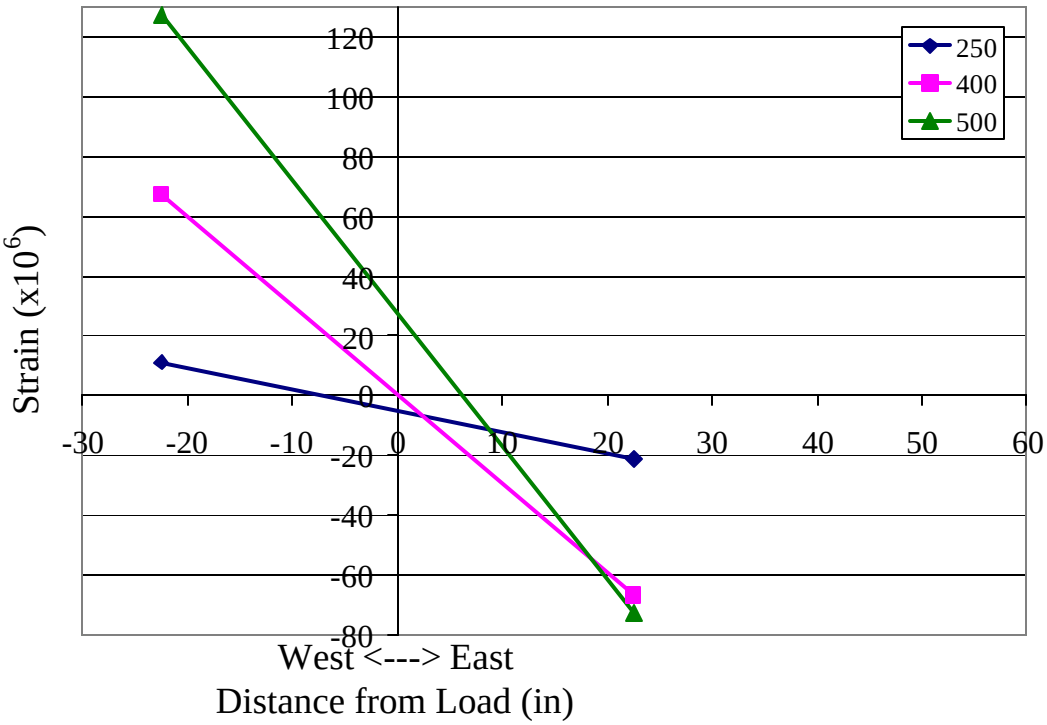

Figure 2.23 - Calculated Membrane Strains at Load

Bending strains are calculated by subtracting the membrane strains from the measured strains. They are plotted in Figure 2.24 through Figure 2.27. As the plots show, for sections close to the loading, the bending strains are higher on the west side than on the east. These could be due to cracking as explained previously.

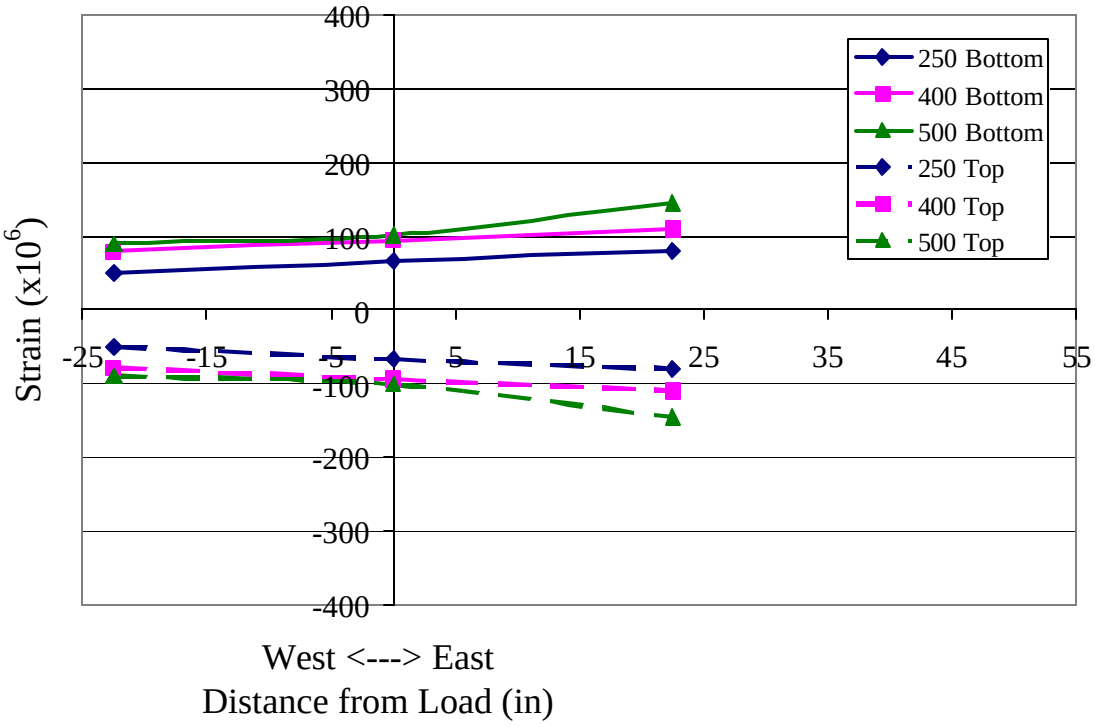

Figure 2.24 - Bending Strains at 52.5 inches North of Load

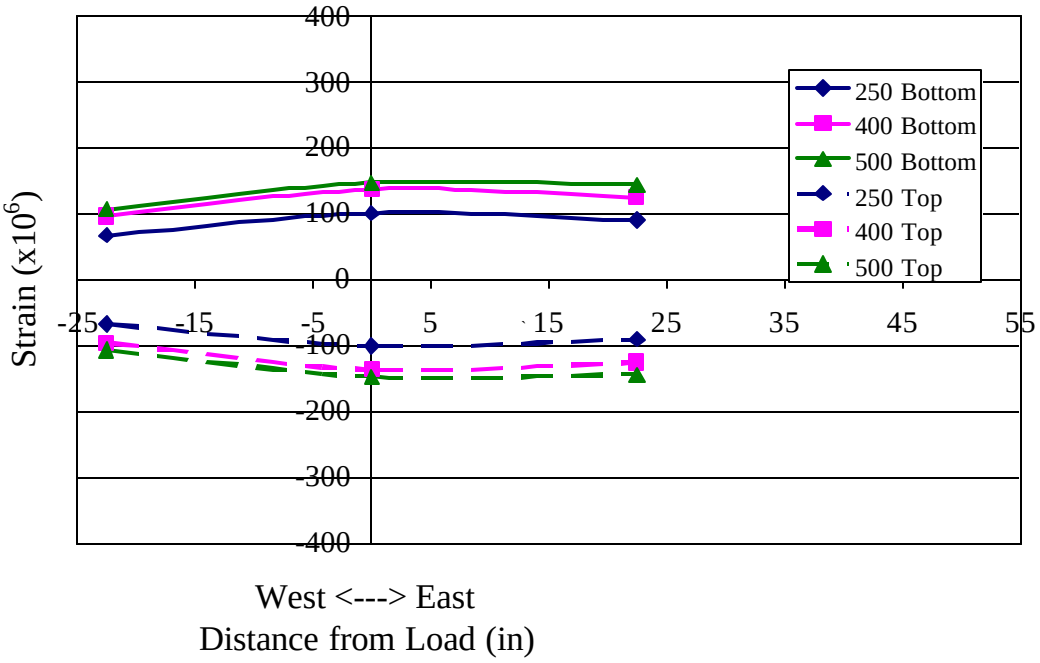

Figure 2.25 - Bending Strains at 37.5 inches North of Load

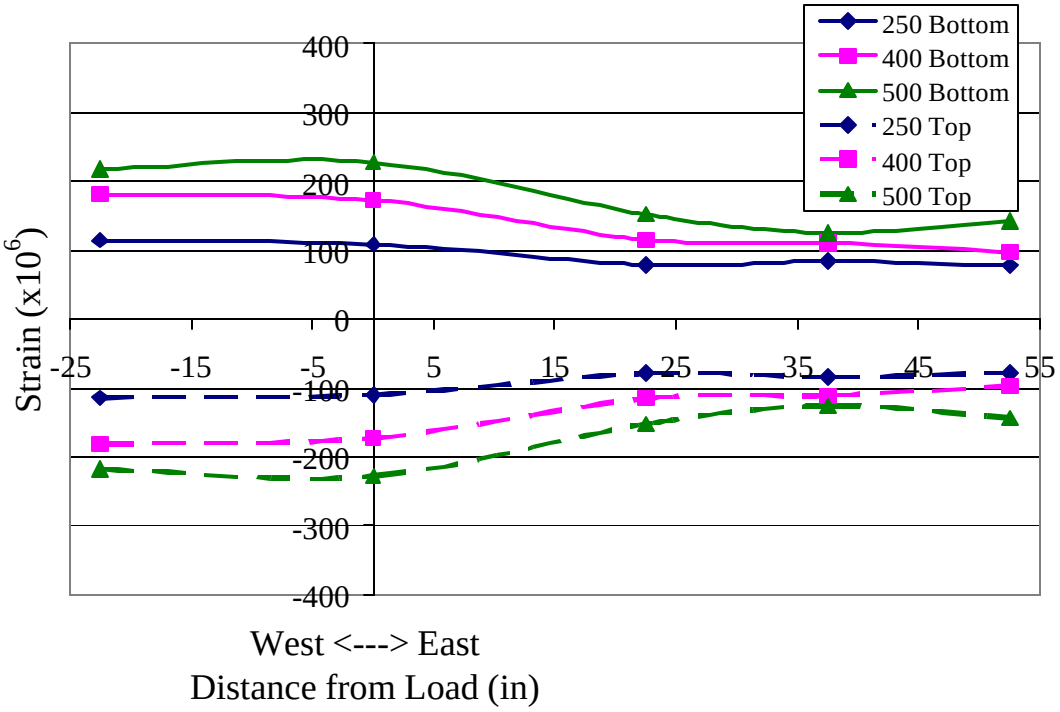

Figure 2.26 - Bending Strains at 22.5 inches North of Load

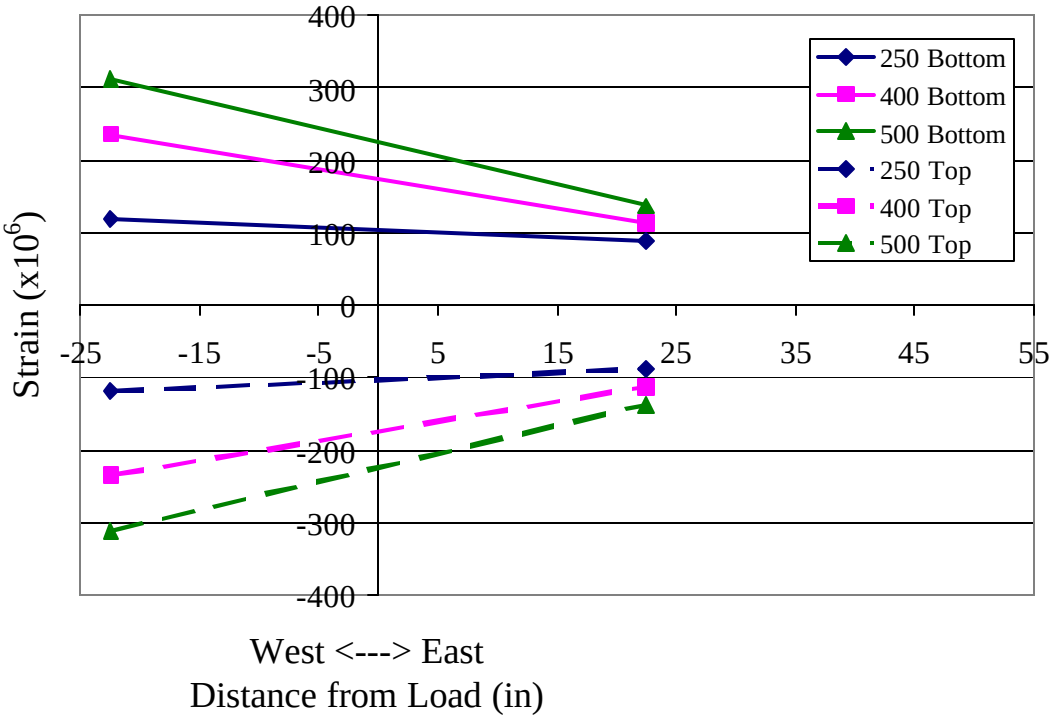

Figure 2.27 - Bending Strains at Load

2.4.3 Beam Behavior

The deflection of the beam at the edge of the deck above the window opening is plotted against the load in Figure 2.28. A linear relation can be observed. The rotation of the beam could not be accurately measured because neither the inclinometers nor the displacement transducers (DT-16, DT-16, and DT-17 as shown in Figure 2.8) in the window opening provided reliable readings. The readings of the inclinometers were adversely affected by the constant movement of the pier induced by the ocean waves and the readings of the displacement transducers were corrupted by the cracking movement in the wall below the window as will be discussed in Section 4.4. Bending strains were measured near the top of the beam above the window opening. They are plotted in Figure 2.29.

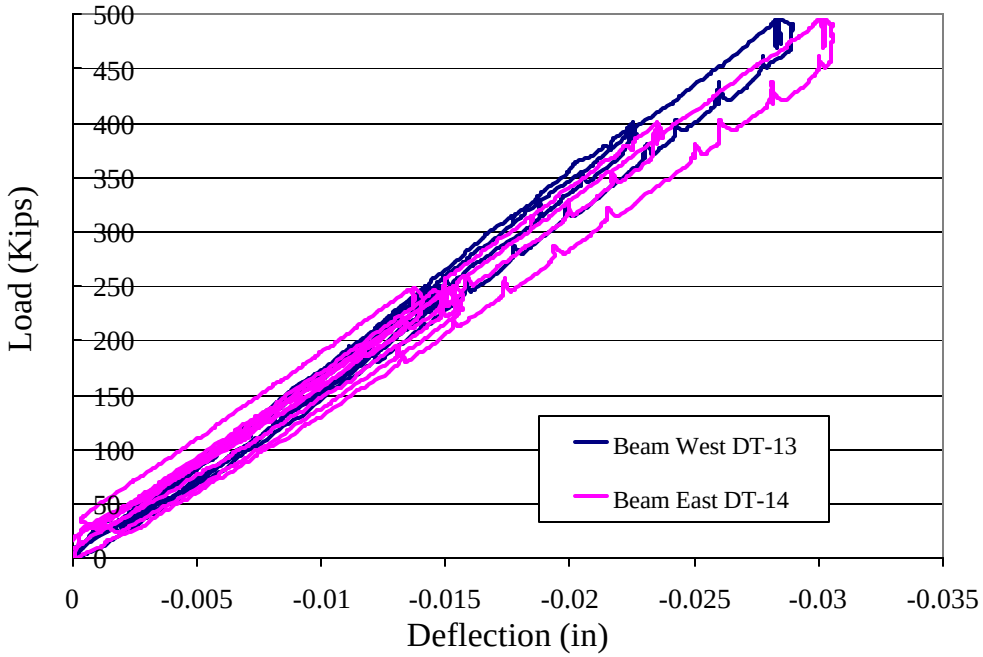

Figure 2.28 - Beam Deflection

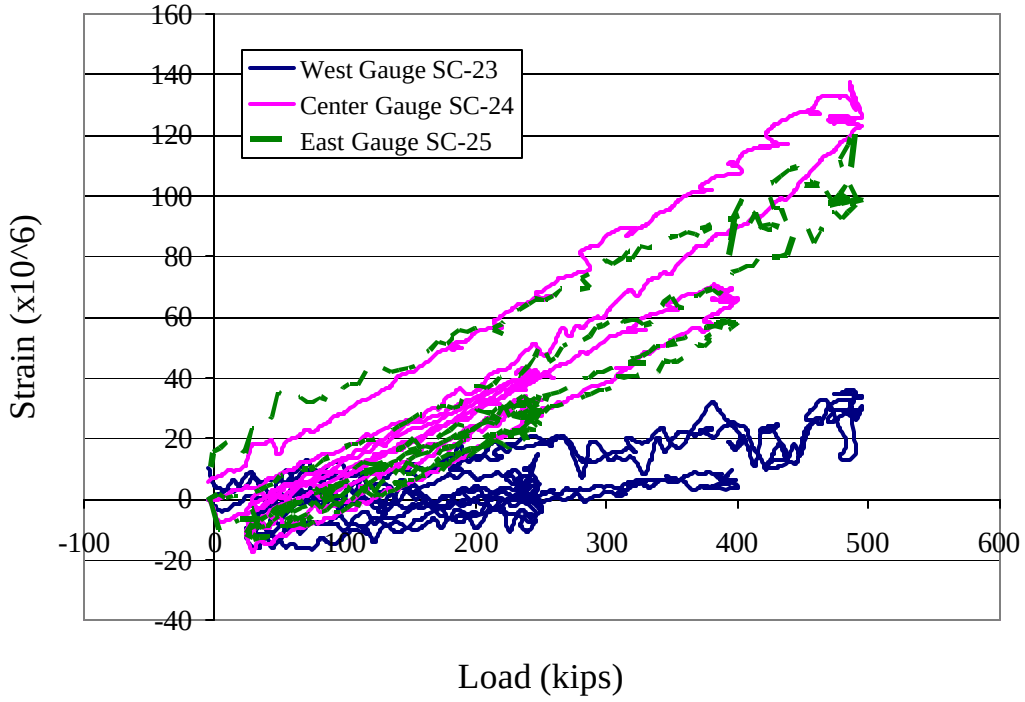

Figure 2.29 - Bending Strains in Beam (2” below Beam-Deck Interface)

2.4.4 Apparatus Issues

A decision was made to load the deck to 500 kips after no damage was observed at the 400-kip level. This additional loading caused slippage between the reaction plate and the wall. Additionally, there was significant cracking in the vicinity of the internal wall post-tensioning anchors below the window opening. The cracking and the slippage movement can be seen in Figure 2.30 and Figure 2.31. Figure 2.31 clearly shows a permanent displacement of 0.014 in., which was probably a combination of the reaction plate slippage and the cracking movement of the wall. The wall of the pier below the service deck was inspected after the test to verify that there was no additional cracking or damage. The cracks below the window opening were not structural damage, and they were filled with epoxy to protect the reinforcement from future corrosion problems.

Figure 2.30 - Cracking in Wall below Window Opening Supporting the Reaction Plate

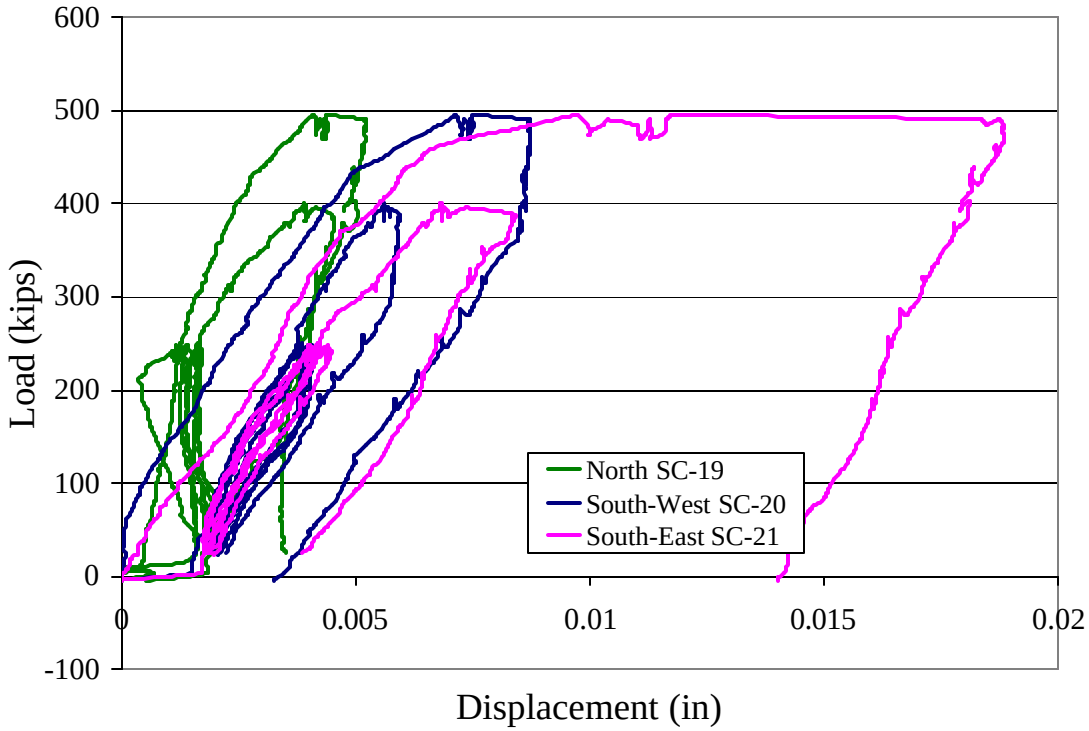

Figure 2.31 - Movement of the Load Transfer Plate with Respect to the Service Deck

3 Bollard Capacity Structural Test

3.1 Introduction

3.1.1 Description of the Bollard

The bollard is made of a steel cylinder that has an outer diameter of 16 in. and an inner diameter of 12.8 in. A picture of the bollard and the design drawings are shown in Figure 3.1 and Figure 3.2, respectively. The cylinder is connected to a 4"-thick base plate with a 1-in. fillet weld all around. The weld size has been increased from the original design of 3/8 in. During the test, the bollard was attached to the deck with four 2-9/16-in.-diameter A449. As shown in Figure 3.1, the original bollard had six bolts. The middle bolts on the north and south sides were removed to reduce the excess capacity. The maximum mooring (service) load expected for the bollard is 200 kips and the bollard is designed to have a factor of safety of 2. In the test, a load was applied to the bollard towards the south with a vertical angle of 11 degrees. This was the critical angle for the tensile fracture of the weld, which was expected to be the governing failure mode as indicated by the pre-test analyses presented in Section 3.2.

Currently, there are few standards for validating the capacity of a bollard. It is anticipated that this full-scale test will be instrumental in creating a test methodology for a future standard.

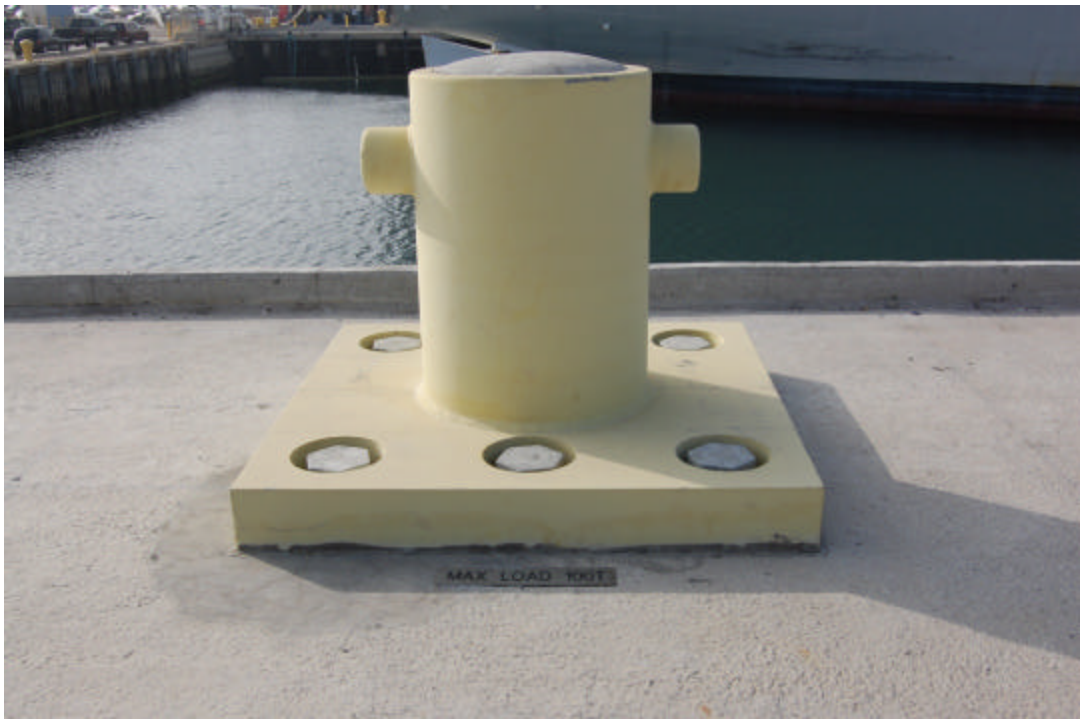

Figure 3.1 - Photograph of the Tested Bollard

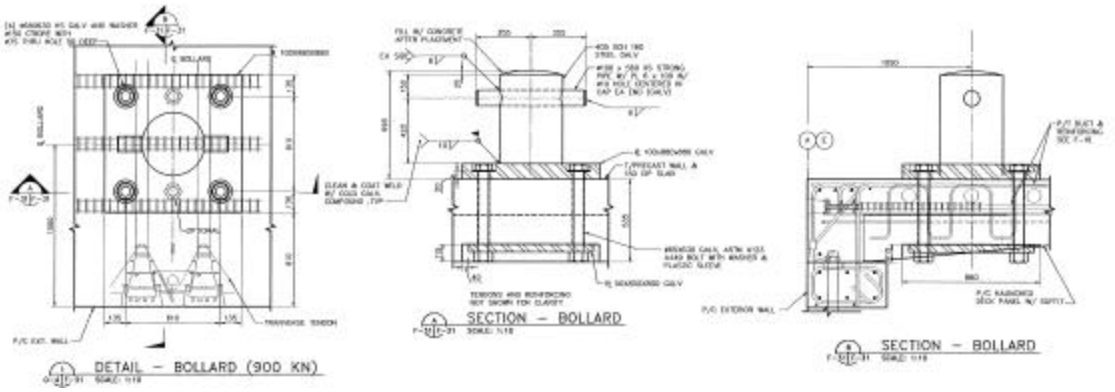

Figure 3.2 - Design of the Bollard

3.1.2 Test Objectives and Scope of Work

The test objective was to validate the load capacity of a full-size bollard that is bolted onto the operations deck on the south side of the MHP. The test was to validate the targeted design capacity but not to induce irreparable damage to the bollard or the deck. Prior to the test, simplified analyses and nonlinear finite element modeling were conducted to identify the failure mechanism and load capacities of the bollard and the supporting deck. Results of these analyses were used to determine the loading protocol and the instrumentation scheme.

3.2 Pre-Test Analyses

The bollard that was selected for the load test is located on the south side of the operations deck. It is made of a steel pipe that has an outside diameter of 16 in. and a wall thickness of 1.594 in. The design of the bollard and the details of its attachment to the operations deck are shown in Figure 3.2. It is connected to a 4-in.-thick base plate with 1-in. fillet weld all around. The base plate is attached to the operations deck with six 2-9/16-in.-diameter A449 bolts, which pass through the holes in the deck and a thick steel plate underneath and are secured with nuts. Before the test, it was decided that two of the bolts be removed to reduce the excess capacity and they would be re-installed afterwards. The bollard is designed to have a mooring service capacity of 200 kips with a factor of safety of 2. Hence, it is expected to sustain a load of 400 kips without being damaged.

In the test, the load was applied towards south with a steel rope wrapped around the bollard right beneath the horns at an angle that was perceived to be the critical loading angle with respect to the horizontal. The critical angle is one that results in the smallest failure load. Analyses were conducted prior to the test to estimate the actual load capacity of the bollard and to determine the governing failure mode and the corresponding critical loading angle. Simplified analyses were first conducted to obtain a good estimate of the bollard capacity. Based on the critical loading angle determined from the analyses, nonlinear finite element analyses of the bollard and the deck were conducted by Hussein Okail at UC San Diego to confirm the analytical results. The analysis results were used to determine the loading protocol and instrumentation scheme for the load test.

3.2.1 Simplified Analyses

In the simplified analyses, a number of potential failure mechanisms were considered, including:

1. Tensile failure of the bollard cylinder.
2. Tensile failure of the weld at the base of the bollard cylinder.
3. Tensile failure of the anchor bolts.
4. Failure of the operations deck due to the prying action of a loaded bollard.

The following sections present the assumptions, reasoning, and calculations used to determine the load capacity and critical loading angle for each of the above

scenarios. Since the load test was to validate the factor of safety in the bollard design and not to induce irreparable damage in the bollard, the capacity of the bollard was considered to be reached when the maximum tensile stress in the cylinder or anchor bolts reaches the yield stress, or that in the weld reaches the tensile strength, whichever comes first. However, for the concrete deck capacity under the prying action, the ultimate strength was estimated, based on which a safe maximum test load could be determined.

Tensile Failure of Bollard Cylinder

The cylindrical body of the bollard is made of a 405 SCH 160 pipe, which has an outside diameter of 16 in. and a nominal wall thickness of 1.594 in. The nominal yield strength s_y = 35 ksi. The steel cylinder is filled with concrete. The loading condition of the bollard is shown in Figure 3.3. The horns have a diameter of 4 in. and the steel wire rope to be used in the test had a nominal diameter of 2-1/2-in.

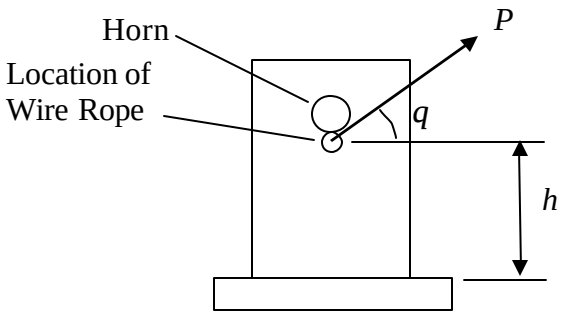

Figure 3.3 - Bollard Loading Condition

Based on the configuration shown in Figure 3.3, the maximum tensile stress induced by the bending and axial force was calculated as

$$s_m = P\left(\frac{h\cos q}{S} + \frac{\sin q}{A}\right) \tag{3.1}$$

in which S is the section modulus and A is the cross-sectional area of the cylinder. It was found that the influence of the concrete core on the bending capacity of the bollard is very small, and, therefore, it was neglected in the analysis. The critical loading angle for this case is one that results in the highest s_m for a given load P. It was obtained from the following equation.

$$\frac{ds_m}{dq} = P\left(\frac{-h\sin q}{S} + \frac{\cos q}{A}\right) = 0 \tag{3.2}$$

which leads to

$$\tan q = \frac{S}{Ah} \tag{3.3}$$

In this case, we have h =13.25 in., A = 72 in.^{2}, and S = 237 in.^{3}. This results in ? = 11.27^o. With Equation (2.1), the maximum load capacity of the bollard was calculated to be 610 kips.

Tensile Failure of Weld

It was conservatively assumed that weld fracture would occur when the maximum tensile stress in the weld reached the tensile strength s_w. The maximum tensile stress in the weld was estimated in a way similar to that for the bollard cylinder

but taking into account of the size of the weld. As a result, the critical loading angle ? would be the same as that for the bollard cylinder, i.e., ? = 11.27^o. Based on Equation (2.1), the maximum tensile stress in the weld was estimated with the following formula.

$$s_{m,w} = P\left(\frac{h\cos q}{S} + \frac{\sin q}{A}\right) \times \frac{t}{T_e} \tag{3.4}$$

in which t is the nominal wall thickness of the bollard cylinder, which is 1.594 in., T_e is the effective throat dimension of the fillet weld, and S is the section modulus and A is the cross-sectional area of the bollard cylinder. For a 1-in. weld, $T_e = 0.707 \times 1$ in. = 0.707 in.

The weld was applied with an E70 electrode. Hence, the nominal tensile strength, s_w, of the weld is 70 ksi. However, with the conservatism used in welding practice, the actual strength could be around 90 ksi. By assuming that weld failure would occur when $s_{m,w}$ reached 70 ksi, the load capacity calculated with Equation (2.4) would be 540 kips. However, in design, the capacity of a weld is normally conservatively based on the shear strength of the weld, which is taken to be 60% of the tensile strength. With this assumption, the capacity of a weld would be governed by the condition that $s_{m,w = 0.6}\ s_w$. With s_w equal to 70 ksi, the load capacity calculated with this condition would be 320 kips. With s_w equal to 90 ksi, the load capacity would be 410 kips. Hence, a conservative estimate of the load capacity of the weld is 320 kips. However, it could be around 540 kips or higher based on the above considerations.

Tensile Failure of Bolts

To estimate the tensile stress in the bolts, the base plate of the bollard was first assumed to be rigid. It would rotate as a rigid body when the bollard was loaded. At first, all six anchor bolts were considered in the analysis. The result indicated an excessive load capacity. Hence, it was subsequently decided that two of the bolts be removed in the test. The calculations presented below are based on a total of four anchor bolts. The idealized load resisting mechanism of the bolts is shown in Figure 3.4.

With the base plate assumed rigid, one can calculate the total force in the two extreme tension bolts as follows.

$$F_2 = P\left(a\sin q + h'\cos q\right)\frac{d_2}{d_1^2 + d_2^2} \tag{3.5}$$

with the geometric parameters defined in Figure 3.4 - Load Resisting Mechanism of Bolts. The critical loading angle for a given load P is given by the following equation.

$$\tan q = \frac{a}{h'} \tag{3.6}$$

Based on the dimensions of the base plate and the bolt locations, a = 17.3 in., h' = 17.25 in., d_1 = 5.3 in., and d_2 = 29.3 in. This results in the critical loading angle q = 40°. For 2-9/16-in.-diameter A449 bolts, the cross-sectional area of the threaded portion of a bolt is about A_b = 4 in.^{2} and the yield strength s_y = 92 ksi. Hence, the maximum F_2 that can develop without yielding the bolts is $F_{2,\max} = 2A_b s_y$ = 736 kips.

With this and Equation (2.5), the maximum load *P* that could be carried without causing bolt failure was estimated to be 920 kips.

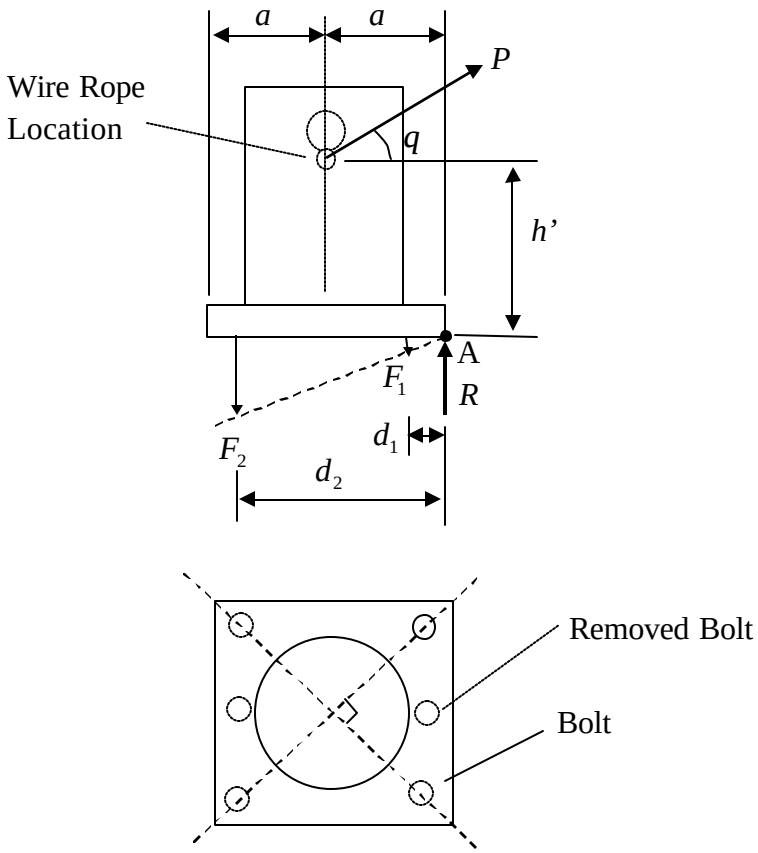

Figure 3.4 - Load Resisting Mechanism of Bolts

Deformable Base

In reality, both the base plate and the concrete deck are deformable. To account for this in a simple and conservative way, the vertical reaction *R* was shifted from point A, the edge of the plate, towards the interior by 4 in. to reduce the moment arm

for F_2 as shown in Figure 3.5. This is a very significant shift and is considered extremely conservative. In this case, the contribution of F_1 is negligible. Hence,

$$F_2 = \frac{P}{d_2 - 4}\left[(a-4)\sin q + h'\cos q\right] \tag{3.7}$$

Equations (2.7) leads to the critical angle q of 33^o and the maximum load capacity of 860 kips.

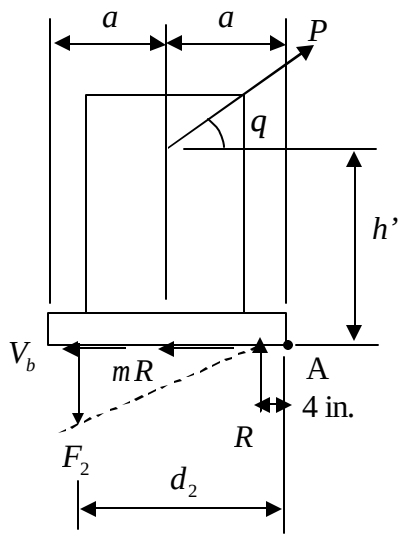

Figure 3.5 - Bolt Resistance with Base Deformation and Friction

Interaction of Tension and Shear

Since bolt tension was not specified for the installation of the bollard, the initial tension in the bolts was assumed zero. Hence, the base plate would very likely slide over the deck surface under a large load, and, subsequently, the bolts could be subjected to shear when they leaned against the wall of the bolt holes. To account for this situation, the capacity of a bolt under simultaneous tension and shear was

estimated using an interaction formula. The total shear demand on the bolts was estimated as

$$V_b = P\cos q - m(F_2 - P\sin q) \tag{3.8}$$

in which F_2 could be conservatively calculated with Equation (2.7) assuming a deformable base. The shear was assumed to be equally shared by all 4 bolts. It was assumed that the coefficient of friction m between the base plate and the deck surface is 0.2 and the interaction between the shear and tensile strengths follows a linear relation. Hence, one can calculate the maximum allowable F_2 with the following formula.

$$\frac{F_2}{F_{2,\max}} + \frac{V_b}{1.2F_{2,\max}} = 1 \tag{3.9}$$

In the above formula, $F_{2,\max} = 2A_b s_y$ = 736 kips, which is the nominal capacity of a pair of bolts when subjected to tension alone, the shear strength of a bolt can be assumed to be 60% of the tensile strength, and F_2 and V_b are given by Equations (2.7) and (2.8), respectively. This results in the critical loading angle q of 25^o and the maximum load capacity of 480 kips.

In summary, with four bolts, the maximum load that could be carried by the bollard without yielding the bolts was estimated to be between 480 and 920 kips. However, the actual capacity would depend on the amount of shear carried by the bolts and the deformability of the base.

3.2.2 Deck Failure

The concrete deck will be subjected to a prying action when the bollard is loaded. The capacity of the deck under the prying action was conservatively assessed assuming a one-way bending action. The thickness of the deck varies along the north-south direction between the supporting walls underneath. The thickness of the deck is about 15 in. for the middle portion and close to 20 in. at the place where the bollard is located. To estimate the nominal moment capacity of the deck, it was conservatively assumed that the deck had a thickness of 15 in. As a result, the nominal moment capacity for positive bending was estimated to be M_n^+ = 153 kip-ft./ft. and the nominal moment capacity for negative bending was M_n^- = 94 kip-ft./ft. The effective bending width was conservatively assumed to be 6 ft., which is about twice the dimension of the bollard base plate. This was proven by the subsequent finite element analysis to be very conservative.

The deck has two continuous spans in the north-south direction over three supporting walls. Even though the deck can be considered as rigidly connected to the supporting walls, the walls are relatively flexible and can provide only limited rotational restraints. Because of the difficulty in finding the exact restraint conditions, a single span was considered with the south end simply supported and the north end fixed, as shown in Figure 3.6, to establish the limiting load. The limiting prying moment and load were calculated with a plastic analysis with the plastic hinge locations shown in Figure 3.6. The load applied to the bollard was assumed to be horizontal and located at 17.25 in. (*h'* in Figure 3.4) above the surface of the deck. The

following values were used for the dimensions shown in the figure: b = 1 ft., $2a$ = 3 ft., and c = 21 ft., which were estimated from the design drawings for the modular pier. Based on the conditions shown in Figure 3.6, the maximum prying moment that could be sustained was calculated to be 840 kip-ft., which corresponds to a maximum horizontal load of 580 kips.

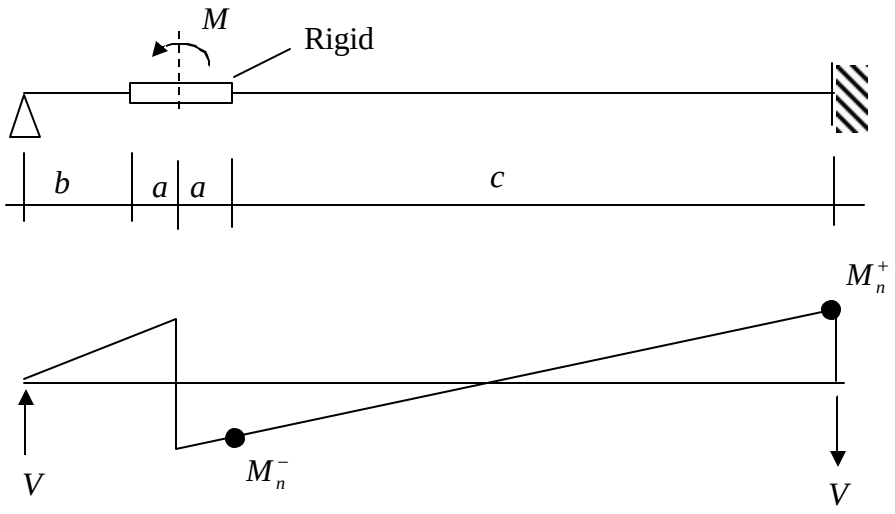

Figure 3.6 - Boundary Conditions for Prying Action

3.2.3 Summary of Simplified Analyses

Results of the simplified analyses are summarized in Table 3.1. It should be mentioned that the nominal moment capacities of the deck were used to estimate its failure load, while the maximum stresses are limited to the yield or tensile strengths at other failure locations. Noticeable damage could occur in the deck when the moment carried reaches 80% of the nominal capacity. Even with this consideration, the weld seems to be the weakest component in the bollard system. For this reason, the loading angle was selected to be 11 degrees for the test.

Table 3.1 - Estimated Failure Loads

Failure Location	**Critical Loading Angle (Degrees)**	**Failure Load (kips)**
Bollard Cylinder	11	610
Weld (1 in.)	11	320-540
Bolts (4)	25-40	480-920
Deck	0 (assumed)	580

3.3 Experimental Setup

3.3.1 Test Setup

The bollard capacity test was designed to simulate the mooring loads introduced by a vessel. The bollard was to be loaded up to the incipience of failure, but not to exceed 400 kips. The design of the test apparatus is general enough to be used as a standard test apparatus for different bollard types. The height and angle of load application can be varied with minor modifications in the test setup should a different failure mechanism be anticipated for a bollard, or to accommodate a particular geometry.

The bollard being tested is on the south side of the operations deck as seen in Figure 1.3. As shown in Figure 3.7 through Figure 3.9, the bollard was loaded with two 300-kip hydraulic jacks. The jacks were attached to a reaction system that consisted of a steel frame that was secured horizontally in place by reacting against the south edge of the operations deck when it was pushed by the jacks, as shown in Figure 3.7. The other ends of the jacks pushed against the W12x252 cross beam, as shown in Figure 3.7 and Figure 3.9, which could slide along an inclined surface that had an 11-degree angle, which was the critical loading direction. The system was completed by a 2-½-inch diameter steel rope that wrapped around the bollard under the bollard horns and was attached to the cross beam with spelter sockets. The rope exerted load onto the bollard as the cross beam was pushed by the jacks. The apparatus extended out over the edge of the modular pier, as seen in Figure 3.7. The concrete in the area of

interest was painted white with a brittle primer to aid in the identification of crack location and size. The test setup was designed for a test load of 400 kips with a factor of safety of 2.

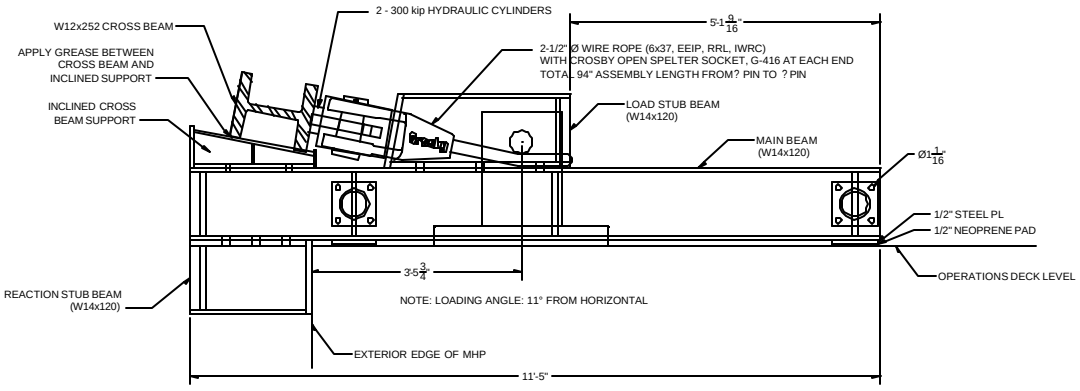

Figure 3.7 - Setup for Bollard Test - Elevation View

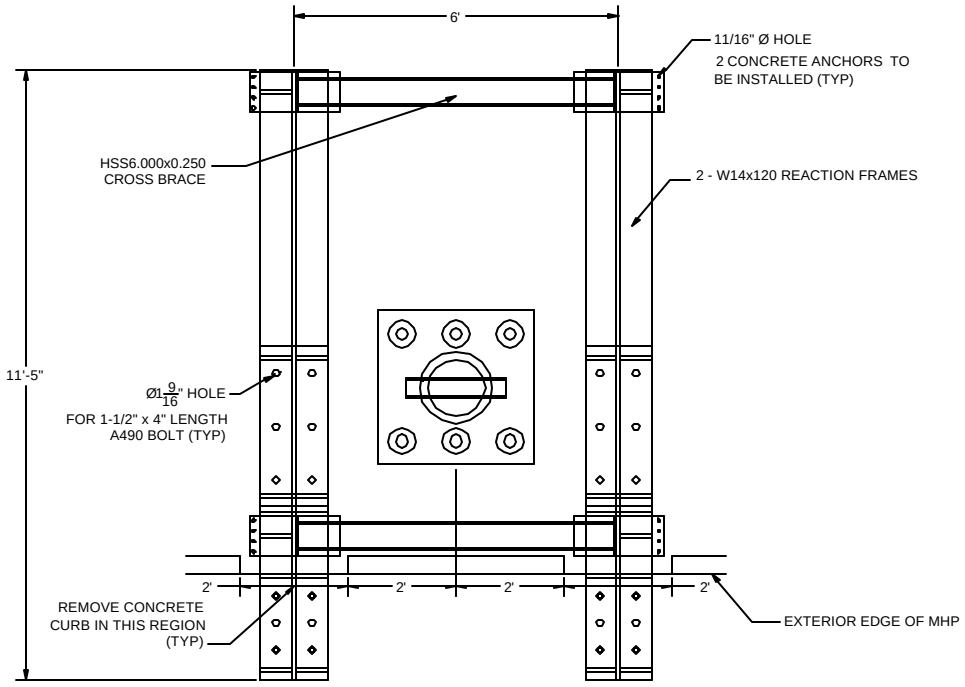

Figure 3.8 - Setup for Bollard Test - Plan View

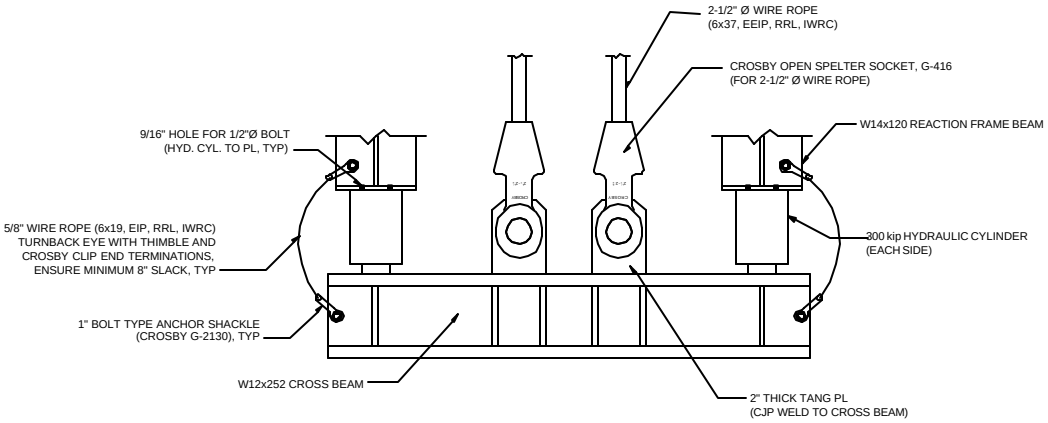

Figure 3.9 - Setup for Bollard Test - Cross Beam Assembly

3.3.2 Instrumentation Scheme

The instrumentation scheme developed and used for the test is shown in Figure 3.10 through Figure 3.12. The scheme was confirmed by the pre-test analyses to be adequate for capturing the key behavior of the bollard system. Four types of sensors were installed: displacement transducers to measure the deflections of the deck and the bollard, strain gages to measure concrete deformation and the strains in the bollard and anchor bolts, inclinometers to record the tilting of the bollard, and pressure transducers to monitor the hydraulic pressure in the jacks. The strains in the north-south direction were measured on the top and the bottom of the operations deck by gages SC-01 through SC-31. Deflections of the operations deck were measured with respect to the service deck by transducers DT-01 through DT-16. Transducers DT-17 and DT-19 measured the possible separation of the operations deck from the supporting beam above the window opening. The displacement of the bollard was measured with respect to a point on the operations deck that was more than 25 ft. away from the south

edge of the deck. Photographs of the instrumentation and setup are shown in Figure 3.13. The strain in each bolt was measured by gages embedded right below the bolt head. Additionally, a camera system with remote control was used to observe the condition of the concrete and to watch for cracking. During the test, the following information was monitored and displayed in real-time with the top displacement of the bollard and the strains in the concrete adjacent to the bollard plotted against the applied load.

1. Applied load.
2. Horizontal displacements of the bollard at top and the base.
3. Base plate uplift.
4. Tilt angle of the bollard.
5. Strains around the bollard right above base plate.
6. Strains in the anchor bolts.
7. Strains at the top and bottom surfaces of the deck at selected locations.
8. Vertical deflections of the deck at selected locations.
9. Concrete crack pattern in the deck during and after loading.
10. Video cameras for observing cracks and damage above and beneath the operations deck.

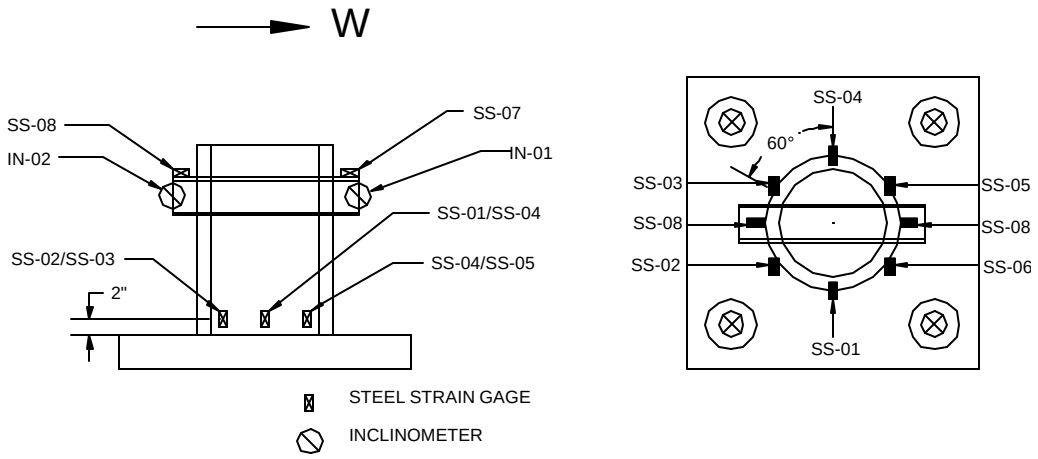

Figure 3.10 - Bollard Instrumentation Plan - Bollard Elevation and Plan Views

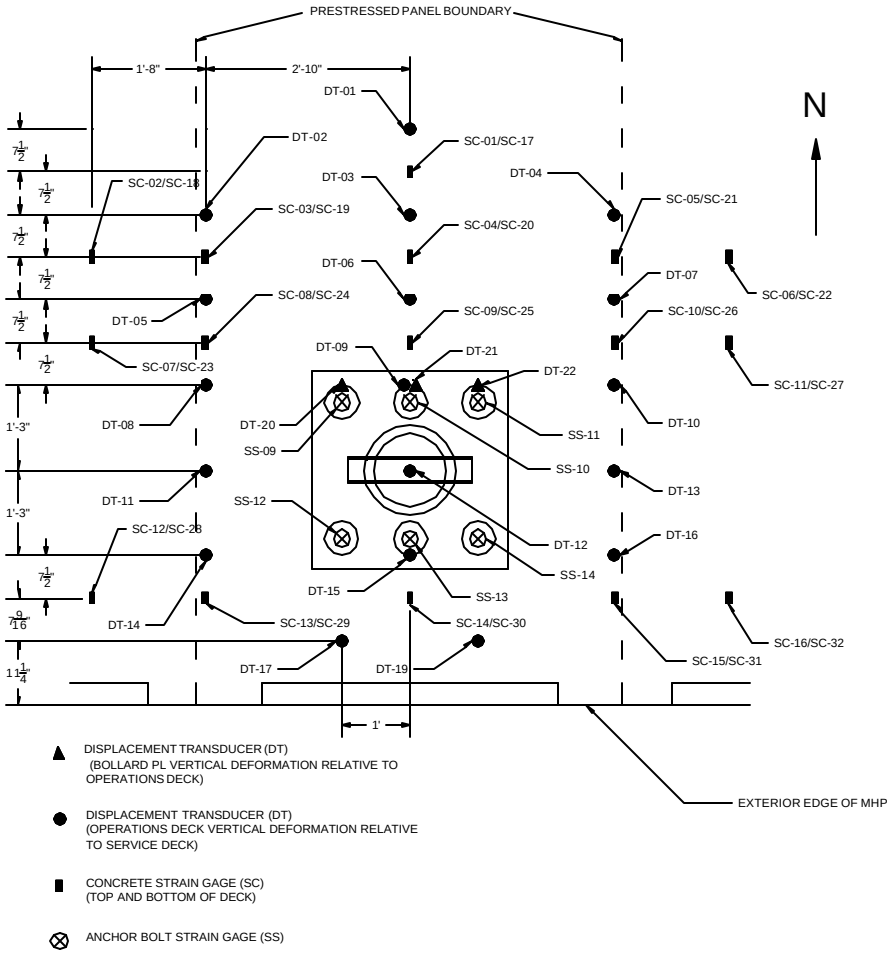

Figure 3.11 - Deck and Bollard Instrumentation Plan - Plan View

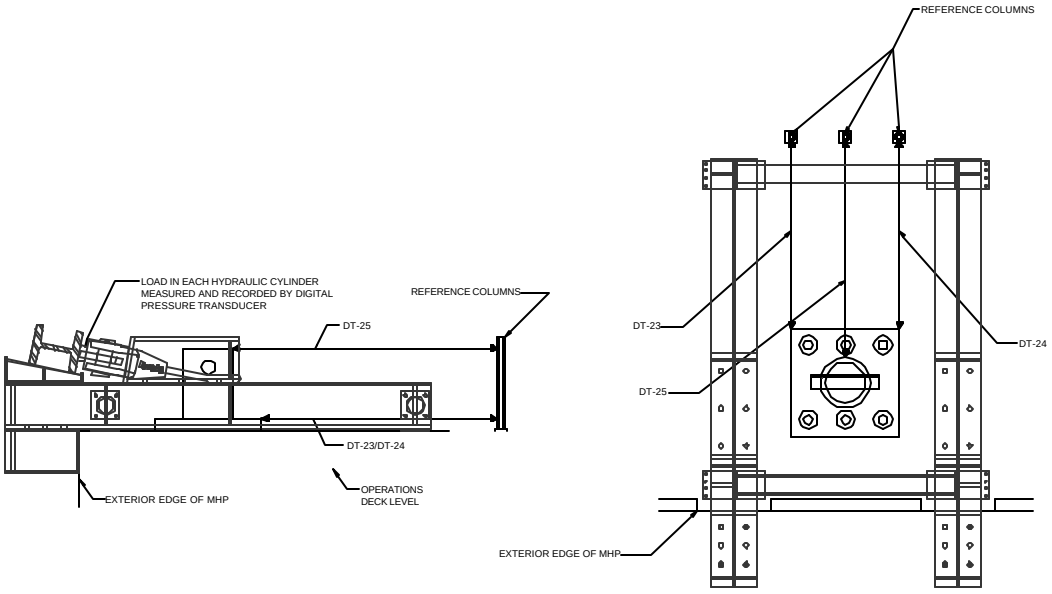

Figure 3.12 - Measurement of Bollard Horizontal Displacements

(a) Looking up from the Service Deck

(b) Wire Rope in Spelter Socket Around Bollard

(c) Cross-Beam and Hydraulic Jacks at 11°

Figure 3.13 - Bollard Test Instrumentation Photos

3.3.3 Loading Protocol

The objective of the test was to see if the bollard is able to resist the maximum service load of 200 kips and assess its reserve capacity. The failure of the bollard was expected to be dominated by the tensile fracture of the weld at the base plate. Based on the finite element analysis, this may occur at a load of 560 kips. The loading protocol was designed to verify that the bollard meets the design requirement with a factor of safety of two. The bollard was subjected to a load that had a vertical angle of 11 degrees, which would result in the minimum load to induce weld fracture.

On the day before the test, the bollard was loaded to 100 kips to validate the test setup. A small horizontal displacement of the bollard occurred. On the day of the test, load testing of the bollard began at 11:00 am. The loading history applied is plotted in Figure 3.14. The load was gradually increased to 200 kips over the next three minutes. This load level was held for 16 minutes. The load was then gradually lowered to 30 kips at approximately the same rate. The load was then cycled between 30 and 200 kips four more times with each cycle taking approximately three minutes. The bollard was then fully unloaded and the service load portion of the test concluded at 12:02 pm.

At 1:57 pm, loading started again to bring the load to 400 kips. When the load reached about 275 kips, a sudden load drop of 40 kips occurred. This was accompanied by a loud noise. After this, the load was almost immediately brought back to 280 kips and was maintained at 280 kips for four minutes. The bollard was then unloaded to 30 kips. The bollard and the testing apparatus were inspected and it

was determined that there was no discernable damage. At 2:29 pm, the bollard was loaded to a maximum load of 410 kips and the load was held for two minutes. The load was then reduced to 200 kips and held for an additional ten minutes for observation. No damage of any sort was observed. The bollard was then unloaded to 30 kips and the load was cycled between 30 and 400 kips twice. The bollard was finally unloaded at 2:56 pm.

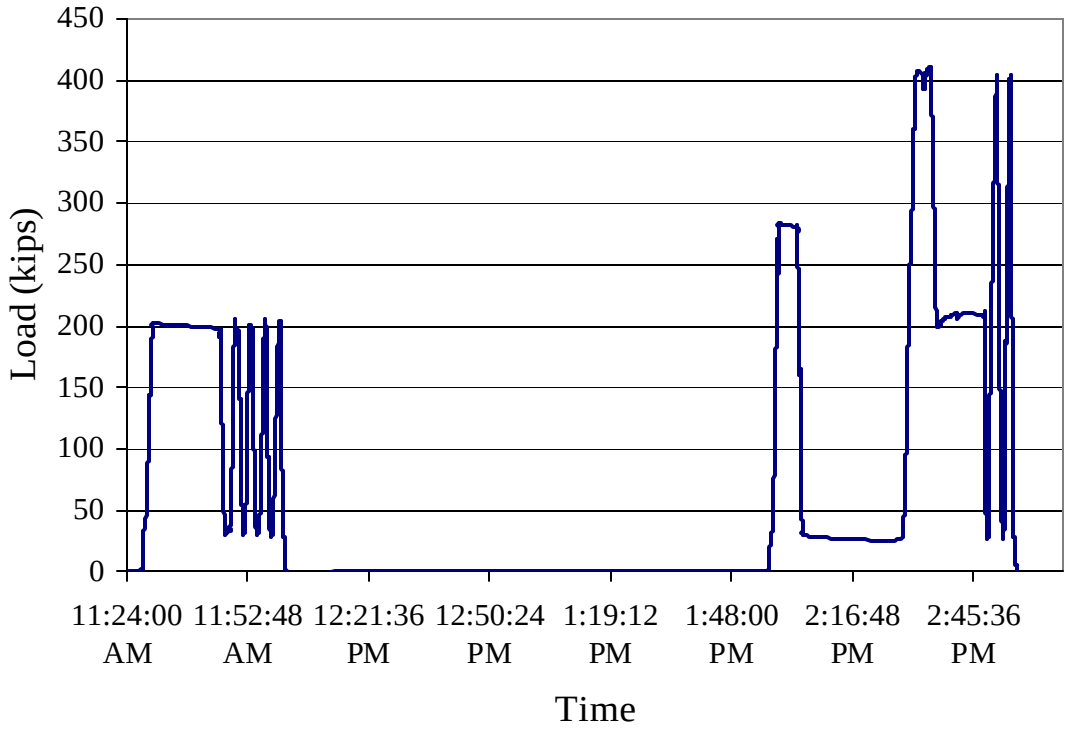

Figure 3.14 - Loading History

3.4 Experimental Results

3.4.1 Observed Performance

The bollard slipped south during both the preliminary equipment checking test conducted on the day before and the bollard capacity test. Additionally, there was a loud noise heard at about 275-kip load during the test. This was most likely caused by some slip in a bolted connection in the testing apparatus. The time lapse video taken during the test clearly shows that the bollard base was sliding back and forth with the loading and unloading cycles as shown by the slip marks due to paint scraping in Figure 3.15. This behavior is due to the tilting and untilting of the anchor bolts against the bolt holes during the load cycles. There were no visible effects of the bollard loading on the operations deck.

Figure 3.15 - Photograph of Slip Marks of the Bollard

3.4.2 Recorded Performance

The overall bollard behavior recorded during the test is a combination of the deformation of the bollard, the deformation of the deck, and the relative motion between the two. A sudden load drop of 40 kips accompanied by a loud noise was observed at about 275 kips. The exact cause of this is not known. It could be due to some slip occurring in a bolted connection of the steel reaction frame. After this, the bollard was reloaded to 280 kips and held at that load level for four minutes. During this period, the west side of the base plate slipped further. The data recorded from the bollard and the deck are presented below.

Bollard Behavior

There were 8 strain gages on the bollard itself, one on the top of each horn and six around the circumference near the base of the bollard (see Figure 3.10). The strain gages were installed on the top of the horns and the compressive strains induced by the steel rope are shown in Figure 3.16. The strains in the two horns were different due to the positioning of the steel rope below. The strains close to the base of the bollard are plotted against the load in Figure 3.17 and they exhibit a linear relation with respect to the applied load. The gage locations are shown in Figure 3.10. The maximum strains reached are way below the yield level as expected from the pre-test analyses. The strains in the bolts are plotted in Figure 3.18. All the bolts were in tension. The strain gage in the southeast bolt did not function correctly and the strain is, therefore, not shown here. Figure 3.18 shows that the northeast bolt started to exhibit a nonlinear

load-strain relation at about a 300-kip load while the other two bolts behaved more or less in a linear fashion. The northeast bolt developed a much larger strain than the northwest bolt during loading and a residual strain upon unloading. However, the maximum strain developed in the northeast bolt is still way below the expected yield strain of 0.003. The exact cause of this is not known. It could be due to the malfunctioning of the strain gage. The strain developed in the northwest bolt is consistent with that obtained in the pre-test finite element analysis, which has indicated that the bolt will yield at a load of 965 kips.

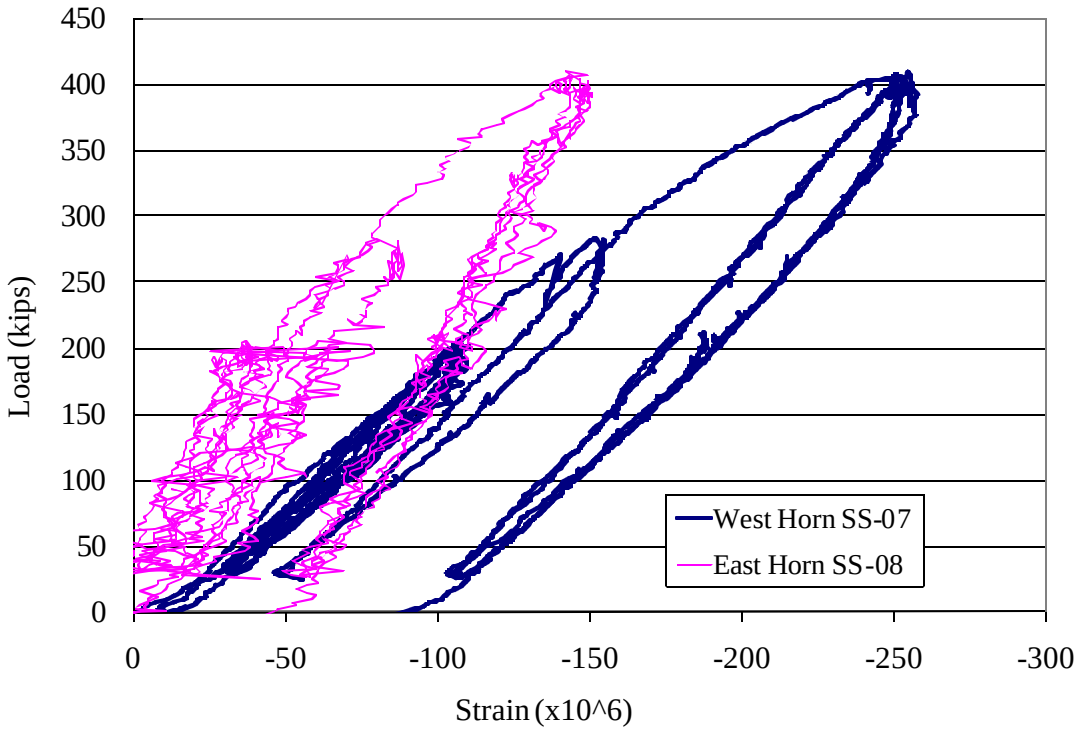

Figure 3.16 - Strains in Bollard Horns

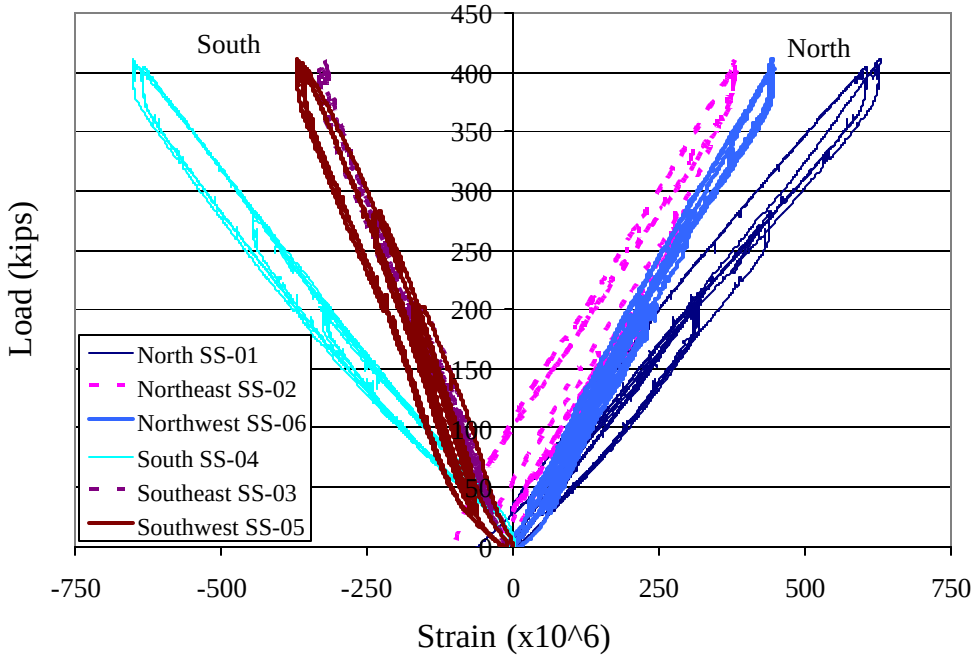

Figure 3.17 - Strains Near the Bollard Base

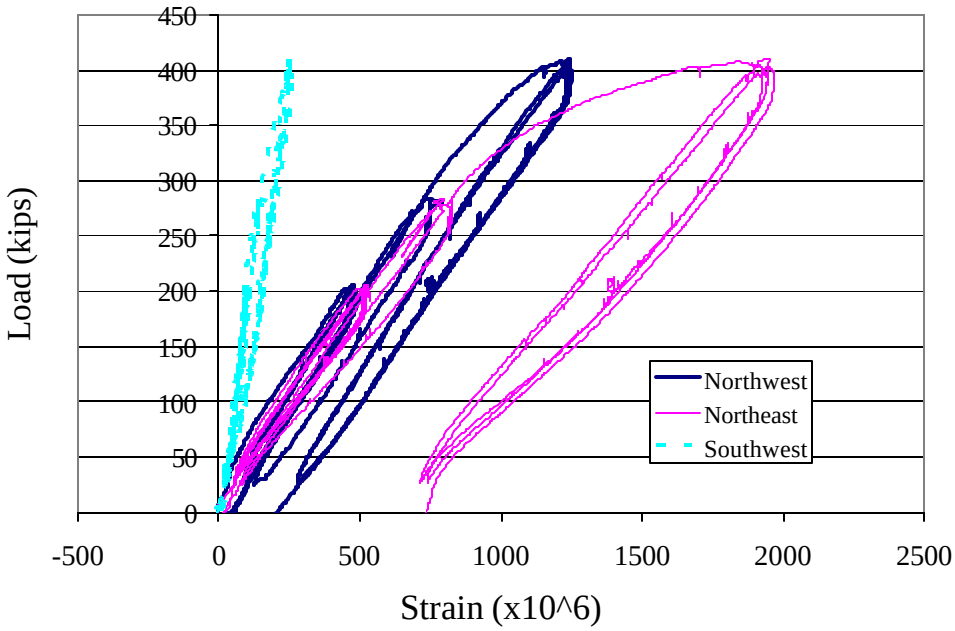

Figure 3.18 - Strains in the Bolts

Figure 3.19 shows the horizontal displacements of the bollard with respect to a fixed reference point on the operations deck that was far away from the bollard. The

transducer locations are shown in Figure 3.12. It can be observed that the west side of the base plate slipped more than the east, especially when the load was held at 280 kips for four minutes. The displacement at the top of the bollard was a combination of the slipping and tilting of the base plate, and the deformations of the bollard and the deck. The additional slippage of about 3/8 in. that occurred during the preliminary equipment checking test is not shown here. The vertical displacement (uplift) of the north edge of the base plate is plotted in Figure 3.20. The vertical displacements on the northeast and northwest sides are about the same. This indicates that the strains in the two north-side bolts should not differ significantly. However, the uplift response shown is slightly nonlinear and is a lot higher that that expected from the bolt elongation shown in Figure 3.18.

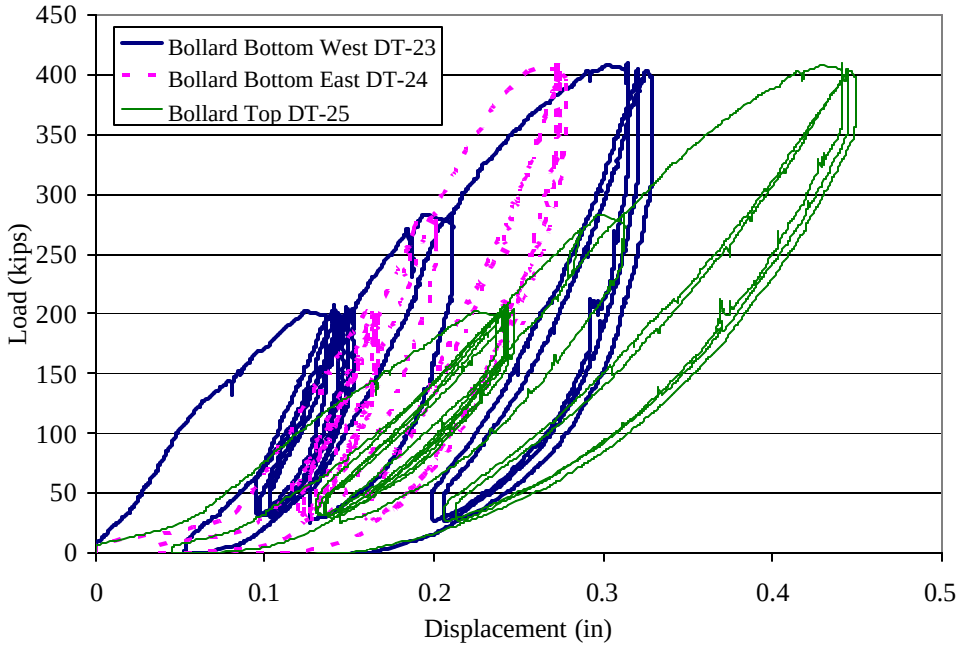

Figure 3.19 - Horizontal Displacements of Bollard

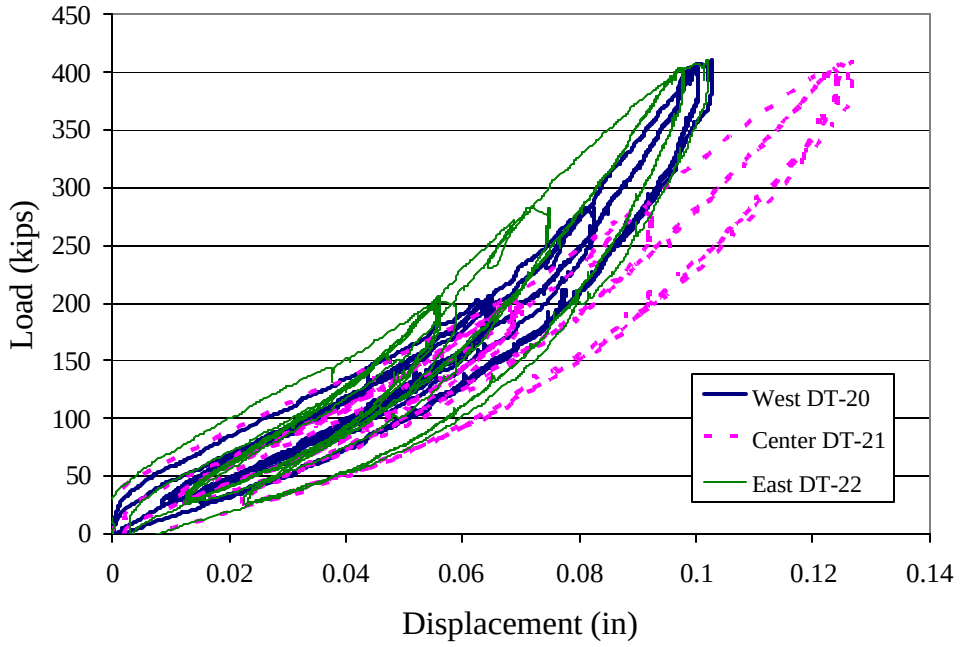

Figure 3.20 - Uplift of the Base Plate

Deck Behavior

Figure 3.21 illustrates the reference lines along which the deflections and strains in the deck are plotted here. The deflection of the deck was measured with respect to reference positions on the service deck, which could be practically considered as fixed as shown by the finite element analysis. A positive reading from a displacement transducer, shown as a circle in Figure 3.21, indicates an upward displacement of the operations deck. The strain gages, shown as rectangles in the figure, were placed at the top and the bottom of the deck, with the lower numbers representing those on top of the deck. Figure 3.22 plots the load against the displacements measured by the transducers installed along line B as shown in Figure 3.21, except for transducer DT-06, which did not function properly. One can observe some hysteretic behavior and residual displacements after unloading. It is believed that

part of the residual displacements could be related to the resolution of the measurement devices as the displacements being measured are extremely small.

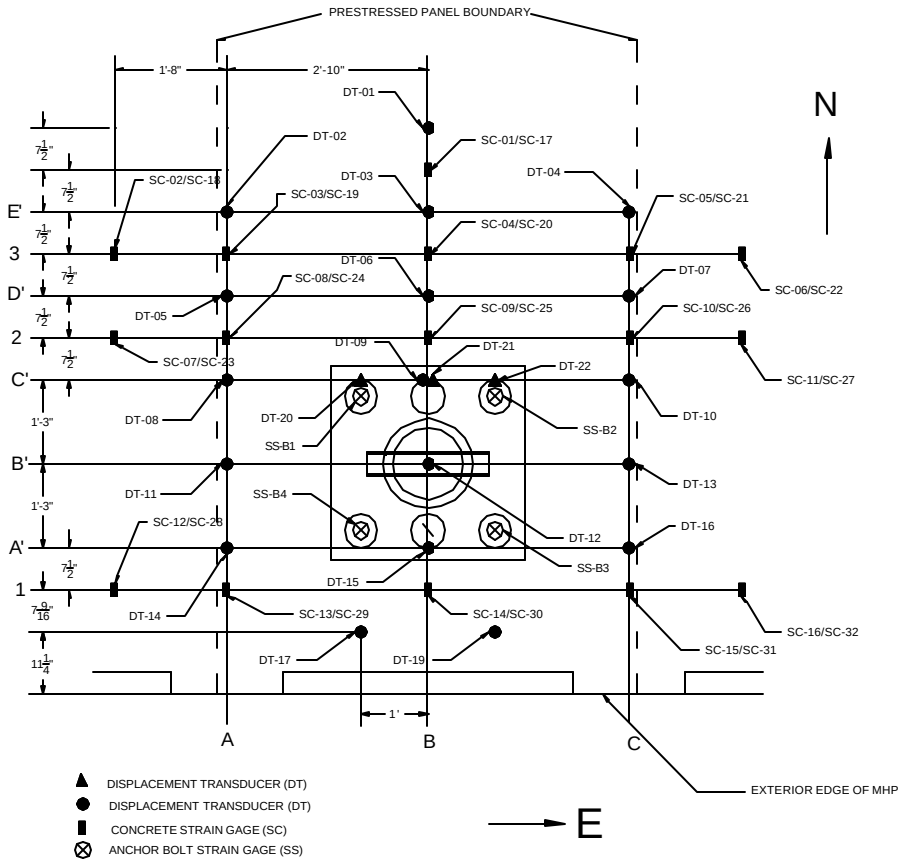

Figure 3.21 - Deck Instrumentation and Reference Lines

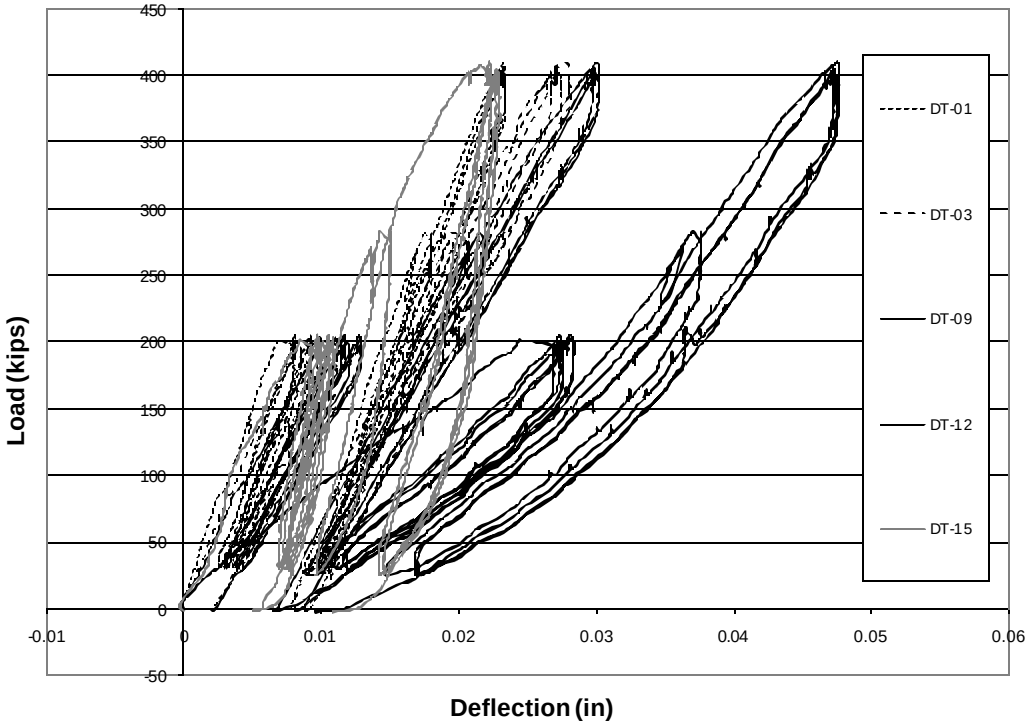

Figure 3.22 - Load-vs.-Deck Deflection Curves

Figure 3.23 plots the maximum deflections along the three north-south lines shown as A, B and C in Figure 3.21 under 200 and 400-kip loads. The deflected shapes are consistent with the prying action of the loaded bollard and the direction of the applied load. It is clear that the whole bollard moved upward. However, the readings from transducer DT-09 seem to be a bit large as compared to those of the other transducers leading to curvatures that are difficult to explain. Deflections along lines A' through E' in the east-west direction are plotted in Figure 3.24 and Figure 3.25. Displacement transducer DT-06, at the intersection of lines D' and B, did not function properly and its reading is, therefore, not shown here. The uplift of the prestressed plank from the supporting beam is shown in Figure 3.26. It was measured

by displacement transducers DT-17 and DT-19. These displacement transducers measured the relative displacement between the top of the beam and the bottom of the operations deck along the north side of the beam.

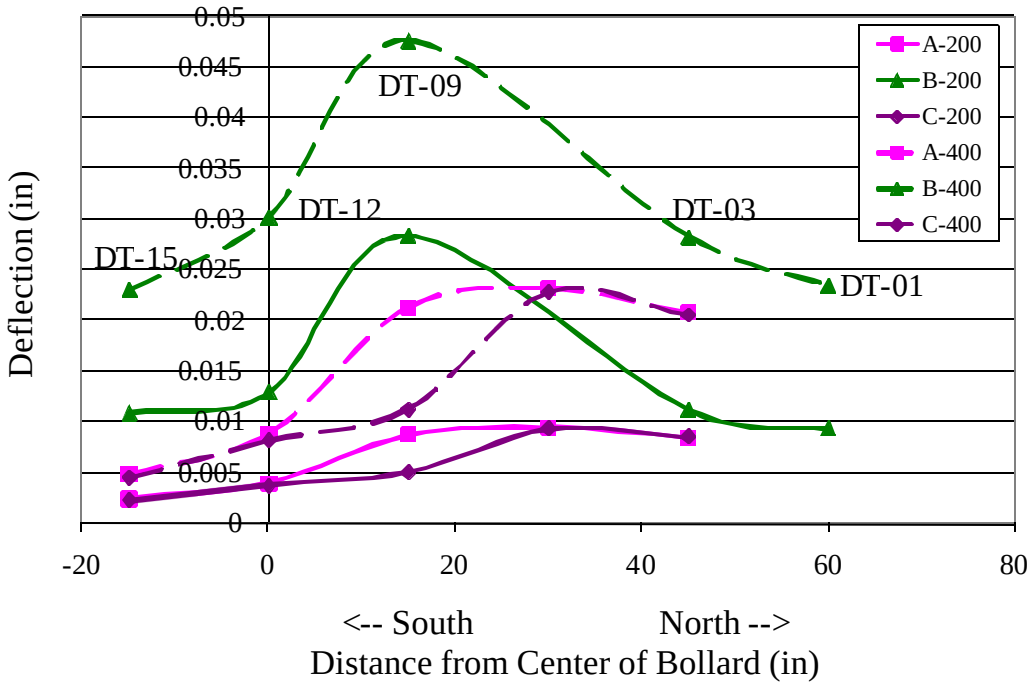

Figure 3.23 - Deflections of Deck Along North-South Lines (A, B, & C) at 200 and 400-Kip Loads

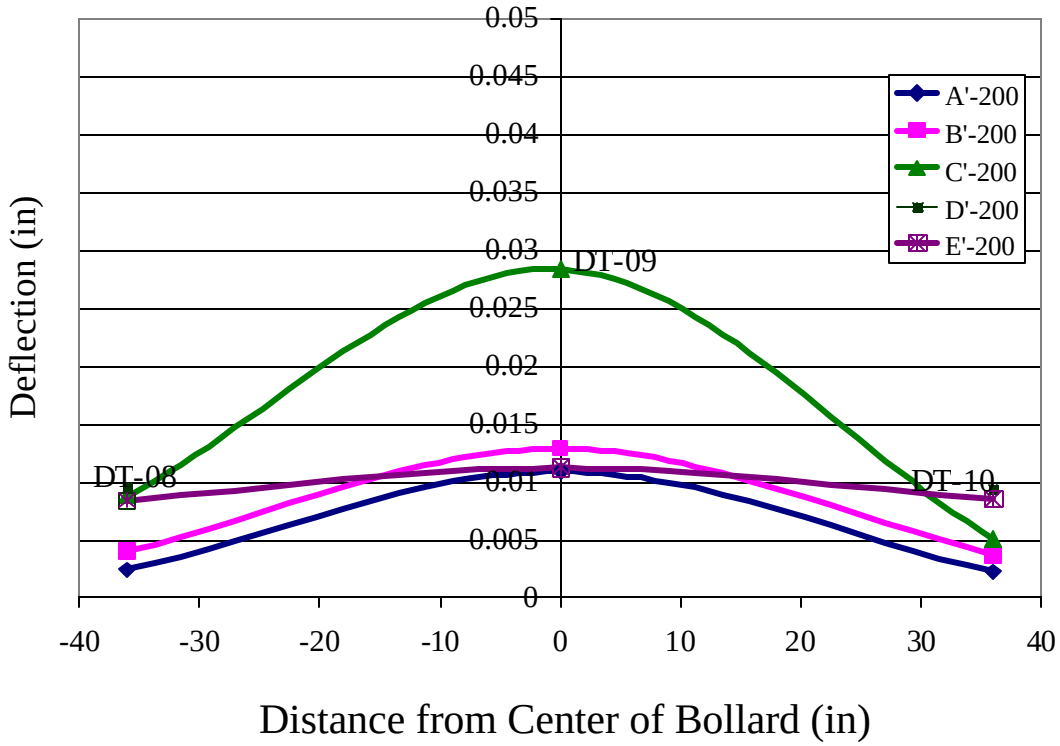

Figure 3.24 - Deflections of Deck at 200 Kips Along East-West Lines (A'-E')

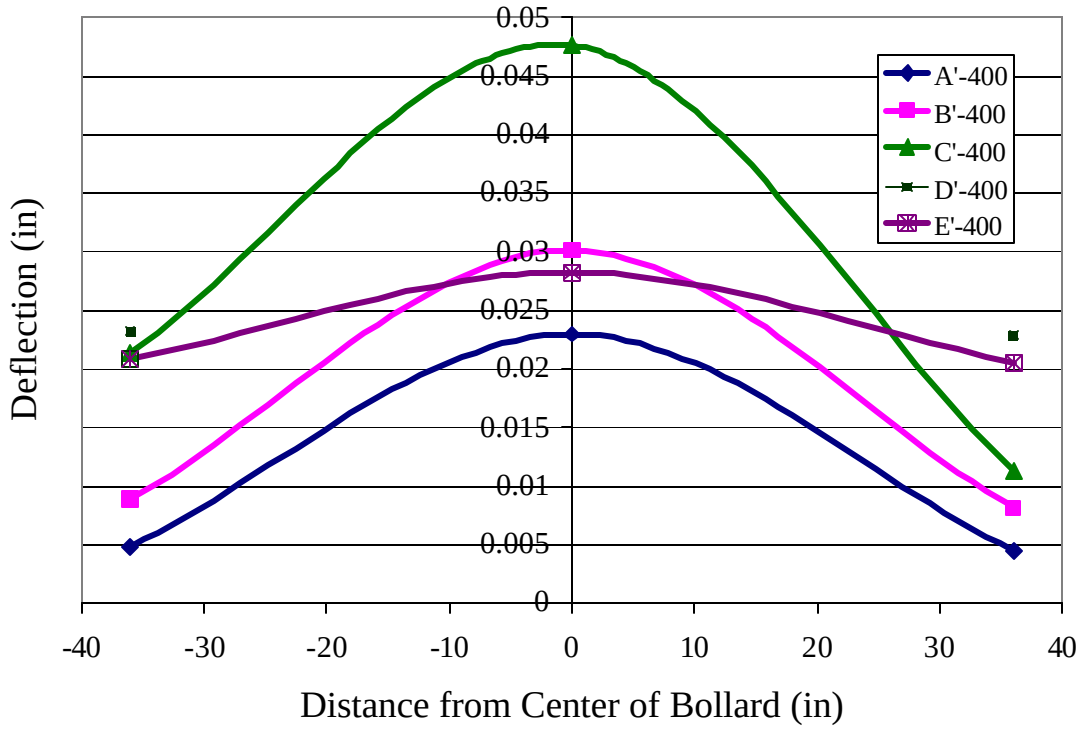

Figure 3.25 - Deflections of Deck at 400 Kips Along East-West Lines (A'-E')

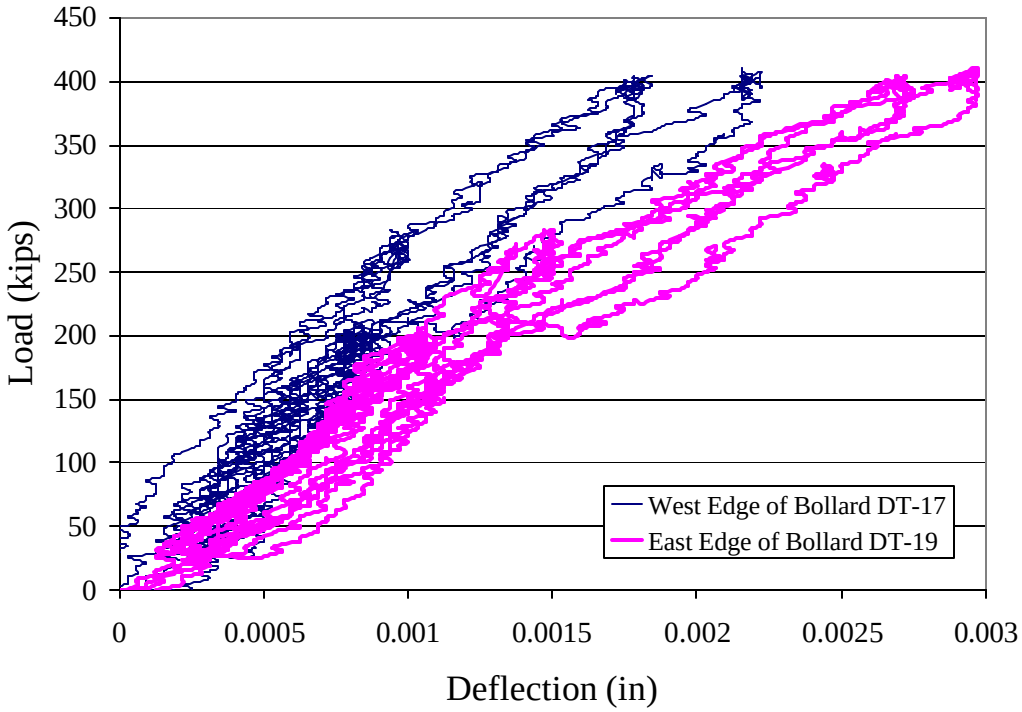

Figure 3.26 - Uplift of Pre-stressed Plank
(measured at beam-deck interface)

The strains in the deck are examined next. Figure 3.27 and Figure 3.28 plot the load against the strains immediately adjacent to the bollard (along lines 1 and 2, respectively, as shown in Figure 3.21). Figure 3.27 shows large tensile strains at the bottom of the deck on the southeast and southwest sides. The strains measured more than thirty inches north of the bollard are very low (all below 100 microstrain). They are illustrated in Figure 3.29. Figure 3.30 and Figure 3.31 plot the strains measured by the gages along lines 1, 2, and 3 against the distance from the center of the bollard. It is interesting to note in the figures that the concrete strains on the extreme east and west sides of the bollard were very low. These locations were in the adjacent precast planks (see Figure 3.11 and Figure 3.13). Figure 3.30 and Figure 3.31 also show that along line 1, the strains right at the east and west sides of the bollard are larger than those at the center, with the tensile strains at the bottom much larger than the compressive strains at the top.

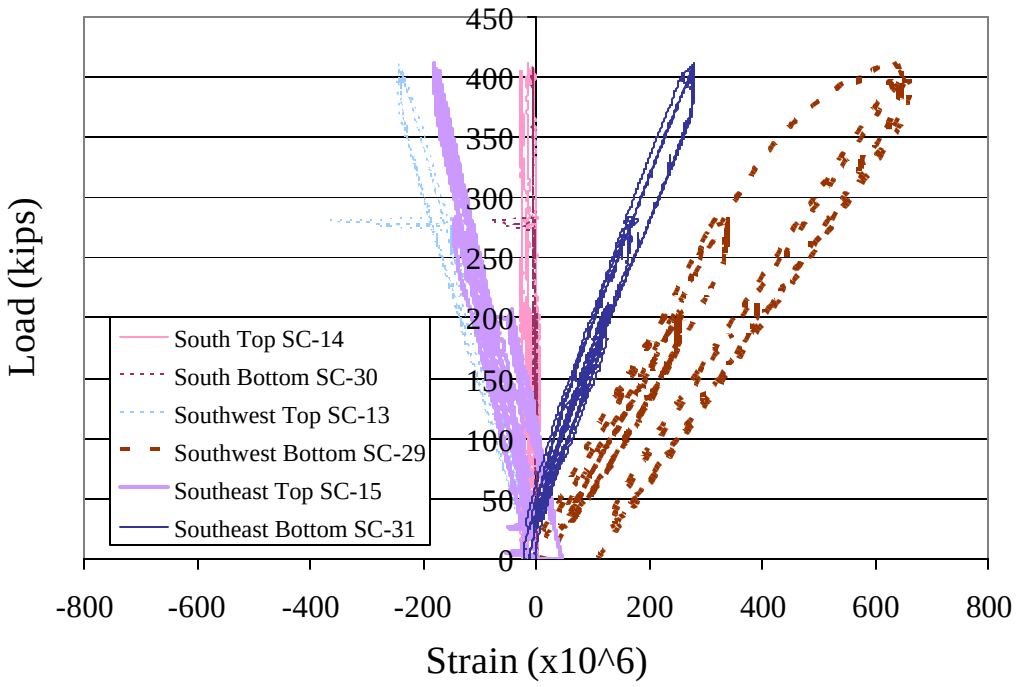

Figure 3.27 - Concrete Strains Immediately South of Bollard (along line 1)

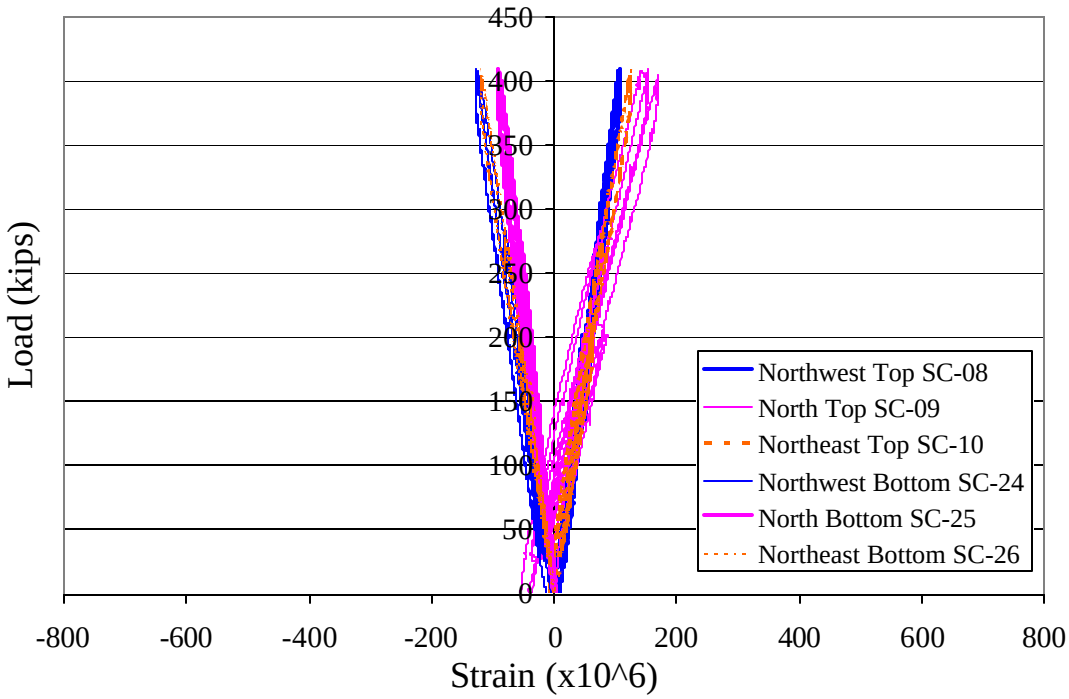

Figure 3.28 - Concrete Strains Immediately North of Bollard (along line 2)

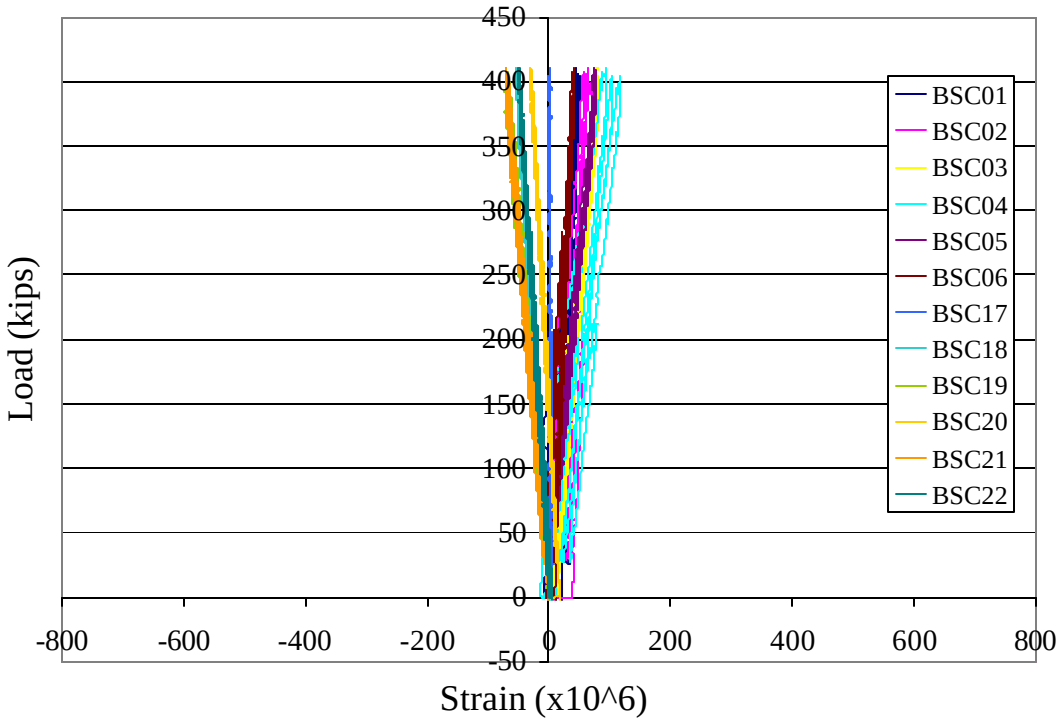

Figure 3.29 - Strains at More Than 30 Inches North of Bollard (along line 3)

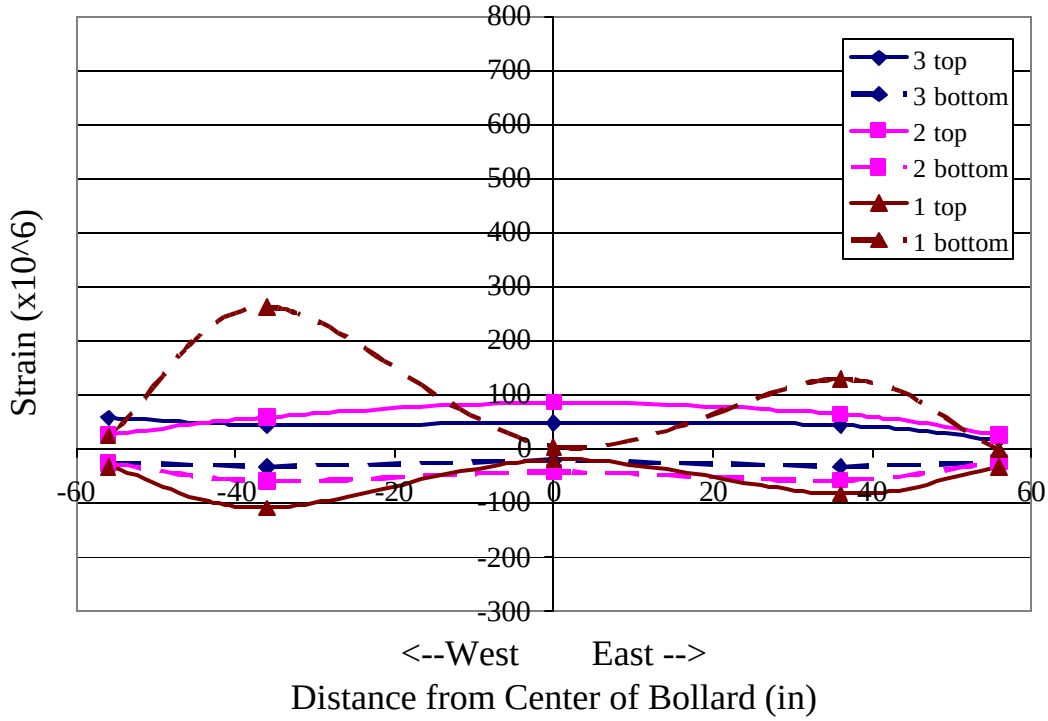

Figure 3.30 - Strains Measured at 200-Kip Load (Along lines 1, 2, & 3)

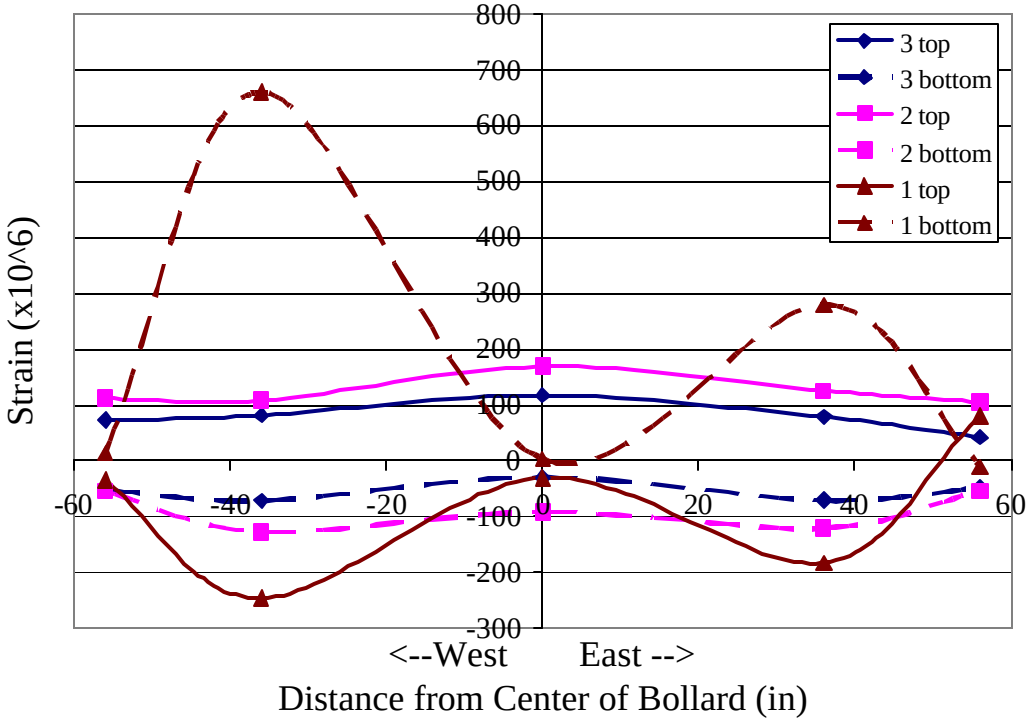

Figure 3.31 - Strains Measured at 400-Kip Load (Along lines 1, 2, & 3)

The difference in the strains at the top and the bottom of the deck can be caused by two factors. One is the membrane force in the deck and the other is the concrete cracking at the gage locations. To examine the likely-hood of the first factor, the "membrane" strains are calculated by averaging the top and bottom strains measured at each location. They are plotted against distance in the east-west direction in Figure 3.32 and Figure 3.33. It can be observed that the strain values are, in general, very small except for one location along line 1. Along line 1, the west side right next to the bollard shows a very large tensile "membrane" strain. A large tensile membrane force in that location is, however, unlikely. Hence, this was most likely caused by the cracking of concrete at the bottom of the deck. The effective prestress in the precast planks is expected be low at the location of line 1 as it is in the stress transfer zone of the precast planks. The maximum tensile strain shown in Figure 3.31 would have way exceeded the cracking strain of concrete if there was no prestress.

Figure 3.34 and Figure 3.35 show the calculated "bending" strains in the deck along lines 1, 2, and 3 (east-west direction). They are the measured strains minus the membrane strains. Figure 3.36 and Figure 3.37 show the "bending" strains along lines A, B, and C (north-south direction). In general, the strains on the west side are higher than those on the east along line 1 and those on the south side of the bollard (along line 1) are larger than those on the north side (except along the center line of the bollard). Hence, line 1 is a critical bending section under the prying action of the bollard. This could be due to the prestress loss in the stress transfer zone of the precast planks, which makes the deck vulnerable to cracking and will also lead to a lower

moment capacity because of the lack of an embedment length. However, during the test, no cracks were observed with the video cameras.

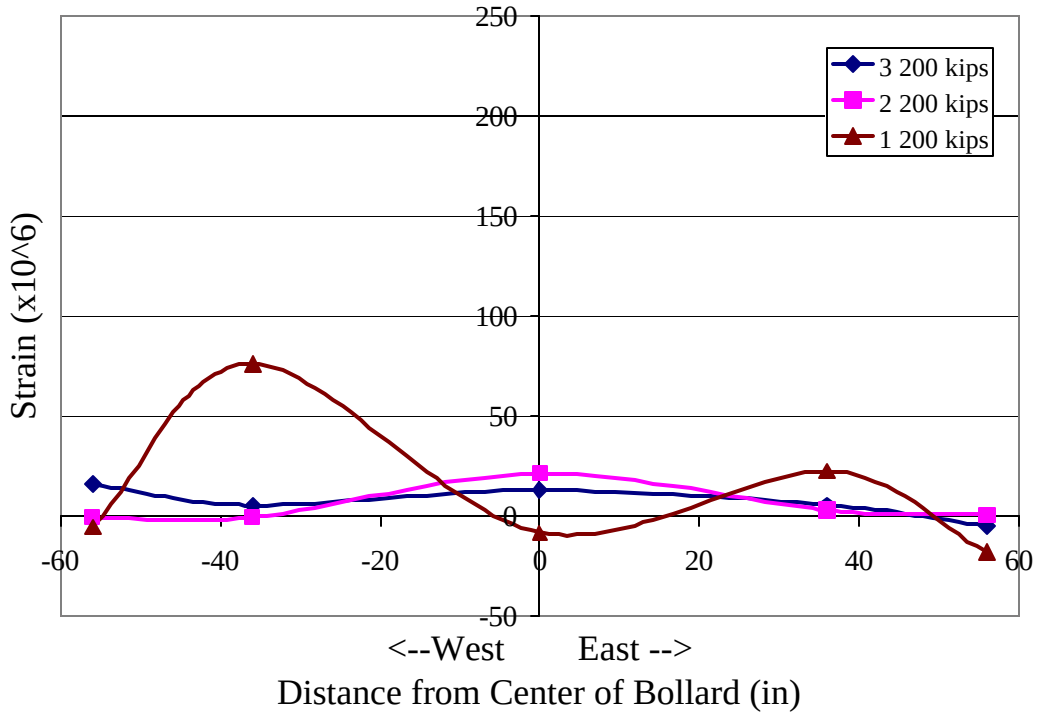

Figure 3.32 - Calculated Membrane Strains at 200-Kip Load (Along lines 1, 2, & 3)

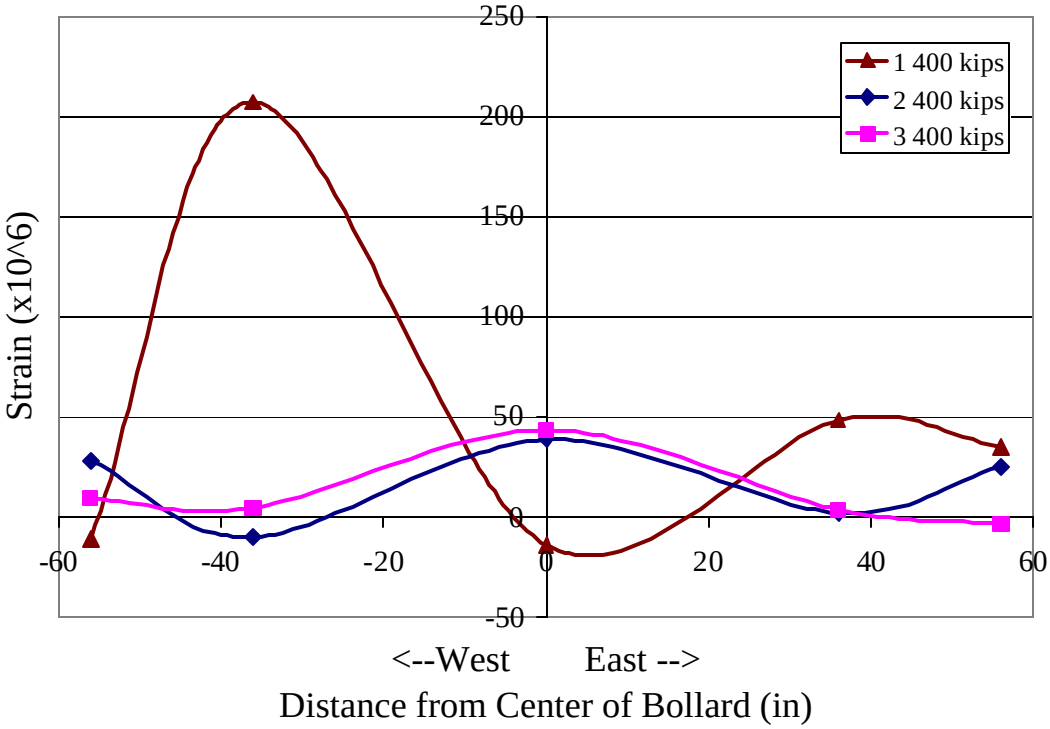

Figure 3.33 - Calculated Membrane Strains at 400-Kip Load (Along lines 1, 2, & 3)

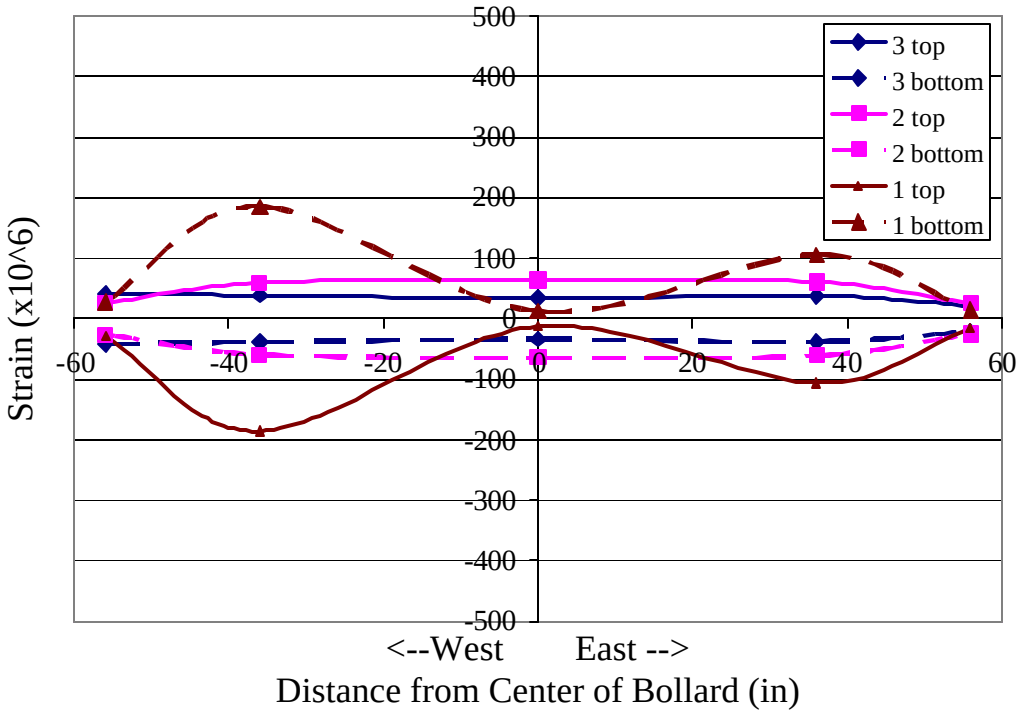

Figure 3.34 - Calculated Bending Strains at 200-Kip Load (Along lines 1, 2, & 3)

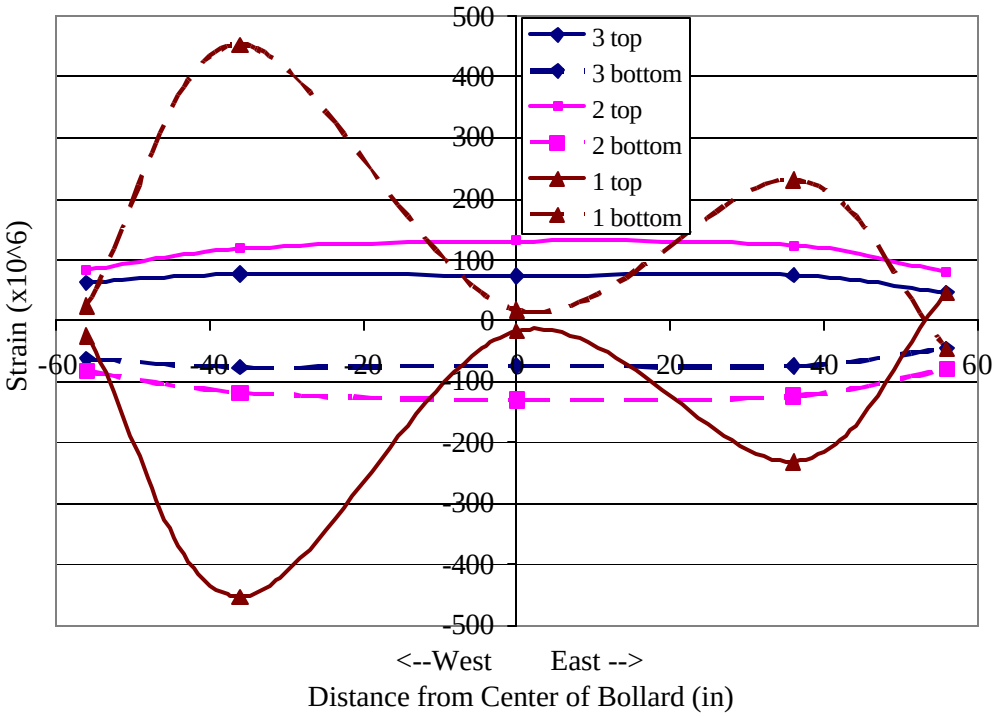

Figure 3.35 - Calculated Bending Strains at 400-Kip Load (Along lines 1, 2, & 3)

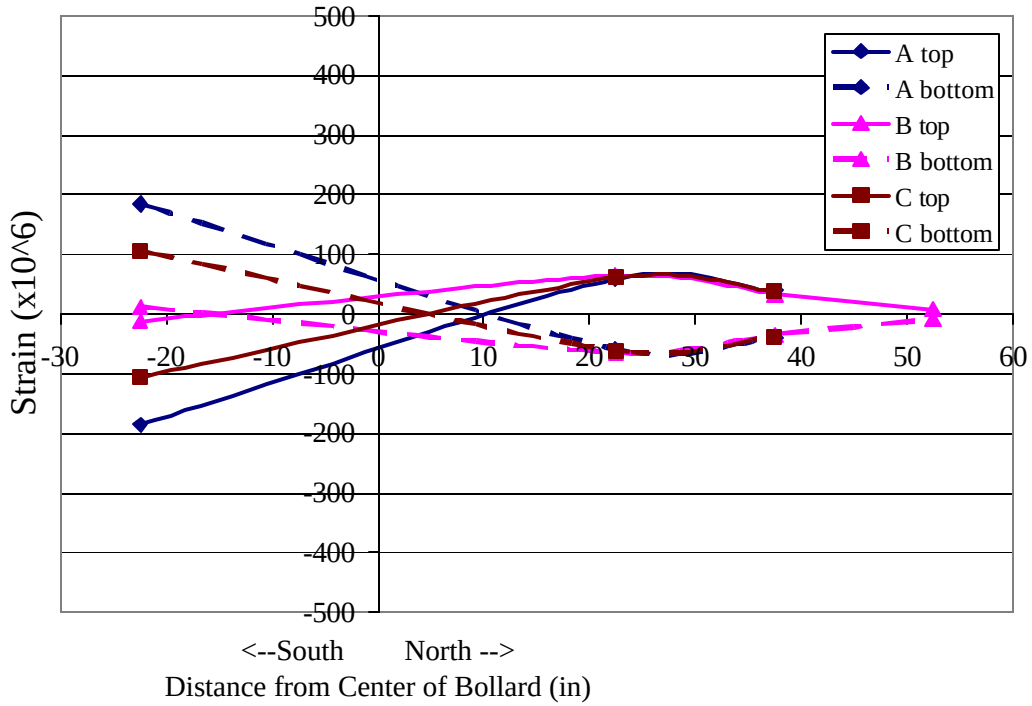

Figure 3.36 - Calculated Bending Strains at 200-Kip Load (Along lines A, B, & C)

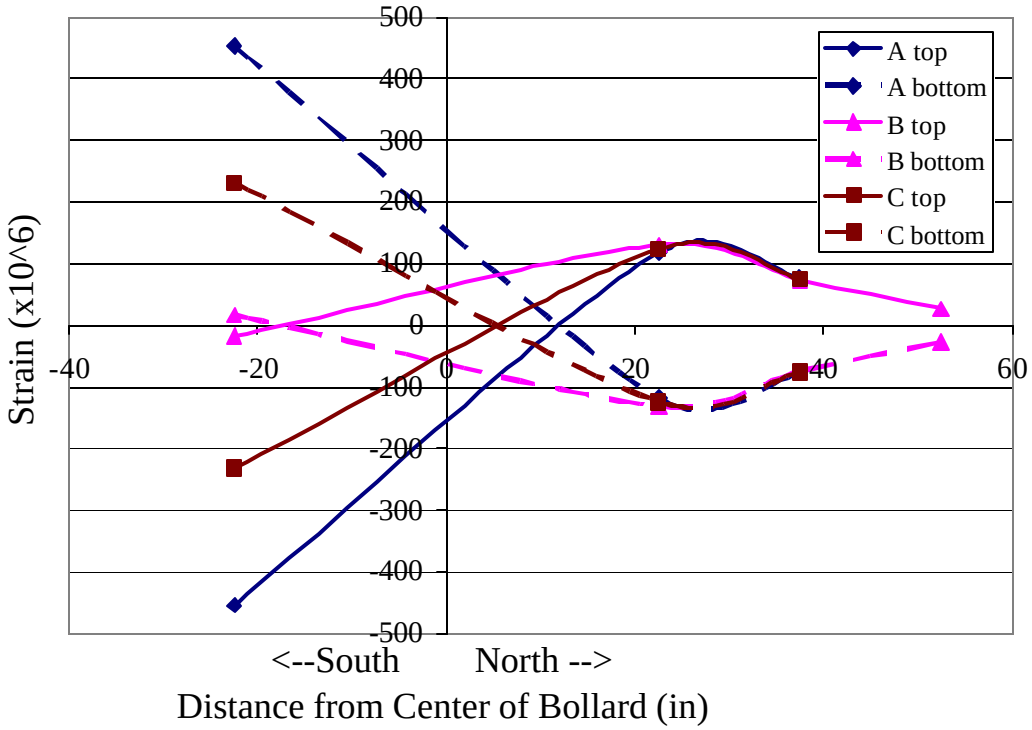

Figure 3.37 - Calculated Bending Strains at 400-Kip Load (Along lines A, B, & C

4 Nonlinear Analysis

4.1 Introduction

A multi-degree-of-freedom analytical model of the Modular Hybrid Pier (MHP) has been created to determine the effects of a seismic event on the structure and the fender system that restrains the MHP. The fluid-structure interaction, soil dynamics, soil-pile interaction, and the deformability of the MHP and the mooring shafts are not considered in this analysis.

The MHP can be built in multiple configurations. The number of modules, number of mooring shafts, and number of fenders can all be varied. The configuration modeled here is a four-module arrangement, as seen in the plan view of the MHP shown in Figure 4.1. Each module is 325-ft. x 88-ft. and the four modules together are 1300-ft. long. For the analysis presented here, the floating concrete structure is assumed to be a rigid block sliding on a frictionless base. There is one "moon pool" in each of the modules. This is a channel through the depth of a module, inside which

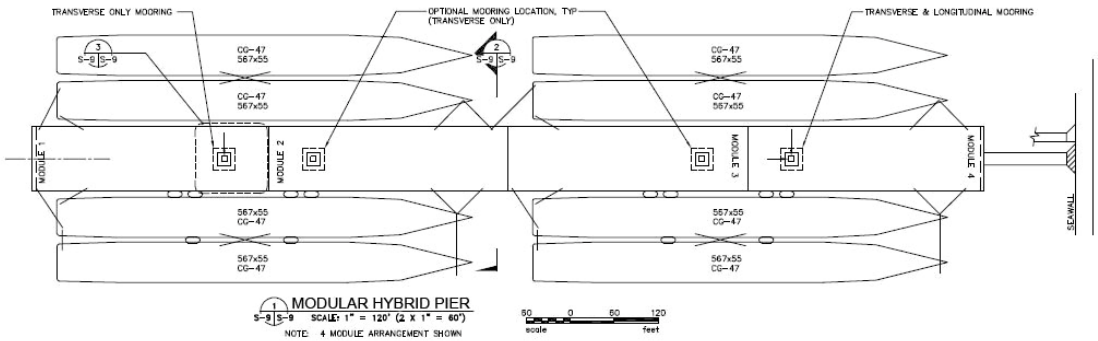

Figure 4.1 - Plan View of the Modular Hybrid Pier

the mooring shaft extends. The mooring shafts are attached to a pile cap at the sea floor. These mooring shafts are assumed to be rigid as well.

The weight of the MHP is estimated to be 68,000 kips. Each module is a reinforced concrete box structure with interior and exterior walls. The floating structure is restrained from moving by the mooring shafts. Each shaft has an appropriate number of fender elements in each direction. The fenders are attached to the MHP inside of the moon pool, but not attached to the mooring shaft. The motion of the structure is induced by the motions of the shafts as a result of earthquake ground motions introduced at the base of each shaft.

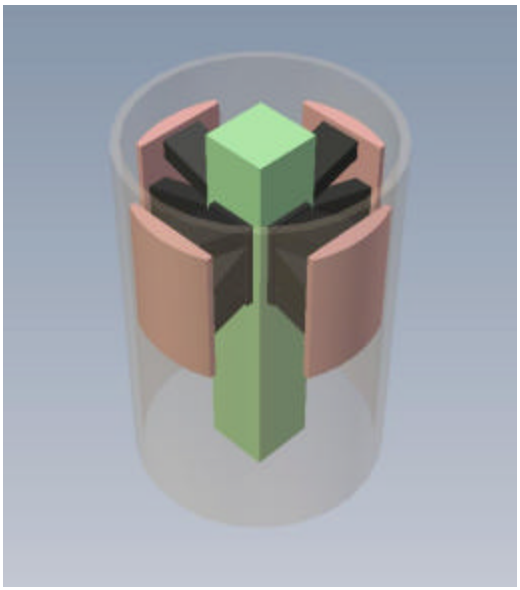

Figure 4.2 - Model of Moon Pool of MHP with Fender Groups

According to the current design, the MHP will be restrained by two pairs of mooring shafts (including the optional ones shown in Figure 4.1). Figure 4.2 shows a model of the moon pool with the mooring shaft and four fender assemblies. Each fender assembly consists of four fender elements attached to an ultra high molecular weight polyethylene (UHMW-PE) pad. Figure 4.3 shows a typical fender assembly with two fender elements.

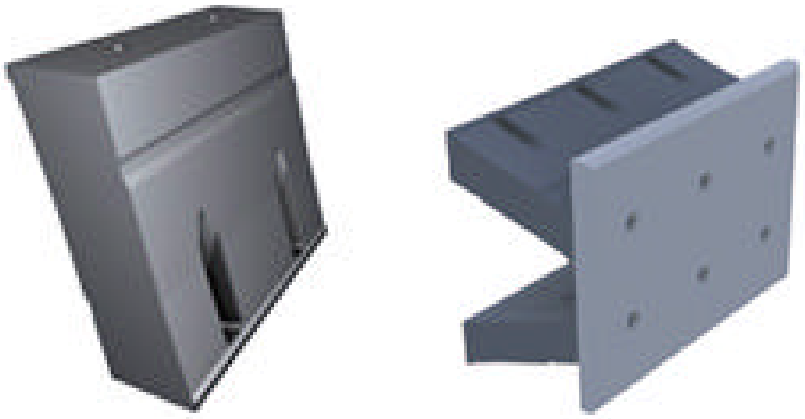

Figure 4.3 - Modular MV Fenders

Three of the four shafts shown in Figure 4.1 will have two fender assemblies on the opposite sides to restrain pier motion in the transverse direction, and one shaft at a far end will be surrounded by four fender assemblies to restrain both the longitudinal and transverse motions of the pier. Each fender assembly will have four fender elements to provide the necessary resistance and energy absorption capability in the axial direction and to limit fender deflection in the lateral direction.

Two different fender systems have been considered in this analysis. One is an initial proposal, which called for two MV1000x1000A and two MV1000x1200A

fender elements for each of the eight fender assemblies restraining the transverse motion, and four MV1000x900A fender elements for each of the two fender assemblies restraining the longitudinal motion. The second system, which is a revised design, calls for larger fenders that have more deflection capability. In this system, the configuration and number of fender assemblies are the same as before but each fender assembly consists of four MV1250x900A elements.

4.2 MHP Model

As shown in Figure 4.1, the moon pools are so located that two mooring shafts are close to each other. In the MHP model, each of these pairs has been idealized as one shaft. Each resulting shaft is located 325 ft. from each end of the 1300-ft. long MHP, and is centered transversely in the 88 ft. direction. The MHP is idealized as a rigid body with three degrees of freedom as shown in Figure 4.4. This is deemed satisfactory in view of the flexibility of the fender systems as compared to that of the

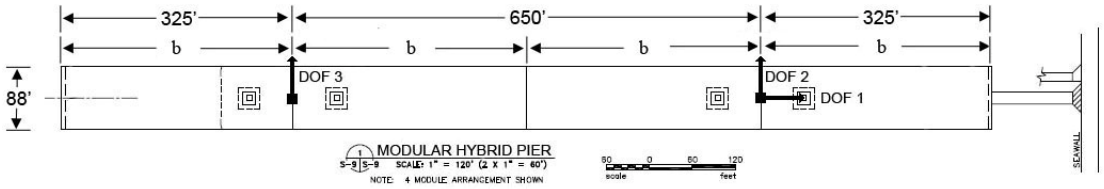

Figure 4.4 - 3-DOFs of MHP

concrete structure. However, this model can be easily extended to account for the flexibility of the concrete structure and the mooring shafts as needed.

With respect to the degrees of freedom shown in Figure 4.4, the equations of motion for the MHP can be expressed as follows:

$$\mathbf{M}\ddot{\mathbf{x}} + \mathbf{C}\dot{\mathbf{x}} + \mathbf{f}_F(\mathbf{x},\dot{\mathbf{x}}) = -\mathbf{M}\ddot{\mathbf{x}}_g \tag{4.1}$$

in which $\mathbf{x}$ is the relative displacement vector that contains the displacement of the MHP relative to that of the shaft at each degree of freedom, $\ddot{\mathbf{x}}_g$ is the vector of shaft accelerations, which in this model are identical to the earthquake ground accelerations used, and $\mathbf{f}_F(\mathbf{x},\dot{\mathbf{x}})$ represents the fender forces that are dependent on the displacements

and velocities of the pier relative to those of the fenders. Since the fenders are expected to provide relatively significant damping, damping from other sources is assumed to be insignificant and the damping matrix **C** is, therefore, assumed to be zero.

To calculate the inertial properties of the MHP, the contribution of the moment of inertia from the outside walls, inside walls, and decks in the individual modules is evaluated first. For simplicity, the center of mass of a module is assumed to coincide with the geometric centroid. According to the pier dimensions provided in the preliminary design drawings and the assumption that the lightweight concrete used for the pier has a unit weight (including the reinforcement) of 140 lbs/ft^3, the mass matrix of each module has been estimated with respect to the degrees of freedom shown in Figure 4.5.

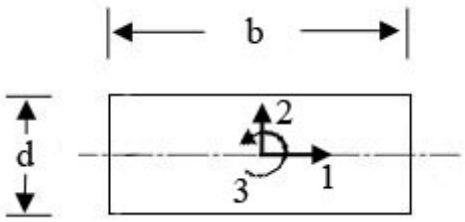

Figure 4.5 - DOFs of One Module

The moment of inertia of the deck of a module about its own centroid can been calculated as follows.

$$I_o = \frac{m(b^2 + d^2)}{12} \tag{4.2}$$

where m = the mass of the deck, b is the length of the module and d is the width of the module, as shown in Figure 4.5. The combined I_o of the two decks and the bottom slab has been found to be $3.376x10^7\,\text{kip}\cdot\text{in}\cdot\text{sec}^2$. The I_o of the outside walls about the centroid of a module has been found to be $1.465x10^7\,\text{kip}\cdot\text{in}\cdot\text{sec}^2$. The two interior walls are 20 ft-3 in from the center of a module. Their I_o about the centroid of the module has been found to be $1.296x10^7\,\text{kip}\cdot\text{in}\cdot\text{sec}^2$. The total $I_{o(Module)}$ of each module is the summation of all the contributions, which is $6.137x10^7\,\text{kip}\cdot\text{in}\cdot\text{sec}^2$, and the total mass $M_{(Module)}$ of a module is $44\,\text{kip}\cdot\text{sec}^2/\text{in}$.

The mass matrix with respect to the center of gravity of the four-module pier is assembled as follows.

$$\mathbf{M}_{COG} = \begin{bmatrix} 4M_{(Module)} & 0 & 0 \\ 0 & 4M_{(Module)} & 0 \\ 0 & 0 & 5b^2M_{(Module)} + 4I_{o(Module)} \end{bmatrix} \tag{4.3}$$

where b is the length of a module. In order to transform the coordinates with respect to the center of gravity to the coordinates shown in Figure 4.4, the following transformation matrix is used.

$$\mathbf{T} = \begin{bmatrix} 1 & 0 & 0 \\ 0 & 0.5 & 0.5 \\ 0 & \dfrac{-1}{2b} & \dfrac{1}{2b} \end{bmatrix} \tag{4.4}$$

Finally, the transformed mass matrix for the 3-DOF system shown in Figure 4.4 is calculated as follows.

$$\mathbf{M} = \mathbf{T}^T \bullet \mathbf{M}_{COG} \bullet \mathbf{T} \tag{4.5}$$

which gives

$$? = \begin{bmatrix} 176 & 0 & 0 \\ 0 & 103 & -15 \\ 0 & -15 & 103 \end{bmatrix} \quad \text{kips} \cdot \sec^2/\text{in.} \tag{4.6}$$

To avoid an iterative solution for the nonlinear system, an explicit time integration method developed by Newmark (1959) is used to evaluate the response of the MHP to earthquake excitations. The procedure is based on equations (4.7) through (4.9). Equation (4.7) is the time discretetized equations of motion, equation (4.8) is the change in displacement from one time step to the next, and equation (4.9) is the change in velocity over the same time step.

$$\mathbf{M}\ddot{\mathbf{x}}_{i+1} + \mathbf{C}\dot{\mathbf{x}}_{i+1} + \mathbf{f}_{F,i+1} = -\mathbf{M}\ddot{\mathbf{x}}_{g,i+1} \tag{4.7}$$

$$\mathbf{x}_{i+1} = \mathbf{x}_i + \Delta t \dot{\mathbf{x}}_i + \frac{\Delta t^2}{2} \ddot{\mathbf{x}}_i \tag{4.8}$$

$$\dot{\mathbf{x}}_{i+1} = \dot{\mathbf{x}}_i + \Delta t \left[(1-g)\ddot{\mathbf{x}}_i + g\ddot{\mathbf{x}}_{i+1} \right] \tag{4.9}$$

where Δt is the integration time step, ? is a parameter that defines the variation of the acceleration over the time step, and $\mathbf{f}_{F,i+1}$ is the vector of fender forces, which depend on the relative displacements between the MHP and the mooring shafts and their rate of variation. In this study, ? is selected to be 0.5, which results in zero numerical

damping. Substituting equation (4.9) into equation (4.7), and solving for the acceleration in the next time step results in equation (4.10).

$$\ddot{\mathbf{x}}_{i+1} = (\mathbf{M} + \Delta t g\,\mathbf{C})^{-1}\{-\mathbf{M}\ddot{\mathbf{x}}_{g,i+1} - \mathbf{f}_{\mathbf{F}}(\mathbf{x}_{i+1}, \dot{\mathbf{x}}_{i+1}) - \mathbf{C}\left[\dot{\mathbf{x}}_i + \Delta t(1-g)\ddot{\mathbf{x}}_i\right]\} \qquad (4.10)$$

To calculate the response in each time step, the new relative displacement at each of the three degrees of freedom is calculated with equation (4.8). The displacements are imposed on the fender models to calculate $\mathbf{f}_{F,i+1}$. As will be presented later, the fenders are modeled as dynamic systems that have natural frequencies much higher than those of the MHP system. Hence, to calculate the response of a fender to the imposed $\mathbf{x}_{i+1}$, the equations of motion for a fender need to be solved with time steps much smaller than Δt. To this end, a subincrementation approach is used and the displacement change within Δt is divided into subincrements by linear interpolation. Once $\mathbf{f}_{F,i+1}$ has been computed, the accelerations of the MHP for this step are then calculated with equation (4.10). Finally, the velocities of the structure are found with equation (4.9). The analysis then moves to the next time step and the process is repeated.

4.3 Fender Model

A Kelvin-Voight rheological model with an elastic spring element and a nonlinear viscous damper element has been developed to model the behavior of a fender element. Each fender element can deform axially and in two lateral directions with bending about the strong and weak axes. However, the resistance derived from bending about the weak axis is neglected in the model. The model has been calibrated with the data provided by the manufacturer, and, in particular, the damper element has been calibrated with the experimental data of Phillips (1993). Currently, the model accounts for the following behavior of a fender.

- Nonlinear axial load-displacement relation.
- Linear lateral force-deformation relation.
- Loading-rate dependency.
- Energy dissipation.
- Gap opening and closing between a fender and a mooring shaft.
- Sliding of the fender pad against the mooring shaft.

With this model, a fender group will exert a force on the concrete structure only when the fender is in contact with the mooring shaft. The model also allows for an initial gap between a fender and the mooring shaft. However, the initial gap is assumed to be zero in the analyses presented here. With the damper element, the fender model has a recovery rate in returning to its un-deformed state when it is

disengaged from the shaft. However, the following features have not been included in the current fender model but may be added in the future.

- Influence of lateral displacement on the axial load capacity.
- The degradation of axial load resistance with loading cycles and its recovery.

Currently, experimental data on the above behavior is not available. It is expected that the proposed fender tests will yield more information on these.

As will be explained below, each fender assembly is modeled as a dynamic system. For each fender element, or fender assembly, a set of equations of motion must be solved. However, due to the nonlinear damping behavior, this is a more complicated process than for the MHP. After each time increment, Δt, the displacement at each degree of freedom of the MHP is subdivided by linear interpolation and input to the fender model, and the force imparted to the MHP is then computed. Figure 4.6 is a schematic of the model representing the axial behavior of a fender, while Figure 4.7 shows the model representing the lateral behavior. The axial behavior has a gap condition, while the lateral behavior has a sliding condition when static friction is overcome. A "penalty spring" is introduced in each direction to facilitate the modeling of the gap and sliding conditions. They are elastic springs with stiffness $\bar{K}^A$ and $\bar{K}^L$, which are considerably stiffer than the fender springs.

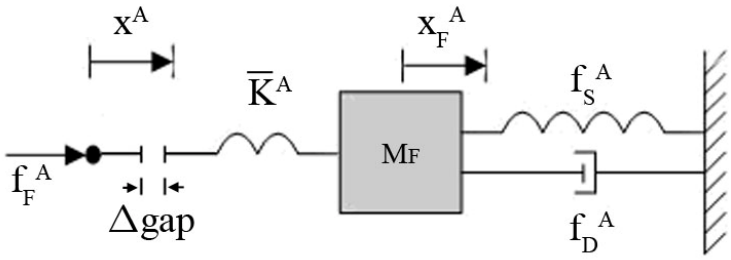

Figure 4.6 - Schematic of Axial Fender Model

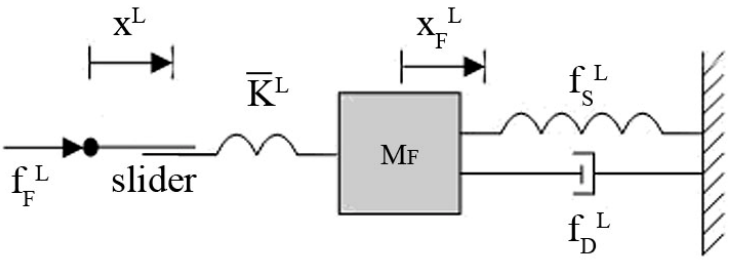

Figure 4.7 - Schematic of Lateral Fender Model

The equations of motion for a fender system can be expressed as follows.

$$\mathbf{M}_F\ddot{\mathbf{x}}_F + \mathbf{f}_D(\dot{\mathbf{x}}_F, \mathbf{x}_F) + \mathbf{f}_S(\mathbf{x}_F) - \mathbf{f}_F(\mathbf{x}, \mathbf{x}_F) = 0 \tag{4.11}$$

where $\mathbf{x}$ is the vector of the relative displacements of the MHP with respect to the shafts; $\mathbf{x}_F$ is the deformation of the fender as shown in Figures 4.6 and 4.7; $\mathbf{M}_F$ is the mass matrix of the fender; $\mathbf{f}_D$ is the vector of damping forces, which are nonlinear functions of fender velocities and displacements; $\mathbf{f}_S$ is the vector of static forces from the axial and lateral resistance of the fender, which are functions of displacements, and $\mathbf{f}_F$ is the vector of forces exerted by the fender on the MHP, which are functions of the relative displacements between the shaft and the fender, i.e., $(\mathbf{x} - \mathbf{x}_F)$.

The axial and lateral behaviors of the fender are assumed to be uncoupled, except for the dependence of the frictional resistance in the lateral direction on the normal force between the fender and the mooring shaft.

The static axial force developed by a fender is calculated with the axial fender deflection. As shown by the inset in Figure 4.8, the fenders buckle when deformed. The curve of the reaction force versus deflection, as shown in Figure 4.8, is provided by Trellex Fender Systems and can be well approximated with a fourth-order polynomial as shown below.

$$f_S^A = \left(a_1 \left| x_F^A \right|^4 + a_2 \left| x_F^A \right|^3 + a_3 \left| x_F^A \right|^2 + a_4 \left| x_F^A \right| \right) \cdot \text{sign}(x_F^A) \qquad (4.12)$$

where the values of a_i can be found experimentally or from manufacturer's data.

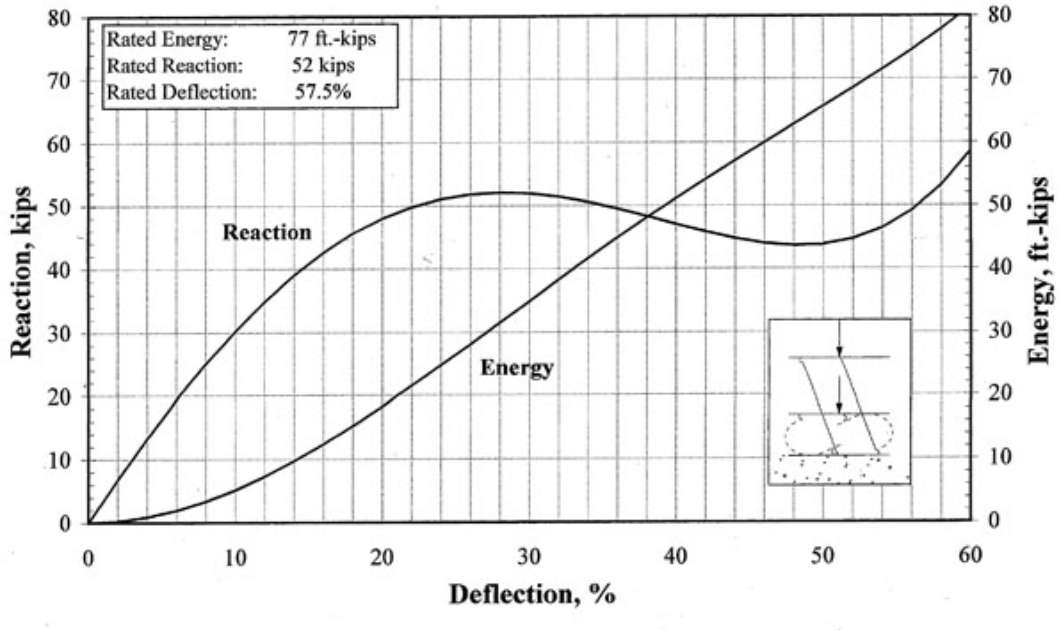

Figure 4.8 - Typical Fender Buckling Behavior (Courtesy of Trellex Fender Systems)

The following dimensionless nonlinear damper model is proposed to model the energy-dissipation and rate-dependent behavior of a fender element.

$$\frac{f_D^A}{\left|f_S^A\right|} = a \cdot \left|\dot{e}\right|^b \dot{e} \tag{4.13}$$

in which $\dot{e}$ is the strain rate, which can be taken to be $\dot{x}_F^A / H$, where *H* is the height of the fender element in the axial (loading) direction, f_S^A is the static force, and *a* and ß are material parameters.

The fenders are not attached to the mooring shaft, therefore, a gap can exist between the shaft and the fender in the axial direction. This can be an initial gap or a result of the fender deformation. If the gap is open, then the fender force is zero. If the gap is closed, then the axial penalty spring is engaged and the force is calculated with the linear penalty spring constant $\bar{K}^A$. This leads to the following relationship.

$$\begin{aligned} f_F^A &= \bar{K}^A (x^A - \Delta_{gap} - x_F^A) \text{ for } (x^A - \Delta_{gap} - x_F^A) > 0 \\ f_F^A &= 0 \text{ for } (x^A - \Delta_{gap} - x_F^A) \le 0 \end{aligned} \tag{4.14}$$

in which Δ_{gap} is the initial gap. The stiffness $\bar{K}^A$ of the axial penalty spring is assumed to be 20 times the initial stiffness of the fender.

For the lateral resistance of a fender element, only the strong direction is considered. Since a fender element is not expected to buckle under lateral loading in the strong direction, the lateral stiffness is assumed to be linearly elastic as follows.

$$f_S^L = K_F^L \cdot x_F^L \tag{4.15}$$

where

$$K_F^L = \frac{K_{bending}^L K_{shear}^L}{K_{bending}^L + K_{shear}^L}$$

As shown above, both the bending and shear stiffnesses are considered. The bending stiffness can be calculated with an assumption of fixed-fixed end conditions as follows.

$$K_{bending} = \frac{12EI}{H^3} \tag{4.16}$$

where E is the Young's Modulus of the material, I is the moment of inertia, and H is the height of the element in the axial direction. The shear stiffness is calculated with the following equation.

$$K_{shear} = \frac{kGA}{H} \tag{4.17}$$

where k is a shape factor, which is 5/6 for a rectangular section, G is the shear modulus, and A is the cross-sectional area of the element.

The same damping model is used for the lateral behavior. Hence, the damping force is given by

$$\frac{f_D^L}{\left| f_S^L \right|} = a \cdot \left| \dot{g} \right|^b \dot{g} \tag{4.18}$$

in which $\dot{g}$ is the strain rate in shear, which can be taken to be $\dot{x}_F^L / H$, where H is the height of the fender element, f_S^L is the static lateral force, and a and ß are material parameters, which can assume the same values as those for the axial direction.

The penalty spring stiffness $\bar{K}^L$ can be assumed to be 20 times the lateral fender stiffness K_F^L. The lateral fender force is non-zero only if the fender is in contact with the mooring shaft. The fender force can be determined with the following rate equation.

$$\dot{f}_F^L = \bar{K}^L (\dot{x}^L - \dot{x}_F^L) \tag{4.19}$$

with

$$\left| f_F^L \right| \le m \left| f_F^A \right| \tag{4.20}$$

in which μ is the coefficient of friction. The magnitude of the lateral fender force is limited by the frictional resistance between the mooring shaft and the ultra high molecular weight polyethylene (UHMW-PE) pad of a fender assembly.

The explicit Newmark integration method is utilized to solve for the displacements, velocities, and accelerations of a fender under an imposed relative displacement vector **x**. However, because of the nonlinear damping, an iterative solution scheme is required even for the explicit integration method. The integration time step dt used here needs to be much smaller than the Δt used to compute the response of the MHP because of the high natural frequencies of a fender assembly.

The time discretized equations of motion for a fender assembly can be expressed as follows together with the displacement and velocity approximations.

$$\mathbf{M}_F \ddot{\mathbf{x}}_{F,i+1} + \mathbf{f}_D(\dot{\mathbf{x}}_{F,i+1}, \mathbf{x}_{F,i+1}) + \mathbf{f}_S(\mathbf{x}_{F,i+1}) - \mathbf{f}_F(\mathbf{x}_{i+1}, \mathbf{x}_{F,i+1}) = 0 \tag{4.21}$$

$$\mathbf{x}_{F,i+1} = \mathbf{x}_{F,i} + dt\dot{\mathbf{x}}_{F,i} + \frac{dt^2}{2}\ddot{\mathbf{x}}_{F,i} \tag{4.22}$$

$$\dot{\mathbf{x}}_{F,i+1} = \dot{\mathbf{x}}_{F,i} + dt\left[(1-g)\ddot{\mathbf{x}}_{F,i} + g\,\ddot{\mathbf{x}}_{F,i+1}\right] \tag{4.23}$$

where $\mathbf{x}_F$ is the vector of fender displacements. In this analysis, *?* is 0.5. Equation (4.23) can be rearranged to:

$$\ddot{\mathbf{x}}_{F,i+1} = \frac{\dot{\mathbf{x}}_{F,i+1} - \dot{\mathbf{x}}_{F,i}}{dtg} + \frac{(g-1)\ddot{\mathbf{x}}_{F,i}}{g} \tag{4.24}$$

Substituting equation (4.24) into the equations of motion, equation (4.21), yields:

$$\mathbf{M}_F\left(\frac{\dot{\mathbf{x}}_{F,i+1} - \dot{\mathbf{x}}_{F,i}}{dtg} + \frac{(g-1)\ddot{\mathbf{x}}_{F,i}}{g}\right) + \mathbf{f}_D(\dot{\mathbf{x}}_{F,i+1}, \mathbf{x}_{F,i+1}) + \mathbf{f}_S(\mathbf{x}_{F,i+1}) - \mathbf{f}_F(\mathbf{x}_{i+1}, \mathbf{x}_{F,i+1}) = \mathbf{0} \tag{4.25}$$

which leads to

$$\frac{\mathbf{M}_F\dot{\mathbf{x}}_{F,i+1}}{dtg} + \mathbf{f}_D(\dot{\mathbf{x}}_{F,i+1}, \mathbf{x}_{F,i+1}) = \mathbf{f}_{i+1} \tag{4.26}$$

where

$$\mathbf{f}_{i+1} = \mathbf{f}_F(\mathbf{x}_{i+1}, \mathbf{x}_{F,i+1}) - \mathbf{f}_S(\mathbf{x}_{F,i+1}) - \frac{\mathbf{M}_F}{g}\left((g-1)\ddot{\mathbf{x}}_{F,i} - \frac{\dot{\mathbf{x}}_{F,i}}{dt}\right) \tag{4.27}$$

in which $\mathbf{x}_{i+1}$ is given and $\mathbf{x}_{F,i+1}$ can be calculated with equation (4.22). Hence, as shown in equation (4.27), $\mathbf{f}_{i+1}$ is a vector of known quantities in each time step, and

therefore, the equilibrium shown in equation (4.26) depends only on the current step's velocities, which are not known. The velocities have to be found with a Newton iteration method as follows. With each trial solution $\dot{\mathbf{x}}_{F,i+1}^{trial}$, we have a residual **R**.

$$\mathbf{R} = \left[\frac{\mathbf{M}_F}{dtg} \dot{\mathbf{x}}_{F,i+1}^{trial} + \mathbf{f}_D(\dot{\mathbf{x}}_{F,i+1}^{trial}, \mathbf{x}_{F,i+1}) \right] - \mathbf{f}_{i+1} \tag{4.28}$$

The goal is to find the exact solution, $\dot{\mathbf{x}}_{F,i+1}$, which results in a residual of **0**, i.e.,

$$\mathbf{0} = \left[\frac{\mathbf{M}_F}{dtg} \dot{\mathbf{x}}_{F,i+1} + \mathbf{f}_D(\dot{\mathbf{x}}_{F,i+1}, \mathbf{x}_{F,i+1}) \right] - \mathbf{f}_{i+1} \tag{4.29}$$

Subtracting equation (4.28) from equation (4.29) results in the following equation.

$$\frac{\mathbf{M}_F}{dtg} d\dot{\mathbf{x}}_{F,i+1} + d\mathbf{f}_D = -\mathbf{R} \tag{4.30}$$

where

$$d\dot{\mathbf{x}}_{F,i+1} = \dot{\mathbf{x}}_{F,i+1} - \dot{\mathbf{x}}_{F,i+1}^{trial} \tag{4.31}$$

$$d\mathbf{f}_D = \mathbf{f}_D(\dot{\mathbf{x}}_{F,i+1,}\mathbf{x}_{F,i+1,}) - \mathbf{f}_D(\dot{\mathbf{x}}_{F,i+1}^{trial}, \mathbf{x}_{F,i+1,}) \tag{4.32}$$

Introducing the tangent damping matrix, $\mathbf{C}_t$, at the current trial solution, we have

$$d\mathbf{f}_D \approx \mathbf{C}_t d\dot{\mathbf{x}}_{F,i+1} \tag{4.33}$$

where

$$\mathbf{C}_t = \frac{d\mathbf{f}_D}{d\dot{\mathbf{x}}_F} = \begin{bmatrix} C_t^A & 0 \\ 0 & C_t^L \end{bmatrix} \tag{4.34}$$

in which $\mathbf{f}_D$ is given by equations (1.13) and (1.18). Hence,

$$\begin{aligned} C_t^A = \frac{df_D^A}{d\dot{x}_F^A} &= \frac{df_D^A}{d(|\dot{x}_F^A| + d)} \cdot \frac{d(|\dot{x}_F^A| + d)}{d\dot{x}_F^A} \\ &= \frac{d\left(\frac{|f_S^A| a}{L^{b+1}} \left(|\dot{x}_F^A| + d \right)^{1+b} \operatorname{sign}(\dot{x}_F^A) \right)}{d(|\dot{x}_F^A| + d)} \cdot \frac{d(|\dot{x}_F^A| + d)}{d\dot{x}_F^A} \\ &= (1+b) \frac{|f_S^A| a}{L^{b+1}} \left(|\dot{x}_F^A| + d \right)^b \end{aligned} \tag{4.35}$$

$$\begin{aligned} C_t^L = \frac{df_D^L}{d\dot{x}_F^L} &= \frac{df_D^L}{d(|\dot{x}_F^L| + d)} \cdot \frac{d(|\dot{x}_F^L| + d)}{d\dot{x}_F^L} \\ &= \frac{d\left(\frac{|f_S^L| a}{L^{b+1}} \left(|\dot{x}_F^L| + d \right)^{1+b} \operatorname{sign}(\dot{x}_F^L) \right)}{d(|\dot{x}_F^L| + d)} \cdot \frac{d(|\dot{x}_F^L| + d)}{d\dot{x}_F^L} \\ &= (1+b) \frac{|f_S^L| a}{L^{b+1}} \left(|\dot{x}_F^L| + d \right)^b \end{aligned} \tag{4.36}$$

Since *ß* is in general negative, equations (1.13) and (1.18) will lead to an infinitely large damping coefficient when the velocity becomes zero. To avoid this problem, a very small constant d is introduced in the above expressions. Substituting equation (4.33) into equation (4.30), one can solve for the incremental change in velocity as follows.

$$d\dot{\mathbf{x}}_{F,i+1} = -\left(\frac{\mathbf{M}_F}{dtg} + \mathbf{C}_t\right)^{-1}\mathbf{R} \tag{4.37}$$

A new trial velocity is found with:

$$\dot{\mathbf{x}}_{F,i+1}^{newtrial} = \dot{\mathbf{x}}_{F,i+1}^{trial} + d\dot{\mathbf{x}}_{F,i+1} \tag{4.38}$$

This value is then used in equation (4.28) to find a new residual and the process is repeated until the residual is below a chosen tolerance. For efficiency, the velocities of the previous time step can be used as the initial trial values. Finally, the accelerations are calculated with equation (4.24). The next increment of $\mathbf{x}$ is then imposed and the computation is repeated. The fender forces are sent back to the MHP model once the entire increment for the time interval Δt has been imposed.

Summary of Solution Scheme

Given:

N = number of time steps dt

$\mathbf{x}_i$ with i=1, ... , N

$\mathbf{x}_{F,0}$

$\dot{\mathbf{x}}_{F,0}$

$\ddot{\mathbf{x}}_{F,0}$

1. Set: $i = 0$
2. Calculate $\mathbf{x}_{F,i+1}$ with equation (4.22).
3. Calculate $f_{S,i+1}^{A}$ with equation (4.12).
4. Calculate $f_{F,i+1}^{A}$ with equation (4.14).
5. Choose a trial velocity: $\dot{x}_{F,i+1}^{Atrial} = \dot{x}_{F,i}^{A}$.
6. Find j_{i+1}^{A} with equation (4.27).
7. Compute residual R^{A} with equations (4.27), (4.28), and (4.13).
8. Check if R^{A} is below tolerance, and go to step 12 if true.
9. Calculate $d\dot{x}_{F,i+1}^{A}$ with equations (4.37) and (4.35).
10. Find $\dot{x}_{F,i+1}^{Anewtrial}$ with equation (4.38).
11. Go to step 7.
12. Set $\dot{x}_{F,i+1}^{A} = \dot{x}_{F,i+1}^{Anewtrial}$.
13. Calculate $\ddot{x}_{F,i+1}^{A}$ with equation (4.24).
14. Calculate $f_{S,i+1}^{L}$ with equation (4.15).

15. Calculate $f_{F,i+1}^{L}$ with the following equations.

    if $\left(f_{F,i+1}^{A} > 0 \right)$, then $f_{F,i+1}^{L} = f_{F,i}^{L} + \bar{K}^{L} \left\{ (x_{i+1}^{L} - x_{F,i+1}^{L}) - (x_{i}^{L} - x_{F,i}^{L}) \right\}$

    if $\left(f_{F,i+1}^{A} = 0 \right)$, then $f_{F,i+1}^{L} = 0$

    if $\left(\left| f_{F,i+1}^{L} \right| \geq m \left| f_{F,i+1}^{A} \right| \right)$, then $f_{F,i+1}^{L} = m \left| f_{F,i+1}^{A} \right| \text{sign}(f_{F,i+1}^{L})$

16. Choose a trial velocity: $\dot{x}_{F,i+1}^{L\,trial} = \dot{x}_{F,i}^{L}$.

17. Find j_{i+1}^{L} with equation (4.27).

18. Compute residual R^{L} with equations (4.27), (4.28), and (4.18).

19. Check if R^{L} is below tolerance, and go to step 23 if true.

20. Calculate $d\dot{x}_{F,i+1}^{L}$ with equations (4.37) and (4.36).

21. Find $\dot{x}_{F,i+1}^{L\,newtrial}$ with equation (4.38).

22. Go to step 18.

23. Set $\dot{x}_{F,i+1}^{L} = \dot{x}_{F,i+1}^{L\,newtrial}$.

24. Calculate $\ddot{x}_{F,i+1}^{L}$ with equation (4.24).

25. When i< N, set $i = i + 1$, and go to step 2.

26. Set $\mathbf{x}_{F,0} = \mathbf{x}_{F,N}$, $\dot{\mathbf{x}}_{F,0} = \dot{\mathbf{x}}_{F,N}$, and $\ddot{\mathbf{x}}_{F,0} = \ddot{\mathbf{x}}_{F,N}$.

27. Send fender forces $\mathbf{f}_{F,N}$ to the MHP model.

4.3.1 Fender Model Calibration

The static axial load-deformation relation for the fenders is deduced from the data provided by the manufactured based on a decreasing velocity test method and the calibrated theoretical rate model shown in Figure 4.11, which will be explained later. Based on the test data provided by the manufacturer (Trelleborg 2007), the following fourth-order polynomial is proposed to model the static axial load-deformation behavior of an MV1000x1000A fender element.

$$f_S^A = \left(0.0024\left|x_F^A\right|^4 - 0.0735\left|x_F^A\right|^3 + 0.0899\left|x_F^A\right|^2 + 12.487\left|x_F^A\right|\right)\cdot sign(x_F^A) \text{ kips} \quad (4.39)$$

in which x_F is the fender deformation in inches. The static resistance of a fender element of other cross-sectional lengths can be scaled accordingly. The above curve is shown in Figure 4.9

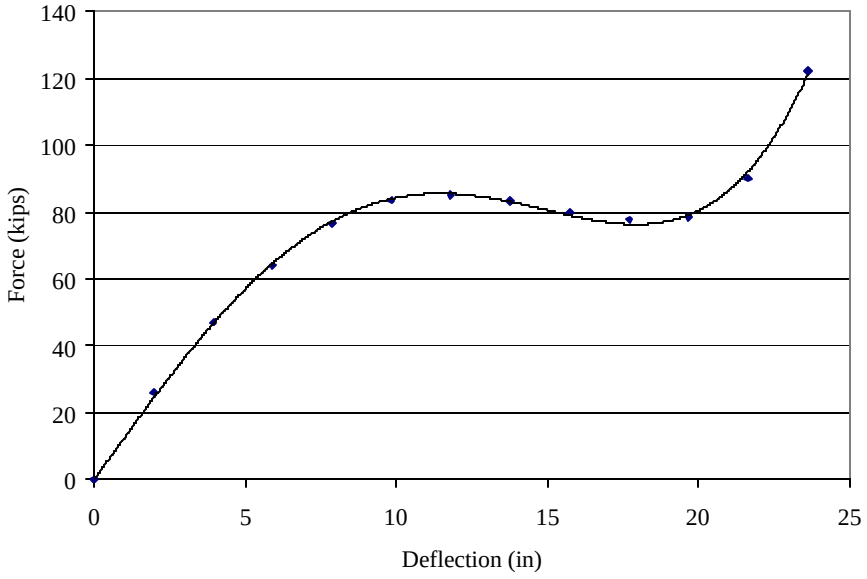

Figure 4.9 - Static Force-Deflection Curve for MV1000x1000A Fender Element

The load-deflection properties of an MV1250x900A element have also been estimated. This fender has more deformation capacity. With the manufacturer's target maximum deflection of 57.5%, it allows for over 28 in of deflection, as opposed to 22.6 in for the MV1000 fender. The following fourth-order polynomial is obtained for the static axial load-deformation behavior of an MV1250x900A fender element.

$$f_S^A = \left(0.0011\left|x_F^A\right|^4 - 0.0408\left|x_F^A\right|^3 + 0.0624\left|x_F^A\right|^2 + 10.836\left|x_F^A\right|\right)\cdot \text{sign}(x_F^A) \text{ kips} \qquad (4.40)$$

in which x_F^A is in inches.

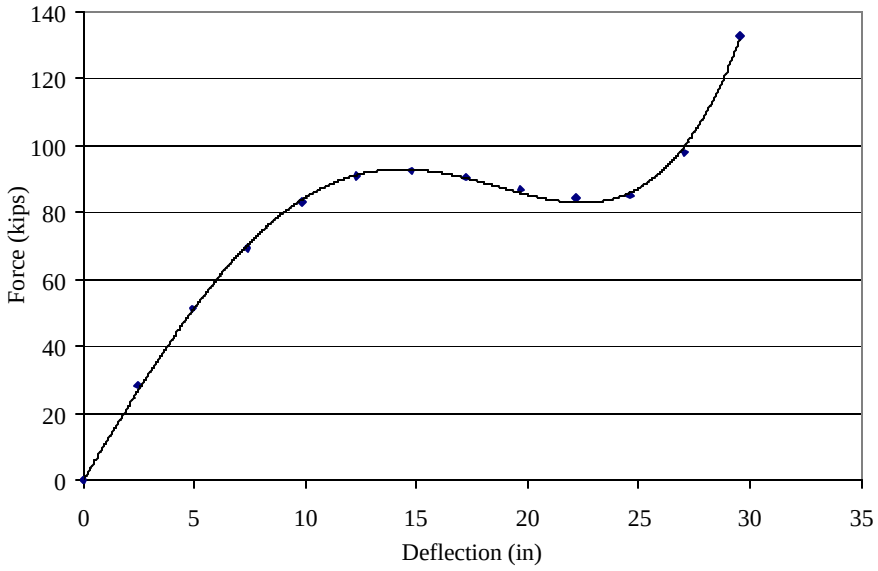

Figure 4.10 - Static Force-Deflection Curve for MV1250x900A Fender Element

The lateral stiffness of a fender is found using equations (4.15) through (4.17), which lead to

$$f_S^L = \left[\frac{\frac{12EI}{H^3} \cdot \frac{kGA}{H}}{\frac{12EI}{H^3} + \frac{kGA}{H}} \right] x_F^L \tag{4.41}$$

with

$$\begin{aligned} I &= \frac{wL^3}{12} \\ G &= \frac{E}{2(1+n)} = \frac{E}{3} \\ A &= wL \end{aligned} \tag{4.42}$$

where E is the Young's modulus, H is the height of the fender in the axial direction, and L is the length and w the width of the fender element cross section. Poisson's ratio of the rubber material is assumed to be 0.5. The Young's modulus is estimated with the initial axial stiffness of a fender element as given by equation (1.39) or (1.40). In the analysis, E is assumed to be 1 ksi.

The damping model has been calibrated with the test data of Phillips (1993) obtained from fender element samples of the same material but of smaller size (MV54x54A). The damping force from the tests has been obtained by subtracting the static resistance from the total force. It is then normalized by the static resistance and plotted against the strain rate as shown in Figure 4.11. The static resistance is assumed to be the force obtained at the slowest strain rate attained in the tests, which is of 0.05

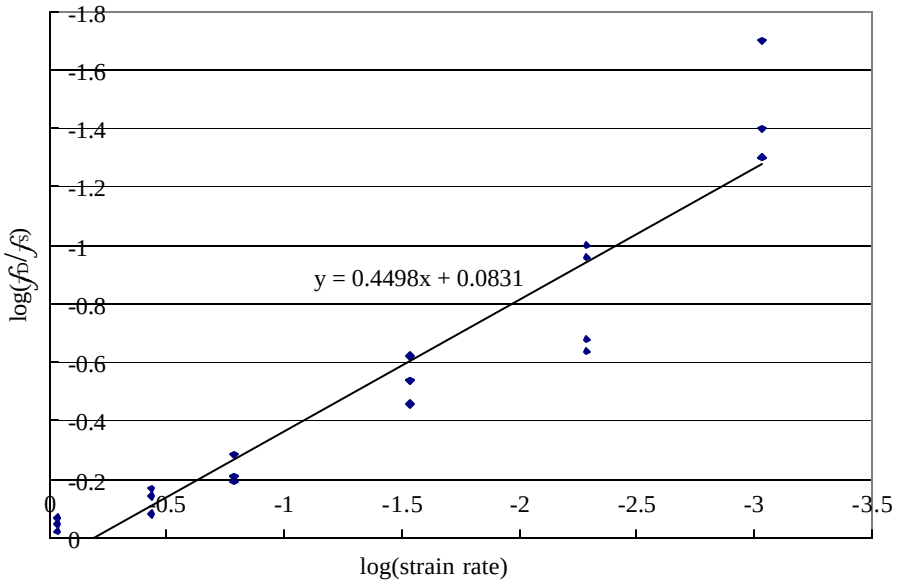

Figure 4.11 - Normalized Damping Force vs. Strain Rate

mm/sec. A least-squares fit has been used to determine the values of a and ß. The value of a has been found to be 1.21 and that of ß is -0.55. To avoid an infinitely large damping coefficient when the velocity becomes zero, a d of 0.0000001 is used. With equation (4.13), the axial damping force of a fender element can be calculated as

$$f_D^A = \left| f_S^A \right| a \cdot \left| \dot{e} \right|^b \dot{e} = \frac{\left| f_S^A \right| \cdot a}{H^{(b+1)}} \left(\left| \dot{x}^A \right| + d \right)^b \left(\dot{x}^A + d \right) \tag{4.43}$$

Similarly, for the lateral direction,

$$f_D^L = \left| f_S^L \right| a \cdot \left| \dot{e} \right|^b \dot{e} = \frac{\left| f_S^L \right| \cdot a}{H^{(b+1)}} \left(\left| \dot{x}^L \right| + d \right)^b \left(\dot{x}^L + d \right) \tag{4.44}$$

From previous tests (Lee et al. 2008), the coefficient of friction between the UHMW-PE pad and the mooring shaft is about 0.15. This agrees well with the manufacturer's recommendations and is used in the analysis.

To model the gap condition, each fender assembly has to be treated as a dynamic system with its mass considered. Each fender assembly consists of four fender elements with an ultra high molecular weight polyethylene (UHMW-PE) pad that has a unit weight of 56.7 lb/ft^3 (0.94 g/cm^3) and a weight of 316 lbs (143 kg) for the smaller fender system and 492 lbs (224 kg) for the larger system. The weight of a fender assembly is assumed to be ½ of that of the elements and the entire weight of the UHMW pad. A four MV1000x900A element fender assembly weighs 2 kips, a two MV1000x1000A plus two MV1000x1200A element fender assembly weighs 2.5 kips, and a four MV1250x900A element assembly weighs 3.2 kips.

For the validation of axial behavior, the MV1000x1000A fender element model is subjected to shifted cosine wave functions with maximum velocities of about 3, 6, and 12 in./sec., respectively. The force-displacement responses of the model to these loading conditions are plotted in Figure 4.12.

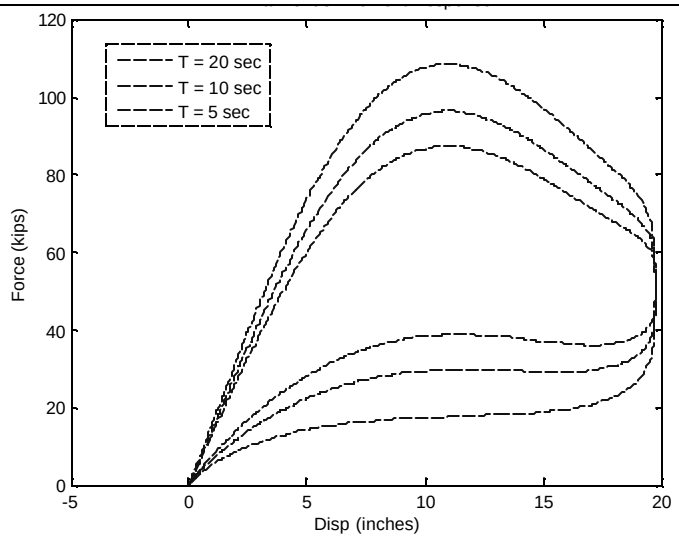

Figure 4.12 - MV1000x1000 Fender Element Subjected to Harmonic Loading

The fender model is also subjected to concurrent axial and lateral deformations. Results from two cases are shown in Figure 4.13 through Figure 4.16. Both cases are for an MV1250x900A fender element. Case 1 consists of an imposed axial displacement that varies linearly with time up to 12 in within 7.5 seconds, after which the displacement is held constant. After 7.5 seconds, with its axial displacement held constant, the fender is loaded laterally to 10 in. of deformation. Figure 4.13 and Figure 4.14 clearly show the decay of the axial damping force and the slipping in the lateral direction at a lateral load of 15% of the axial force. Note the small difference in the imposed axial displacement and the response. This is due to the compression of the penalty spring.

Case 2, whose results are plotted in Figure 4.15 and Figure 4.16, has a similar loading scheme as Case 1 except that the axial load is removed after 12.5 seconds. The rebound of the fender in both the axial and lateral directions can be seen.

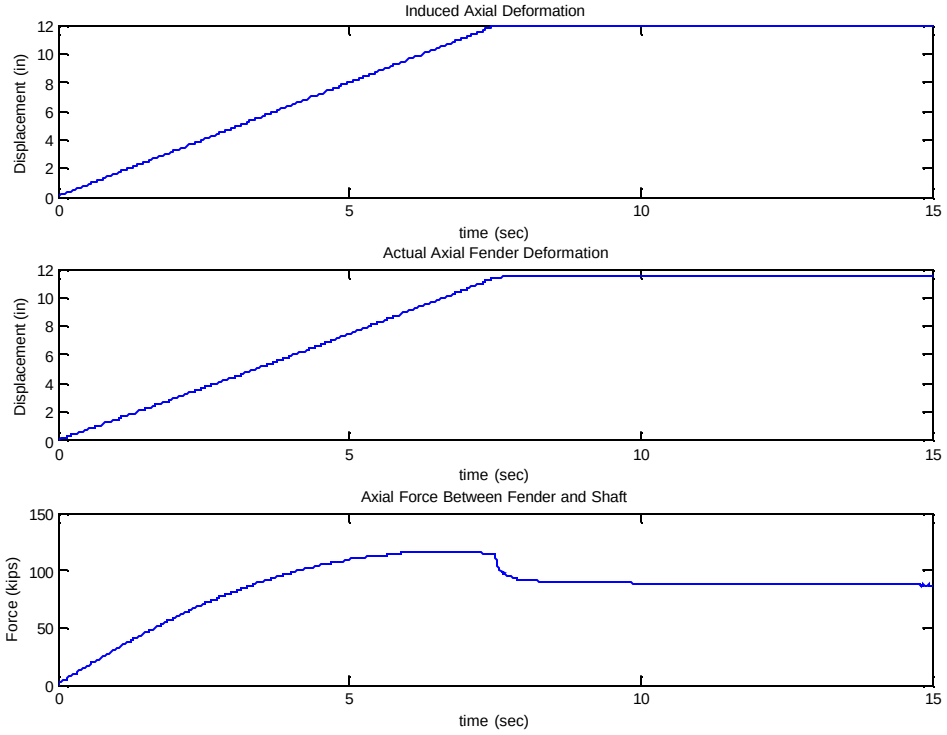

Figure 4.13 - Axial Response of Fender Element (Case 1)

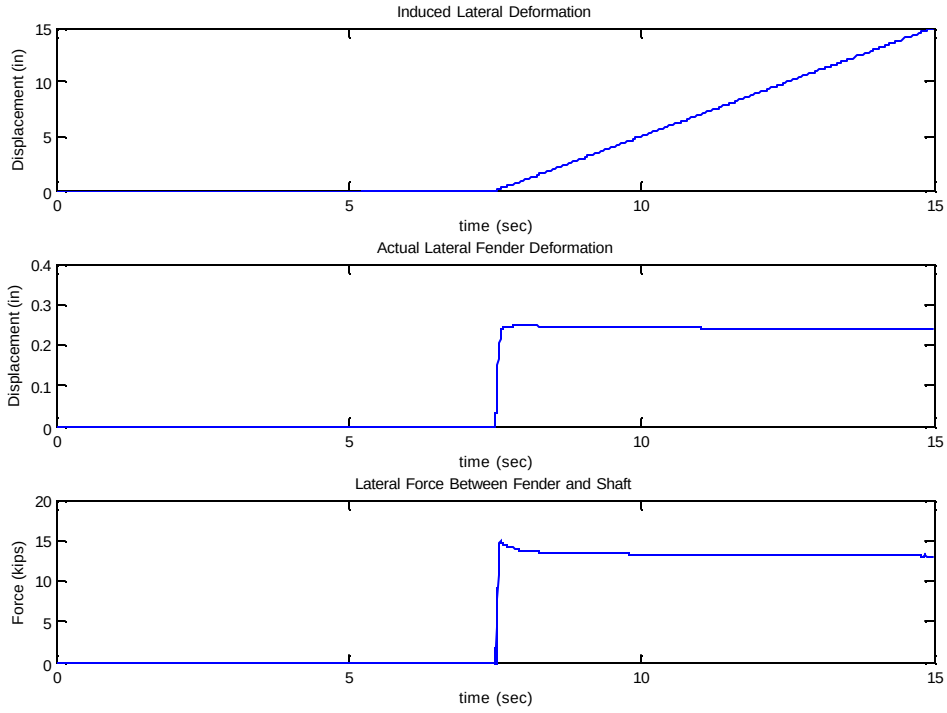

Figure 4.14 - Lateral Response of Fender Element (Case 1)

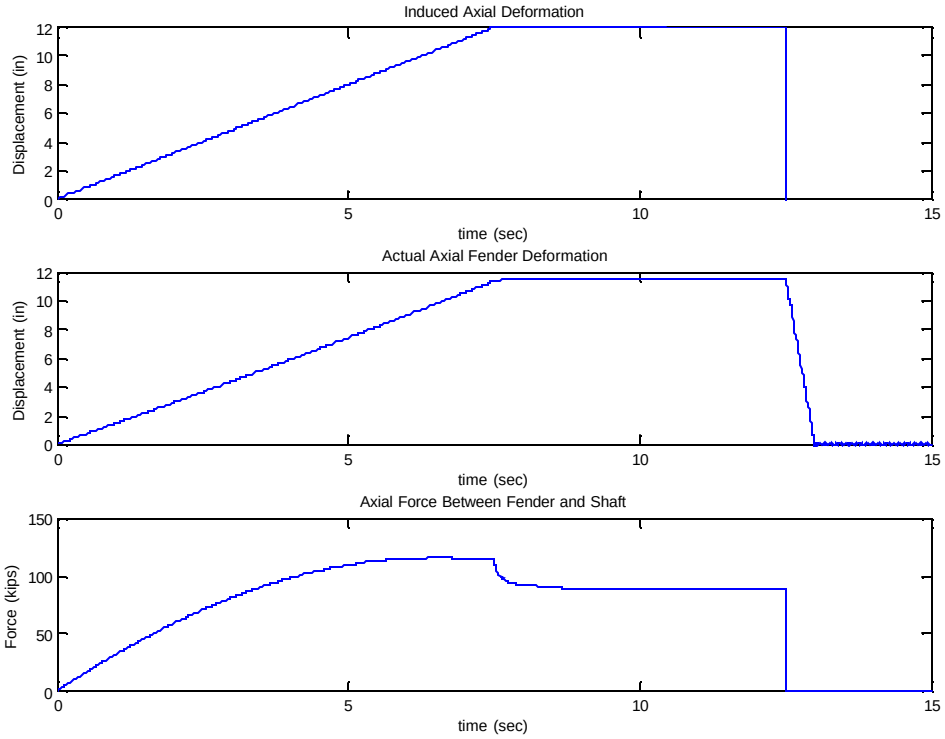

Figure 4.15 - Axial Response of Fender Element (Case 2)

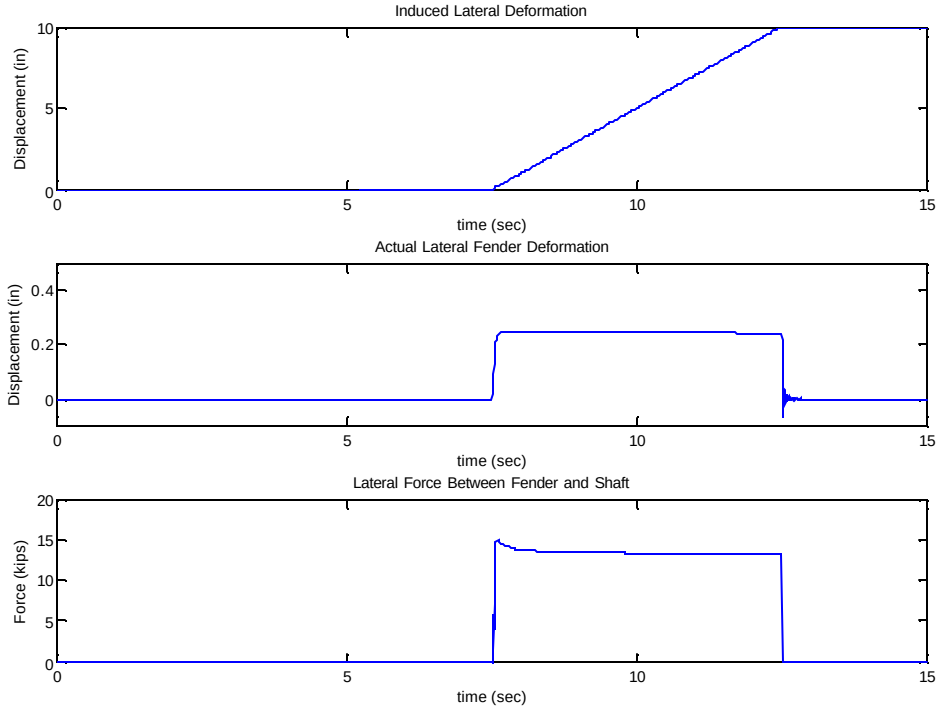

Figure 4.16 - Lateral Response of Fender Element (Case 2)

4.4 Seismic Analyses

The natural frequencies of the MHP in the longitudinal and transverse directions are 15 and 8 sec, respectively. Four groups of earthquake ground motion records are considered in the seismic analyses. They are provided by URS Corporation. Each group has five records. The first two groups are representative of free-field ground motions at the mud-line level for the San Diego Bay with return periods of 475 and 975 years, respectively. The third and forth groups have the same return periods but are representative of ground motions 69 ft. (21m) below the mud-line at the same elevation as the base of the pile groups supporting the mooring shafts. The latter motions are derived from those at the mud-line using a deconvolution analysis. The motions at the mud-line level are scaled ground motions from the 1979 Imperial Valley, 1995 Kobe, 1999 Kocaeli, 1992 Landers, and 1989 Loma Prieta Earthquakes. The response spectra of the ground motions are shown in Figure 4.17. The first two fundamental periods of the MHP are 8 and 15 sec. As can be seen from the figure, for these periods, the ground motions at the two elevations will result in the same spectral accelerations. Hence, only the results for the motions 69 ft. (21 m) below the mud-line are presented here. The integration time step, Δt, for the MHP analysis is the same as the time discretization intervals of the earthquake records. This value is 0.005 sec for all of the records except for the Kobe record. The time interval is 0.02 sec for the Kobe record. The integration time step, dt, for evaluating the fender response is 0.001 sec in all cases.

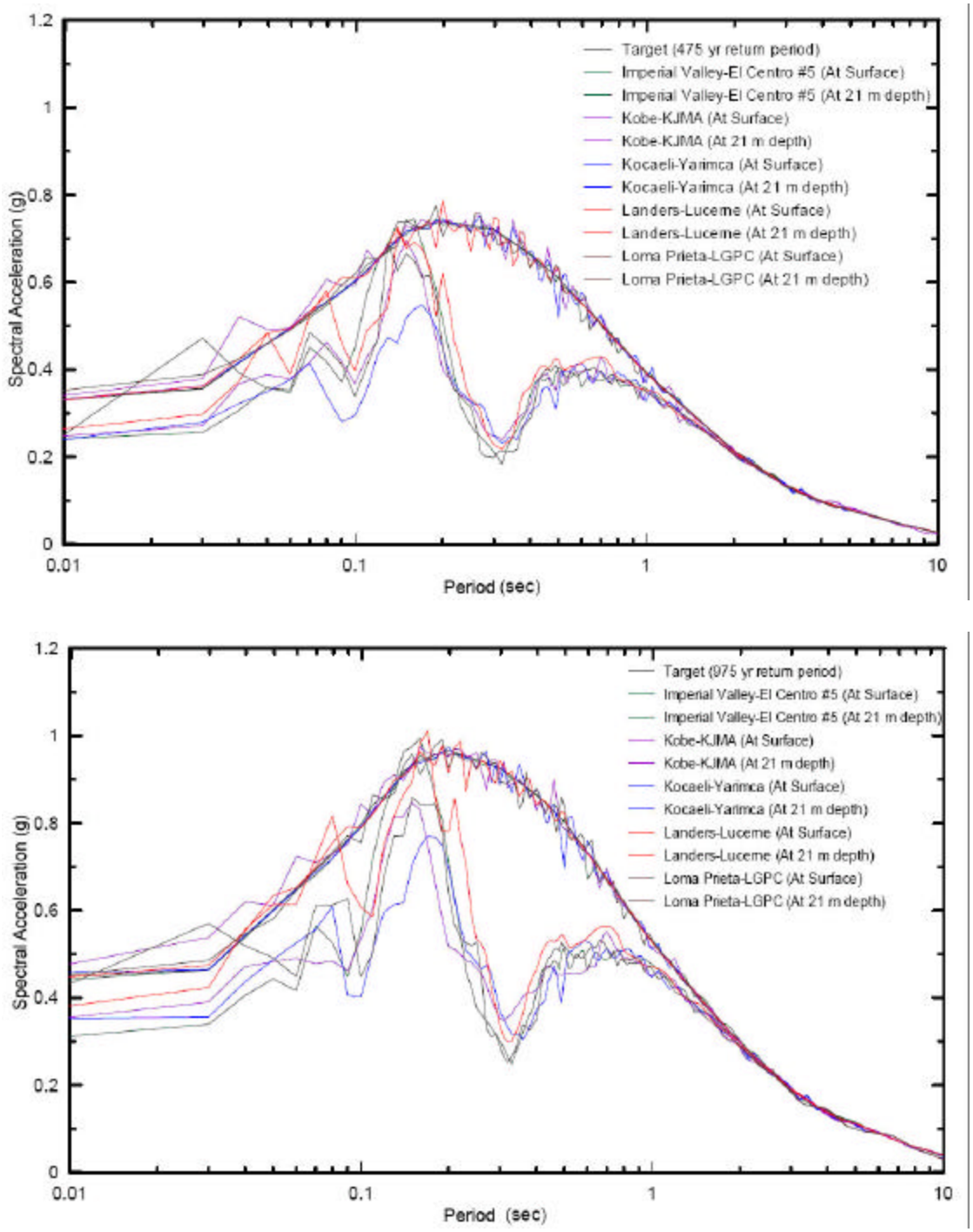

Figure 4.17 - Response Spectra of Earthquake Ground Motions (Courtesy of URS)

In the analyses, the same ground motion record is applied simultaneously in the longitudinal and transverse directions to represent the worst scenario. All fender assemblies in the transverse direction experience more or less the same displacements. The yaw of the MHP is negligible

Figure 4.18 and Figure 4.19 show the relative displacements of the MHP with the MV1000 fender system for the El Centro and Kobe grounds motions that have a return period of 975 years. The displacements are with respect to the positions of mooring shafts. It can be observed that the peak relative displacements obtained exceed the allowable displacement for the fender system. Since only one fender system is engaged in the axial or lateral direction at each location at a time, the solid and dashed lines in the plots represent different fender assemblies. This prompted a change in the size of the fender elements to MV1250.

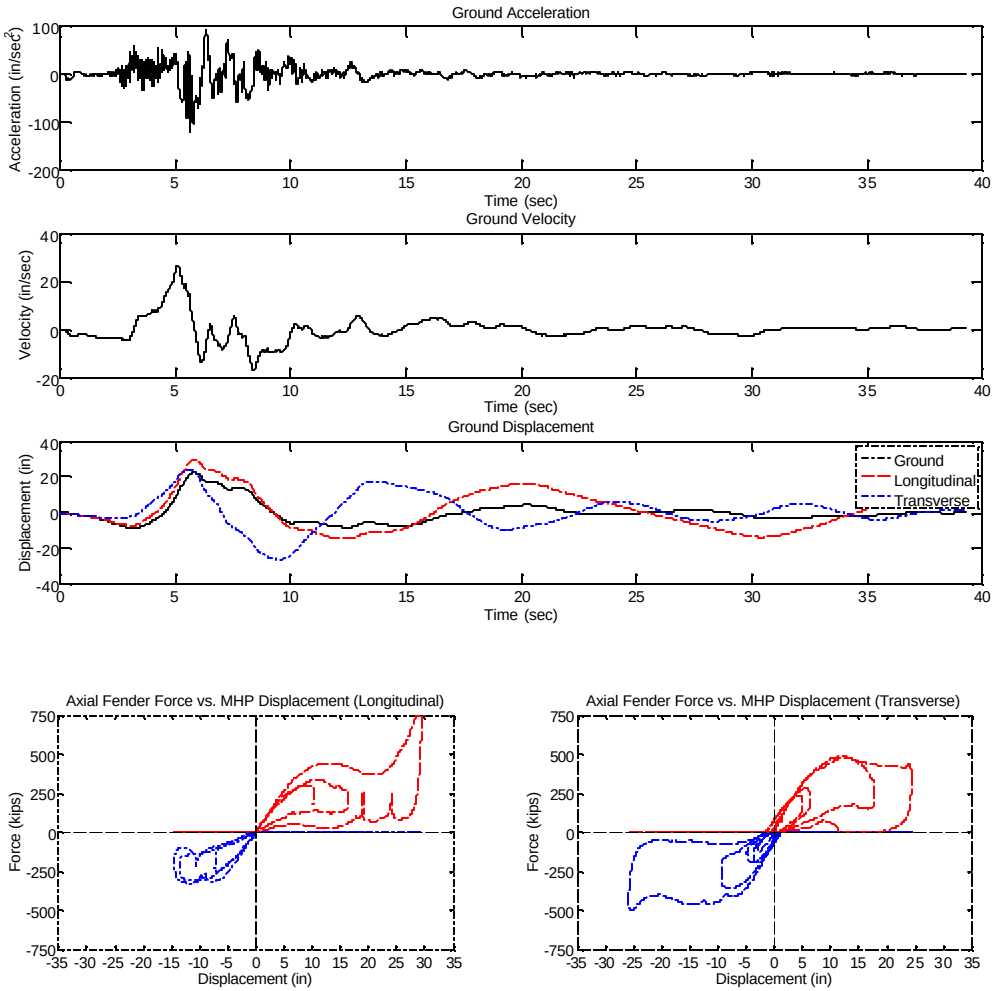

Figure 4.18 - Seismic Response with MV1000 under
1979 Imperial Valley - El Centro (975-year)

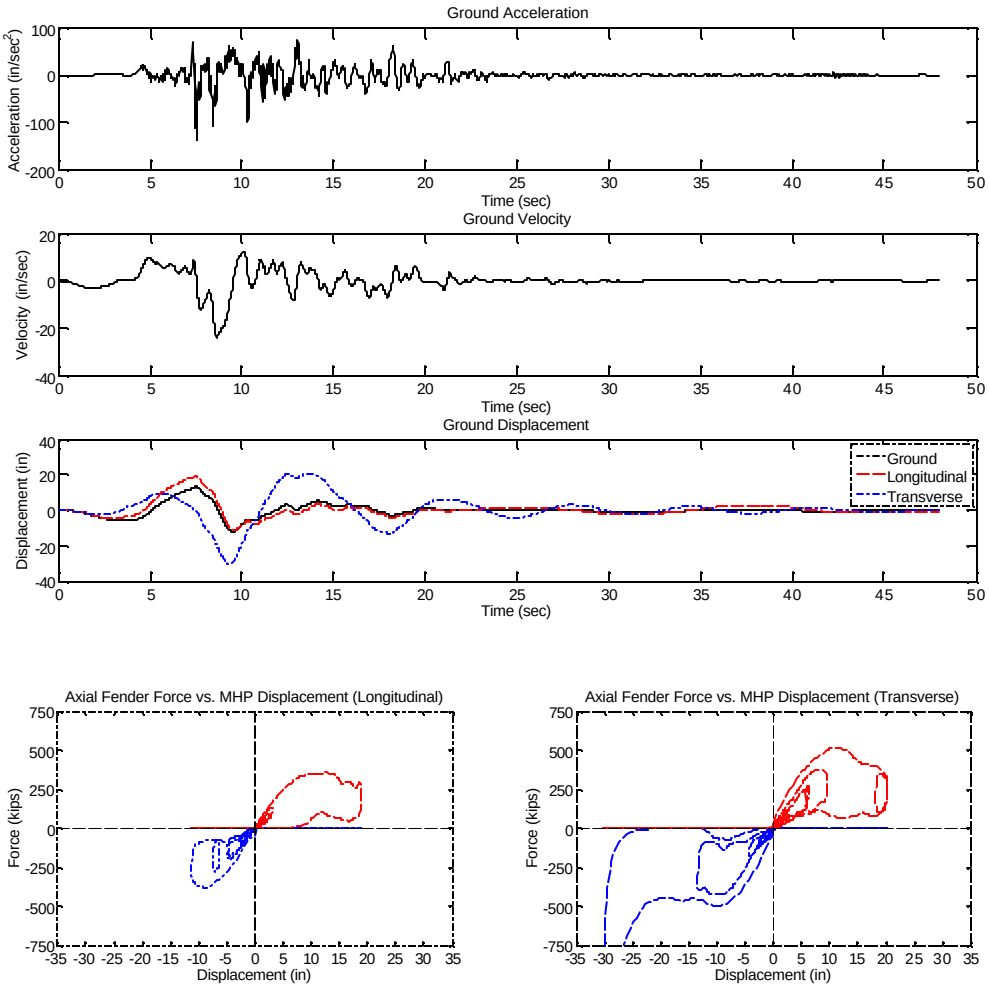

Figure 4.19 - Seismic Response with MV1000 under
1995 Kobe, Japan - KJMA (975-year)

With the revised fender system (MV1250x900A), the responses of the MHP to the ten earthquake records are analyzed. The results of the analyses are presented in Figure 4.20 through Figure 4.29. In each figure, the acceleration, velocity, and displacement time histories of the earthquake ground motion are presented. The displacement of the ground and the relative displacements of the MHP in the longitudinal and transverse directions are plotted together. Below these three graphs, the responses of the fender assemblies in the longitudinal and transverse directions are plotted. The responses of the transverse fenders at degree-of-freedom 2 and 3, as identified in Figure 4.4, are very similar and, therefore, only one is presented here. For each of the principle directions of the MHP, four plots are presented with a total of eight plots. The axial and lateral forces of a four-element fender assembly are each plotted against the relative displacements of the MHP in each of the principle directions. Since only one fender system is engaged in the axial or lateral direction at each location at a time, the solid and dashed lines in the plots represent different fender assemblies. The scales for the axial and lateral forces differ significantly, as the lateral force is in general an order of magnitude smaller than the axial force. The axial and lateral displacement time histories of the fenders are shown in the last four plots of each figure. It can be observed that the displacements of the fenders are within the allowable limits for all cases.

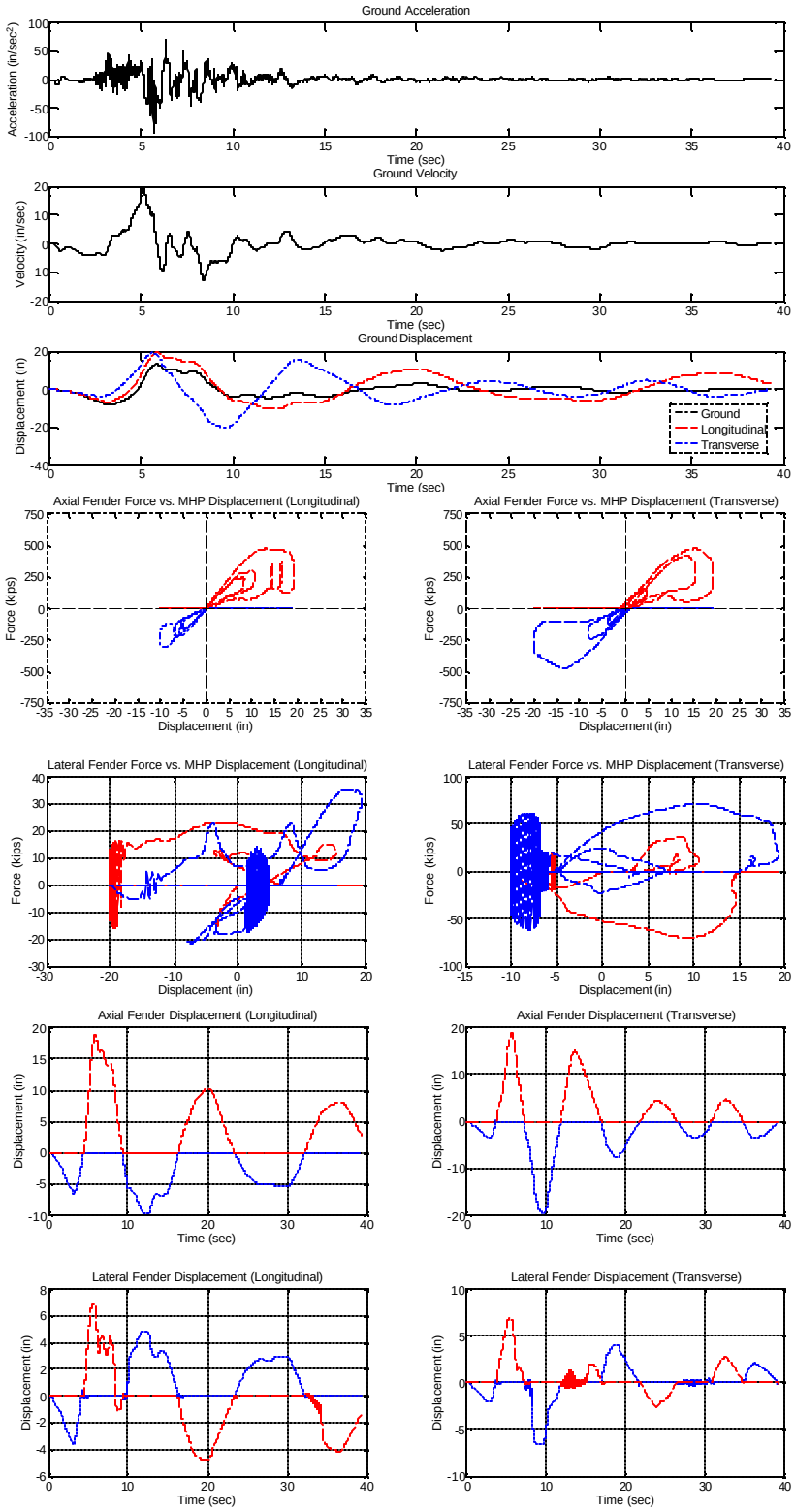

Figure 4.20 - Seismic Response with MV1250 under 1979 Imperial Valley - El Centro (475-year)

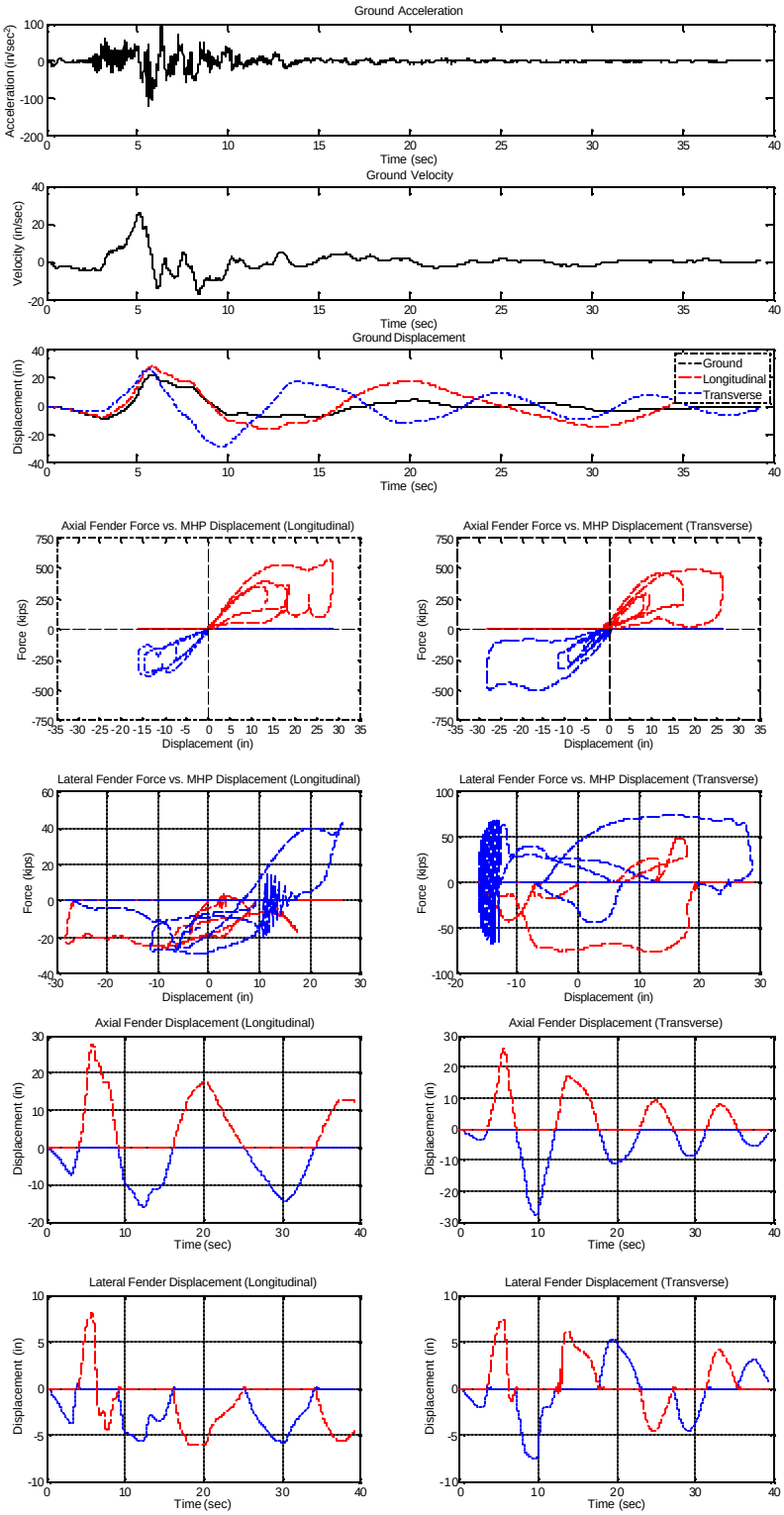

Figure 4.21 - Seismic Response with MV1250 under 1979 Imperial Valley - El Centro (975-year)

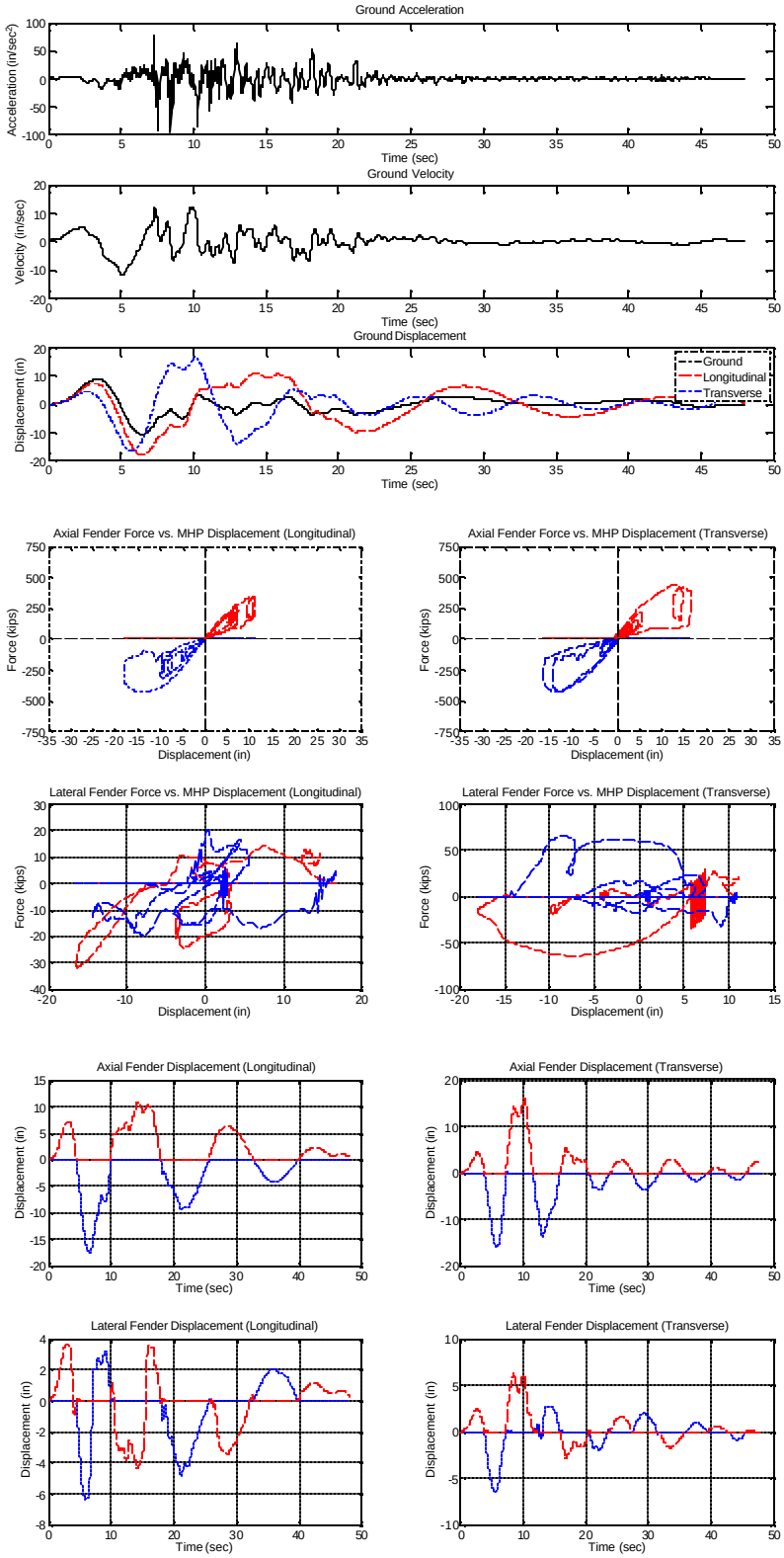

Figure 4.22 - Seismic Response with MV1250 under 1995 Kobe, Japan (475-year)

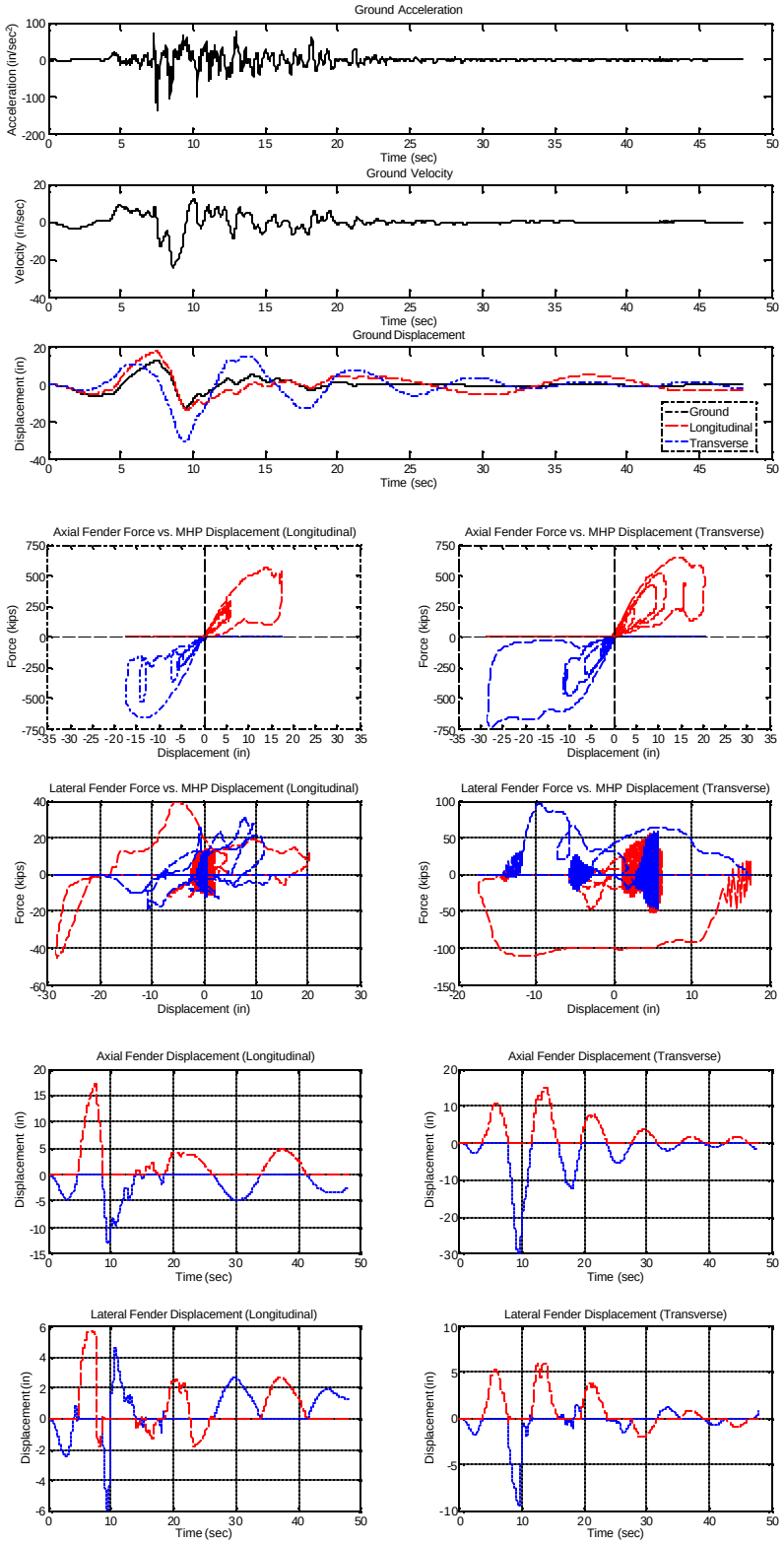

Figure 4.23 - Seismic Response with MV1250 under 1995 Kobe, Japan (975-year)

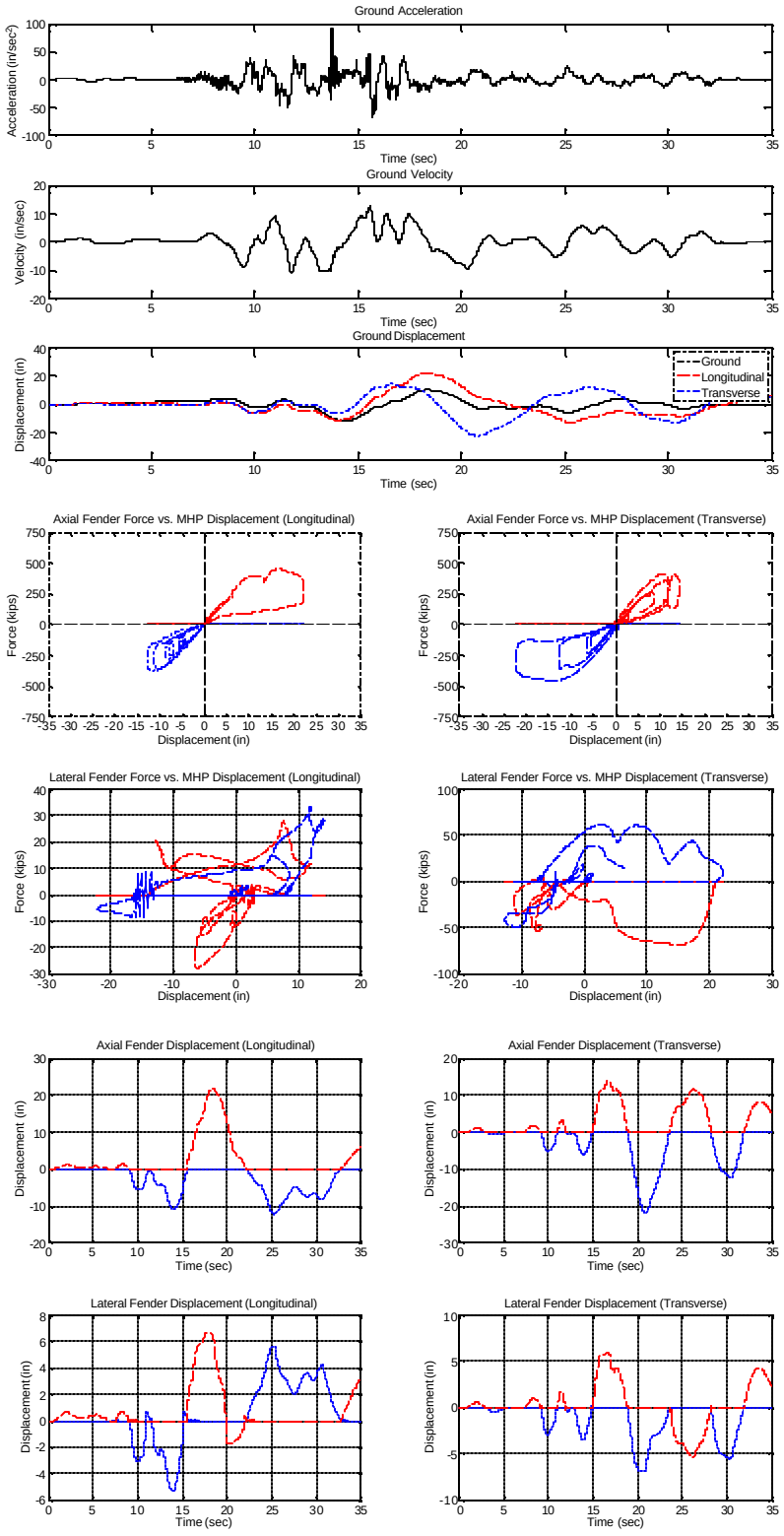

Figure 4.24 - Seismic Response with MV1250 under 1999 Kocaeli - Yarimca (475-year)

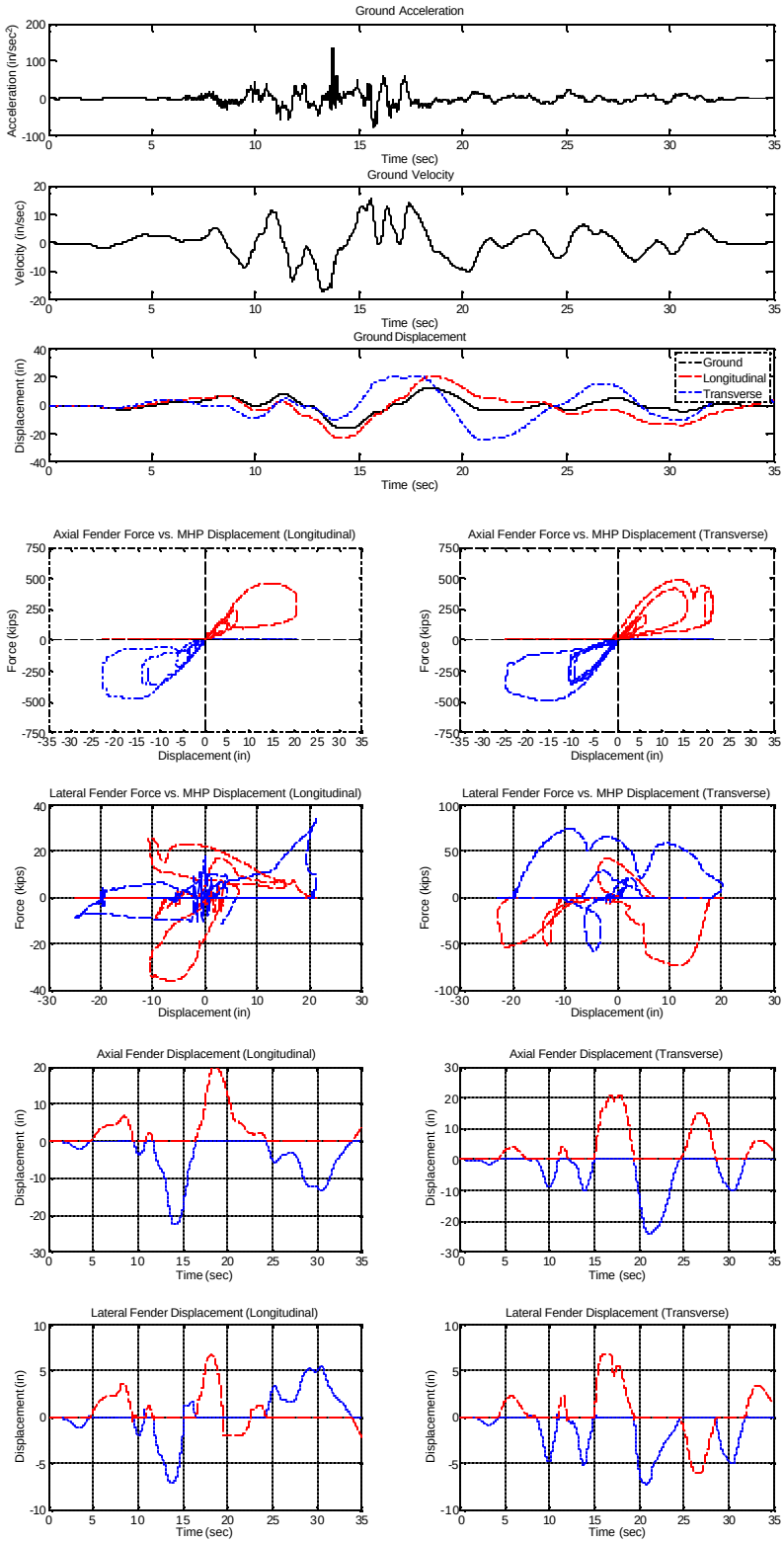

Figure 4.25 - Seismic Response with MV1250 under 1999 Kocaeli - Yarimca (975-year)

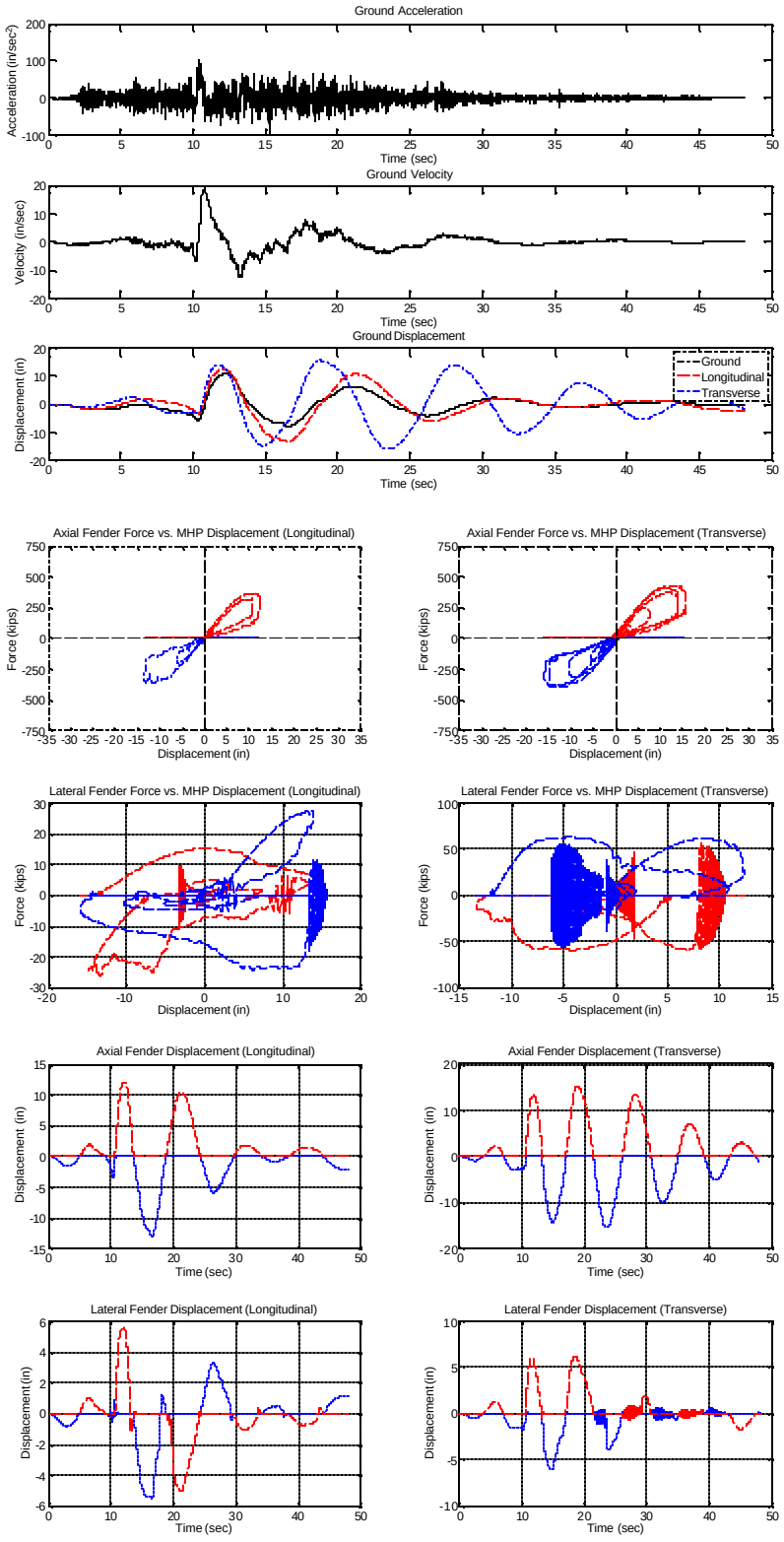

Figure 4.26 - Seismic Response with MV1250 under 1992 Landers - Lucerne (475-year)

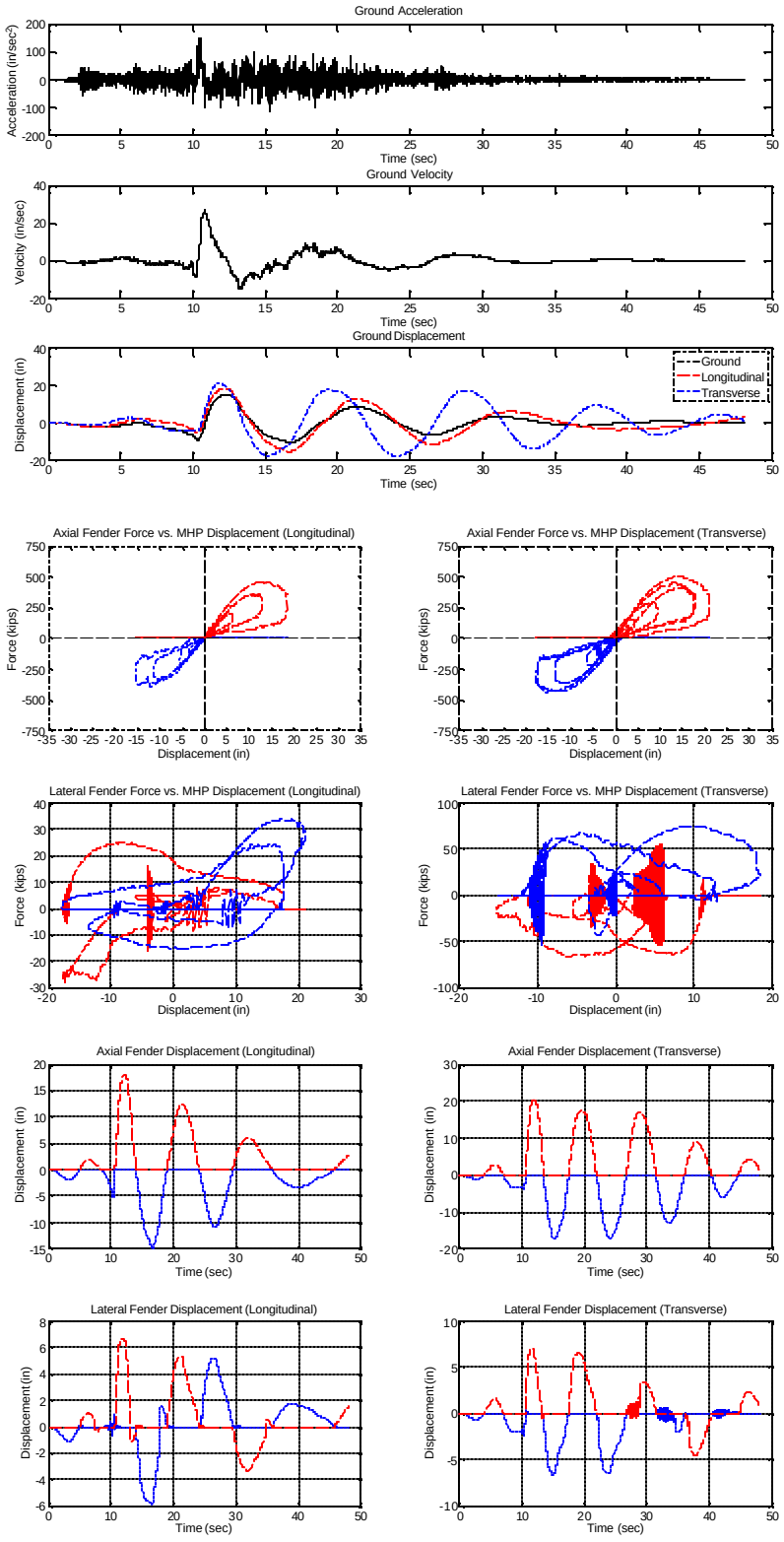

Figure 4.27 - Seismic Response with MV1250 under 1992 Landers - Lucerne (975-year)

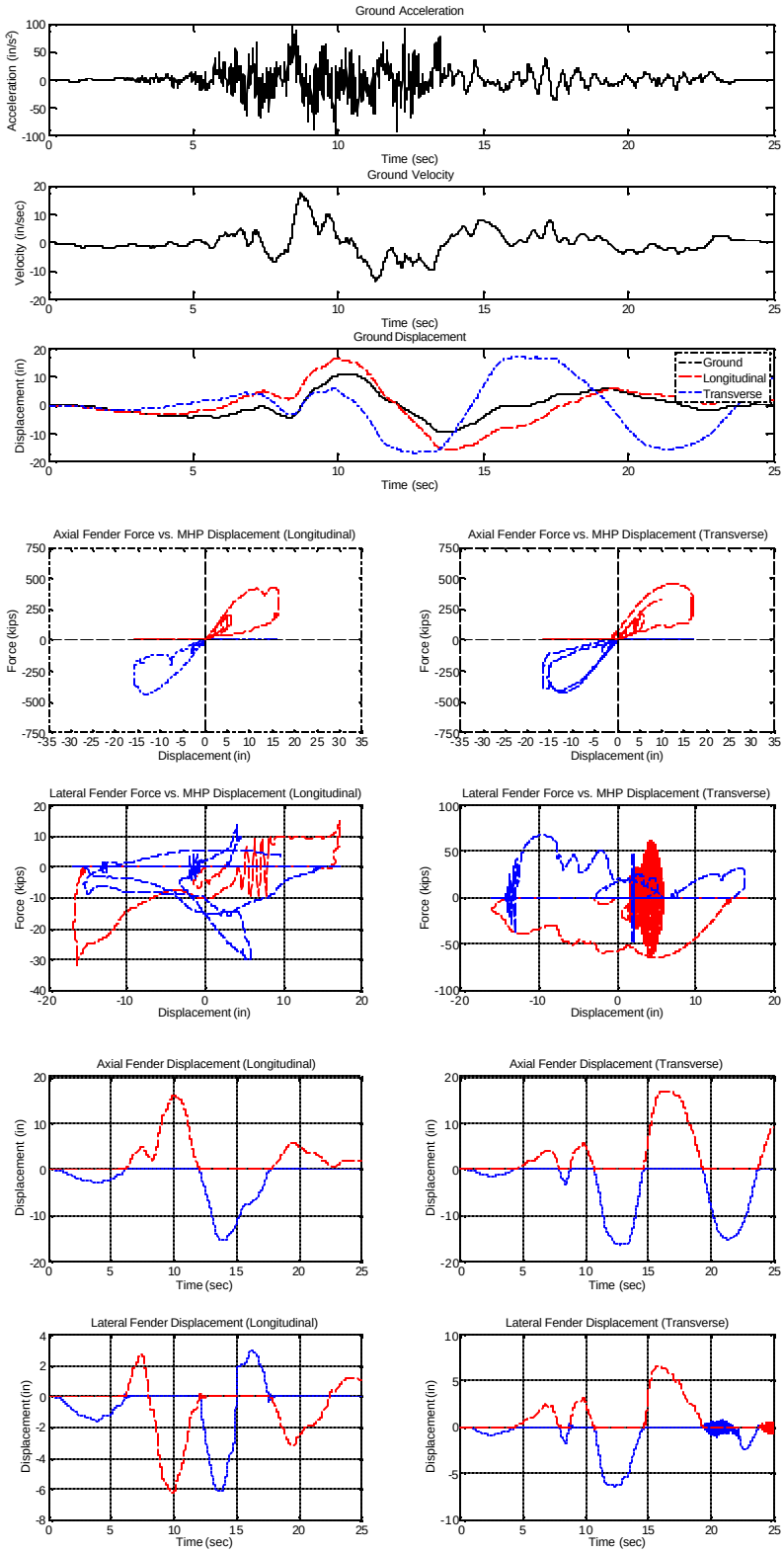

Figure 4.28 - Seismic Response with MV1250 under 1989 Loma Prieta (475-year)

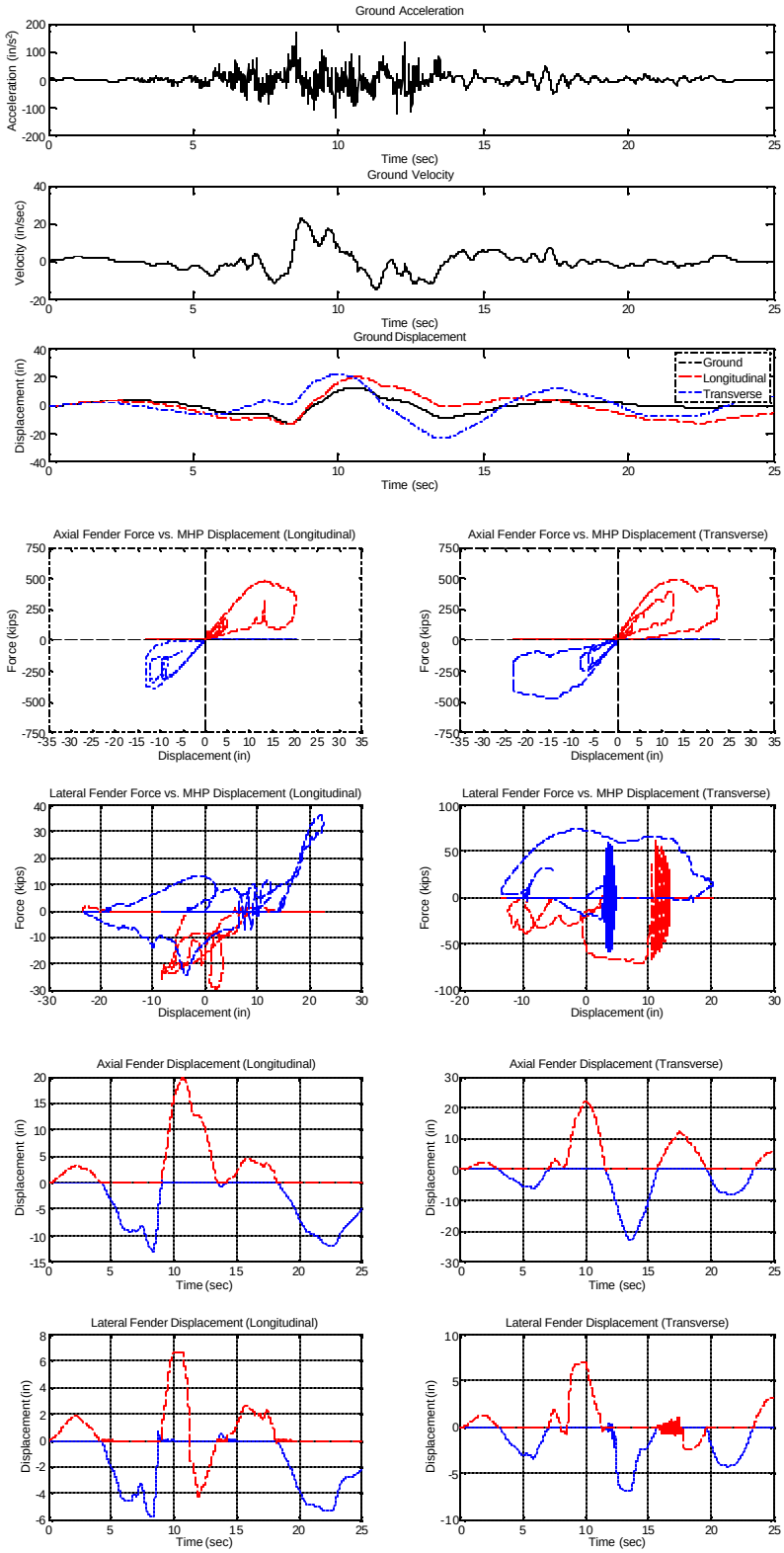

Figure 4.29 - Seismic Response with MV1250 under 1989 Loma Prieta (975-year)

5 Conclusion

5.1 Summary

During the load test of the operations deck of the modular hybrid pier behaved in a linear manner up to the maximum applied load of 500 kips, as predicted by the finite element analyses. However, the deck exhibited a little cracking near the drain hole, which was probably due to the reduction of the pre-compression at the bottom of the deck in the stress transfer zone for the prestress tendons as well as the stress concentration introduced by the drain hole. The cracks were first observed at a load of 500 kips on the west side of the load, but they could have occurred earlier. They closed upon load release. Large tensile strains were also measured at the bottom of the deck on the west side of the load, indicating a high possibility of concrete cracking. In spite of this, the deck performed in a satisfactory manner without structural damage during the load test.

There was no observable damage in the operations deck of the modular hybrid pier during the bollard test, and the bollard performed according to the design requirements in terms of the load capacity. However, the large tensile strains observed at the bottom of the deck on the south side of the bollard could be an indication of minor flexural cracks, which are not of a concern from the serviceability standpoint. There was significant sliding of the bollard base even at the service load level of 200 kips due to the size difference of the anchor bolts and the bolt holes in the deck and also the fact that the bolts were not tightened enough to develop the necessary friction.

The base sliding and uplift and the friction in the moving components are the main cause of the nonlinear load-displacement relation of the bollard observed in the test. However, the strains at the base of the bollard cylinder exhibit a linear relation with the applied load. The loading apparatus performed according to design and can be used in future tests. The observed performance of the bollard-deck system is consistent with the results of the pre-test analyses, which include nonlinear finite element modeling. However, the pre-test finite element model of the pier showed a lower stiffness than the test results.

The analysis and test results have indicated that the base plate of the bollard can be assumed rigid in assessing the tensile stress in the anchor bolts, and that the concrete infill can be ignored in calculating the tensile strain in the bollard cylinder using the simple beam theory. Furthermore, the effective bending width of the deck in resisting the prying action of the bollard can be conservatively assumed to be 10 ft., which is about three times the dimension of the bollard base plate.

The seismic analysis was instrumental in assessing the feasibility of the initial fender configuration. Having found this design to be inadequate, the model was used to validate the redesigned configuration.

5.2 Other Considerations and Recommendations for Future Work

Currently, there is little experimental data available on the punching shear capacity of concrete slabs made of high-strength concrete or subjected to a high prestress level. Further experimental study of this issue is needed to acquire appropriate data to evaluate the current ACI provisions. Finite element models have their limitation in capturing the punching shear capacity of a slab, due to stress locking, and should only be used with caution.

The performance of the operations deck of the modular hybrid pier studied here satisfies the design requirements. However, the design seems to be a little conservative and could probably be further optimized to reduce the weight and cost.

Currently, there is a trend towards double-decked piers in traditional pier construction, as well as for modular hybrid piers. These would have similar bollard design and installations. This study has not provided a conclusive assessment of the load capacity of the weld at the base of the bollard cylinder because of possible limitations of the constitutive models used in the finite element analysis. The capacity of a bollard under different horizontal angles of applied load is also worth further investigation. Laboratory testing of bollards to failure will clarify these issues and provide a definitive assessment of the finite element modeling capability.

The sliding of a bollard is an issue. The clearance between an anchor bolt and the bolt hole should be reduced or adequate tension needs to be specified for the anchor bolts to develop sufficient friction to prevent sliding. The use of a rubber pad

between a bollard and the deck may also reduce the friction. It can be replaced by hydrostone to provide a good contact surface.

Further laboratory tests would be invaluable in calibrating the seismic model. The addition of fluid-structure interaction, the soil dynamics of the site and the soil-pile system, and the deformability of the MHP and the mooring shaft would add to the accuracy and completeness of the model.

6 Bibliography

1. ABAQUS Manual (2006): *Example Problems, Verification, Theory. Version 6.61*, Hibbit, Karlsson and Sorenson, Inc.
2. ACI-318 (2005). *Building Code Requirements for Reinforced Concrete.* American Concrete Institute, Farmington Hills, MI.
3. Bogage, A. et al. (2007). *Bollard Capacity Test for a Modular Hybrid Pier*. UCSD SSRP-07/26. UC San Diego.
4. Bogage, A. et al. (2007). *Load Capacity Tests of Operations Deck of a Modular Hybrid Pier*. UCSD SSRP-07/25. UC San Diego.
5. Chopra, A. (2001). *Dynamics of Structures, Second Edition*, Prentice Hall.
6. Lee, J. et al. (2008). *Modular Hybrid Pier Structural Capacity Tests: Short Term Fender Tests*. UCSD SSRP-07/27. UC San Diego.
7. Trelleborg Marine Systems. (2007).*Safe Berthing and Mooring.* Trelleborg.
8. Wong, I. et al. (2008). *Site-Specific Probabilistic Seismic Hazard Analysis and Development of Time Histories for the Prototype MHP Mooring System Design*. URS Corporation.

7 Appendix

MatLab software used in analysis.

```
%*****************************************************************
%***                                                           ***
%***          Seismic Non-Linear MHP Analysis                  ***
%***                                                           ***
%***  Programmer          :      Adam Bogage                   ***
%***  Date                :      Spring 2008                   ***
%***  Version             :      3.0                           ***
%***  Advisor             :      Professor Shing               ***
%***  File Name           :      Final_MHP.m                   ***
%***                                                           ***
%*****************************************************************
%*****************************************************************

function [] = Final_MHP()

close all
clear all
clc

fprintf(1,'\nSeismic Analysis of the Modular Hybrid Pier\n');
fprintf(1,' \n');
fprintf(1,'\n');

% Fenders
for i=1:6

% fenderProp(i).mass = 3.2/(32.2*12); % UHMW PE pad and 1/2 of fenders
% fenderProp(i).length = 35.43; % in inches (900 mm)
% fenderProp(i).height = 49.2; % in inches (1250 mm)
% fenderProp(i).width = 15.79; % in inches (401 mm)
% fenderProp(i).youngs =  1; %ksi
% fenderProp(i).gap= 0;  % in inches (each side of mooring column)
% fenderProp(i).NumAxial = 8; % Number of Axial fender elements
%
%
% if ( i==1 || i == 2)
%     fenderProp(i).NumAxial = 4; % Number of Axial fender elements
% end


   if ( i==1 || i == 2)
fenderProp(i).mass = 2.076/(32.2*12); % UHMW PE pad and 1/2 of fenders
fenderProp(i).length = 35.4; % in inches (900 mm)
fenderProp(i).height = 39.4; % in inches (1000 mm)
fenderProp(i).width = 12.7; % in inches (322 mm)
fenderProp(i).youngs =  1; %ksi
fenderProp(i).gap= 0.01;  % in inches (each side of mooring column)
fenderProp(i).NumAxial = 4; % Number of Axial fender elements

   else
fenderProp(i).mass = 2.469/(32.2*12); % UHMW PE pad and 1/2 of fenders
fenderProp(i).length = 43.3; % in inches (900 mm)
fenderProp(i).height = 39.2; % in inches (1000 mm)
```

```
fenderProp(i).width = 12.7; % in inches (322 mm)
fenderProp(i).youngs =  1; %ksi
fenderProp(i).gap= 0.01;  % in inches (each side of mooring column)
fenderProp(i).NumAxial = 8; % Number of Axial fender elements

  end

% Deformation (Axial, Lateral)
fenderDef(i).uD = zeros(2,1);  % Displacement (in inches)
fenderDef(i).uDdot = zeros(2,1);   % Velocity
fenderDef(i).uDddot = zeros(2,1);  % Acceleration
% Force
fenderForce(i).RLat(1) = 0;  % Lateral Force Tracking
fenderForce(i).RAxial = 0; % Axial Force Tracking
end

% Initial Constants
% MDOF for MHP
Sv = zeros(3,1);     % Displacement
Svdot = zeros(3,1);  % Velocity
Svddot = zeros(3,1);  % Acceleration

% Timestep
% see forcing function for EQ
dT = .001;        % Timestep for fender

M = Mass();    % Initialize Mass Matrix

% Newmark Constants
gamma = .5;

% Initialize Damping (MHP not Fender (Fluid/Structure)

% Damping Ratio chosen
% z = 0.00;
% w1 = 0.477;
% w2 = 0.954;

% Create Rayleigh Damping Matrix
%a0 = (z*2*w1*w2)/(w1+w2);
%a1 = z*2/(w1+w2);
%C = a0*M + a1*K

% Forcing Function (Time must be updated above)
fid = fopen('loma975.txt','r');
EQData = fscanf(fid,'%g');
fclose(fid);
deltaT = .005;    % Timestep for Pier (from EQ in seconds)

%
   f = 1 * EQData * 32.2*12; % % of EQ in in/s^2
   fdot = cumsum(f)*deltaT;  fdot = fdot - mean(fdot); % vel
   fpos = cumsum(fdot)*deltaT;  fpos = fpos - mean(fpos); %disp
```

```
    % Forcing Function
    forcing = f * ones(1,3);

    F = M * forcing';

length = size(f);

i = 1;

while (i < length(1))


    % MHP displacement step
    Sv(:,i+1) = Sv(:,i) + deltaT*Svdot(:,i) + (deltaT^2/2)*Svddot(:,i);

%%%%%%%%%%%%%%%%%%%%%%%%%%%%%%%%%%%%%%%%%%%%%%%%%
%%%%%%%%%%%%%%%%%%%%%%%%


    %%%%%%%%%%%%%%%%%%%%%%%%%%%%%%
    % Force from non-linear fender %
    %%%%%%%%%%%%%%%%%%%%%%%%%%%%%%

    % Total Disp vector

    changeDisp = (Sv(:,i+1) - Sv(:,i)); % change in MHP displacement (i step)
    steps = deltaT/dT; % Number of fender steps per MHP step
    stepsize = changeDisp / steps; % step for fender (j) iterations

    for p=1:3

        if stepsize(p) ~=0
            disp(p,:) = Sv(p,i):stepsize(p):Sv(p,i+1);
        else
          for w = 1:(steps+1)

            disp(p,w) = (Sv(p,i+1)) ; % Creates vectors of if no change

          end

        end

    end


        %fender loops
        for fnum = 1:6

        [newDef,newForce] =
Fender_final(steps,disp,fenderProp(fnum),fenderDef(fnum).uD(:,i),fenderDef(fnum).uDdot(:,i),fenderD
ef(fnum).uDddot(:,i),fenderForce(fnum).RAxial,fenderForce(fnum).RLat(i),fnum);
```

```
      fenderDef(fnum).uD(1,i+1) = newDef.vD(1);
      fenderDef(fnum).uDdot(1,i+1) = newDef.vDdot(1);
      fenderDef(fnum).uDddot(1,i+1) = newDef.vDddot(1);
      fenderDef(fnum).uD(2,i+1) = newDef.vD(2);
      fenderDef(fnum).uDdot(2,i+1) = newDef.vDdot(2);
      fenderDef(fnum).uDddot(2,i+1) = newDef.vDddot(2);

      fenderForce(fnum).RAxial = newForce.RAxial;
      fenderForce(fnum).RLat(i+1) = newForce.RLat;

      end

      % Axial Force from Fenders in Global
      R(1, i+1) = (fenderForce(1).RAxial + fenderForce(2).RAxial );  % Force in Long. Direction
      R(2, i+1) = (fenderForce(3).RAxial + fenderForce(4).RAxial ); % Force in Transverse 1
      R(3, i+1) = (fenderForce(5).RAxial + fenderForce(6).RAxial ); % Force in Transverse 1

      % Lateral Force from Fenders in Global

      RL(1, i+1) = (fenderForce(3).RLat(i+1) + fenderForce(4).RLat(i+1) + fenderForce(5).RLat(i+1) +
fenderForce(6).RLat(i+1));
      RL(2, i+1) = (fenderForce(1).RLat(i+1) + fenderForce(2).RLat(i+1)); % Force in Transverse 1
      RL(3, i+1) = 0; % Force in Transverse 2


      % Vector of Forces for plotting

      for w=1:6
         Fplot(w,i+1) = fenderForce(w).RAxial;
         LatPlot(w,i+1) = fenderForce(w).RLat(i+1);
      end

   %Calculate Acceleration Step

   %vddot(:,i+1) = inv(M+deltaT*gamma*C)*(F(:,i+1)-R(:,i+1)-C*(vdot(:,i)+deltaT*(1-
gamma)*vddot(:,i)));
    Svddot(:,i+1) = inv(M)*(F(:,i+1)-R(:,i+1)+ RL(:,i+1));

   %Calculate Velocity Step
   Svdot(:,i+1) = Svdot(:,i) + deltaT*((1-gamma)*Svddot(:,i)+ gamma*Svddot(:,i+1));

   time(i+1) = i*deltaT;
   i = i+1;


end


figure('DefaultAxesFontSize',16);

subplot(3,1,1)

plot(time,f,'k', 'LineWidth',2);
```

```
title('Ground Acceleration','fontsize',16)
ylabel('Acceleration (in/sec^2)','fontsize',16)
xlabel('Time (sec)','fontsize',16)
axes('fontsize',16)
subplot(3,1,2)
plot(time,fdot,'k', 'LineWidth',2);
title('Ground Velocity','fontsize',16)
ylabel('Velocity (in/sec)','fontsize',16)
xlabel('Time (sec)','fontsize',16)

subplot(3,1,3)
plot(time,fpos,'k', 'LineWidth',2);
hold on
plot(time,Sv(1,:),'--r', 'LineWidth',2);
plot(time,Sv(2,:),'-.b', 'LineWidth',2);
title('Ground Displacement','fontsize',16)
ylabel('Displacement (in)','fontsize',16)
xlabel('Time (sec)','fontsize',16)
legend('Ground','Longitudinal','Transverse')


% to plot 0 axes lines
xline1 = (-35:35:35);
xline2(3) = (0);
yline1 = (-750:750:750);
yline2(3) = (0);

figure('DefaultAxesFontSize',16);

subplot(2,2,1)
plot (Sv(1,:),Fplot(1,:), 'b', 'LineWidth',2)
hold on

plot (Sv(1,:),Fplot(2,:), '--r', 'LineWidth',2)
plot (xline1, xline2,'k')
plot (yline2,yline1,'k')
axis([-35,35,-750,750])
set(gca,'XTick',-35:5:35)
set(gca,'YTick',-750:250:750)
title('Axial Fender Force vs. MHP Displacement (Longitudinal)','fontsize',16)
xlabel('Displacement (in)','fontsize',16)
ylabel('Force (kips)','fontsize',16)


subplot(2,2,3)
plot (Sv(2,:),LatPlot(1,:),'--r', 'LineWidth',2)
hold on
grid on
plot (Sv(2,:),LatPlot(2,:), 'b', 'LineWidth',2)

title('Lateral Fender Force vs. MHP Displacement (Longitudinal)','fontsize',16)
xlabel('Displacement (in)','fontsize',16)
ylabel('Force (kips)','fontsize',16)
```

```
subplot(2,2,2)
plot (Sv(2,:),Fplot(5,:)/2, 'b', 'LineWidth',2)
hold on

plot (Sv(2,:),Fplot(6,:)/2, '--r', 'LineWidth',2)

plot (xline1, xline2,'k')
plot (yline2,yline1,'k')
axis([-35,35,-750,750])
set(gca,'XTick',-35:5:35)
set(gca,'YTick',-750:250:750)
title('Axial Fender Force vs. MHP Displacement (Transverse)','fontsize',16)
xlabel('Displacement (in)','fontsize',16)
ylabel('Force (kips)','fontsize',16)

subplot(2,2,4)
plot (Sv(1,:),LatPlot(5,:), '--r', 'LineWidth',2)
hold on
grid on
plot (Sv(1,:),LatPlot(6,:), 'b', 'LineWidth',2)

title('Lateral Fender Force vs. MHP Displacement (Transverse)','fontsize',16)
xlabel('Displacement (in)','fontsize',16)
ylabel('Force (kips)','fontsize',16)


figure('DefaultAxesFontSize',16);

subplot(2,2,1)
plot (time,fenderDef(1).uD(1,:), 'b', 'LineWidth',2)
grid on
hold on
plot (time,fenderDef(2).uD(1,:), '--r', 'LineWidth',2)
title('Axial Fender Displacement (Longitudinal)','fontsize',16)
xlabel('Time (sec)','fontsize',16)
ylabel('Displacement (in)','fontsize',16)

subplot(2,2,2)
plot (time,fenderDef(3).uD(1,:), 'b', 'LineWidth',2)
grid on
hold on
plot (time,fenderDef(4).uD(1,:), '--r', 'LineWidth',2)
title('Axial Fender Displacement (Transverse)','fontsize',16)
xlabel('Time (sec)','fontsize',16)
ylabel('Displacement (in)','fontsize',16)

subplot(2,2,3)
plot (time,fenderDef(1).uD(2,:), 'b', 'LineWidth',2)
grid on
hold on
plot (time,fenderDef(2).uD(2,:), '--r', 'LineWidth',2)
```

```
title('Lateral Fender Displacement (Longitudinal)','fontsize',16)
xlabel('Time (sec)','fontsize',16)
ylabel('Displacement (in)','fontsize',16)

subplot(2,2,4)
plot (time,fenderDef(3).uD(2,:), 'b', 'LineWidth',2)
grid on
hold on
plot (time,fenderDef(4).uD(2,:), '--r', 'LineWidth',2)
title('Lateral Fender Displacement (Transverse)','fontsize',16)
xlabel('Time (sec)','fontsize',16)
ylabel('Displacement (in)','fontsize',16)

%title('1979 Imperial Valley - El Centro #5 (475 year)')
%title('1979 Imperial Valley - El Centro #5 (975 year)')
%title('1995 Kobe, Japan - KJMA (475 year)')
%title('1995 Kobe, Japan - KJMA (975 year)')
%title('1999 Koccaeli - Yarimca (475-year)')
%title('1999 Koccaeli - Yarimca (975-year)')
%title('1992 Landers - Lucerne (475 years)')
%title('1992 Landers - Lucerne (975 years)')
%title('1989 Loma Prieta - LGPC (475 year)')
%title('1989 Loma Prieta - LGPC (975 year)')

% figure
% plot (v(3,:),Fplot(5,:), 'b', 'LineWidth',2)
% hold on
% plot (v(3,:),Fplot(6,:), 'b', 'LineWidth',2)
% title('Force inparted to MHP from fenders')
% xlabel('Disp')
% ylabel('Force')


fprintf(1,'\nSeismic Analysis Successful\n');
fprintf(1,'\nSee Output\n');
fprintf(1,' \n');

end
```

```
%*****************************************************************
%***                                                           ***
%***          Seismic Non-Linear MHP Analysis                  ***
%***                                                           ***
%***  Programmer            :      Adam Bogage          ***
%***  Date                  :      Spring 2008          ***
%***  Version               :      3.0                  ***
%***  Advisor               :      Professor Shing      ***
%***  File Name             :      Final_MHP.m          ***
%***                                                           ***
%*****************************************************************
%*****************************************************************

function [] = Final_MHP()

close all
clear all
clc

fprintf(1,'\nSeismic Analysis of the Modular Hybrid Pier\n');
fprintf(1,' \n');
fprintf(1,'\n');

% Fenders
for i=1:6
fenderProp(i).mass = 3.2/(32.2*12); % UHMW PE pad and 1/2 of fenders
fenderProp(i).length = 35.43; % in inches (900 mm)
fenderProp(i).height = 49.2; % in inches (1250 mm)
fenderProp(i).width = 15.79; % in inches (401 mm)
fenderProp(i).youngs =  1; %ksi
fenderProp(i).gap= 0;  % in inches (each side of mooring column)
fenderProp(i).NumAxial = 8; % Number of Axial fender elements


if ( i==1 || i == 2)
   fenderProp(i).NumAxial = 4; % Number of Axial fender elements
end


%     if ( i==1 || i == 2)
% fenderProp(i).mass = 2.076/(32.2*12); % UHMW PE pad and 1/2 of fenders
% fenderProp(i).length = 35.4; % in inches (900 mm)
% fenderProp(i).width = 12.7; % in inches (322 mm)
% fenderProp(i).youngs =  20; %ksi
% fenderProp(i).gap= 0.01;  % in inches (each side of mooring column)
% fenderProp(i).NumAxial = 4; % Number of Axial fender elements
%
%    else
% fenderProp(i).mass = 2.469/(32.2*12); % UHMW PE pad and 1/2 of fenders
% fenderProp(i).length = 43.3; % in inches (900 mm)
% fenderProp(i).width = 12.7; % in inches (322 mm)
% fenderProp(i).youngs =  20; %ksi
% fenderProp(i).gap= 0.01;  % in inches (each side of mooring column)
```

```
% fenderProp(i).NumAxial = 8; % Number of Axial fender elements

%    end

% Deformation (Axial, Lateral)
fenderDef(i).uD = zeros(2,1);  % Displacement (in inches)
fenderDef(i).uDdot = zeros(2,1);   % Velocity
fenderDef(i).uDddot = zeros(2,1);  % Acceleration
% Force
fenderForce(i).RLat(1) = 0;  % Lateral Force Tracking
fenderForce(i).RAxial = 0; % Axial Force Tracking
end

% Initial Constants
% MDOF for MHP
Sv = zeros(3,1);     % Displacement
Svdot = zeros(3,1);  % Velocity
Svddot = zeros(3,1);  % Acceleration

% Timestep
% see forcing function for EQ
dT = .001;        % Timestep for fender

M = Mass();    % Initialize Mass Matrix

% Newmark Constants
gamma = .5;

% Initialize Damping (MHP not Fender (Fluid/Structure)

% Damping Ratio chosen
% z = 0.00;
% w1 = 0.477;
% w2 = 0.954;

% Create Rayleigh Damping Matrix
%a0 = (z*2*w1*w2)/(w1+w2);
%a1 = z*2/(w1+w2);
%C = a0*M + a1*K

% Forcing Function (Time must be updated above)
fid = fopen('Kobe975.txt','r');
EQData = fscanf(fid,'%g');
fclose(fid);
deltaT = .02;    % Timestep for Pier (from EQ in seconds)

%
   f = 1 * EQData * 32.2*12; % % of EQ in in/s^2
   fdot = cumsum(f)*deltaT;  fdot = fdot - mean(fdot); % vel
   fpos = cumsum(fdot)*deltaT;  fpos = fpos - mean(fpos); %disp

  % Forcing Function
   forcing = f * ones(1,3);
```

```
    F = M * forcing';

length = size(f);

i = 1;

while (i < length(1))


   % MHP displacement step
    Sv(:,i+1) = Sv(:,i) + deltaT*Svdot(:,i) + (deltaT^2/2)*Svddot(:,i);

%%%%%%%%%%%%%%%%%%%%%%%%%%%%%%%%%%%%%%%%%%%%%%%%%%%%%%%%%%%%%%%%%%%%%%%%%%%%%%%%%%%%%%%%%%%%%%%%%%%%
%%%%%%%%%%%%%%%%%%%%%%%%%%%%%%%%%%%%%%%%%%


   %%%%%%%%%%%%%%%%%%%%%%%%%%%%%%%%%%%%%%%%%%%%%%%%%%%%%%%%%%%%%%%%%
   % Force from non-linear fender %
   %%%%%%%%%%%%%%%%%%%%%%%%%%%%%%%%%%%%%%%%%%%%%%%%%%%%%%%%%%%%%%%%%

   % Total Disp vector

   changeDisp = (Sv(:,i+1) - Sv(:,i)); % change in MHP displacement (i step)
   steps = deltaT/dT; % Number of fender steps per MHP step
   stepsize = changeDisp / steps; % step for fender (j) iterations

   for p=1:3

      if stepsize(p) ~=0
          disp(p,:) = Sv(p,i):stepsize(p):Sv(p,i+1);
      else
         for w = 1:(steps+1)

          disp(p,w) = (Sv(p,i+1)) ; % Creates vectors of if no change

         end

       end

   end


      %fender loops
      for fnum = 1:6

      [newDef,newForce] =
Fender_1250_final(steps,disp,fenderProp(fnum),fenderDef(fnum).uD(:,i),fenderDef(fnum).uDdot(:,i),fe
nderDef(fnum).uDddot(:,i),fenderForce(fnum).RAxial,fenderForce(fnum).RLat(i),fnum);

      fenderDef(fnum).uD(1,i+1) = newDef.vD(1);
      fenderDef(fnum).uDdot(1,i+1) = newDef.vDdot(1);
      fenderDef(fnum).uDddot(1,i+1) = newDef.vDddot(1);
```

```
        fenderDef(fnum).uD(2,i+1) = newDef.vD(2);
        fenderDef(fnum).uDdot(2,i+1) = newDef.vDdot(2);
        fenderDef(fnum).uDddot(2,i+1) = newDef.vDddot(2);

        fenderForce(fnum).RAxial = newForce.RAxial;
        fenderForce(fnum).RLat(i+1) = newForce.RLat;

        end

        % Axial Force from Fenders in Global
        R(1, i+1) = (fenderForce(1).RAxial + fenderForce(2).RAxial );  % Force in Long. Direction
        R(2, i+1) = (fenderForce(3).RAxial + fenderForce(4).RAxial ); % Force in Transverse 1
        R(3, i+1) = (fenderForce(5).RAxial + fenderForce(6).RAxial ); % Force in Transverse 1

        % Lateral Force from Fenders in Global

        RL(1, i+1) = (fenderForce(3).RLat(i+1) + fenderForce(4).RLat(i+1) + fenderForce(5).RLat(i+1) +
fenderForce(6).RLat(i+1));
        RL(2, i+1) = (fenderForce(1).RLat(i+1) + fenderForce(2).RLat(i+1)); % Force in Transverse 1
        RL(3, i+1) = 0; % Force in Transverse 2


        % Vector of Forces for plotting

        for w=1:6
            Fplot(w,i+1) = fenderForce(w).RAxial;
            LatPlot(w,i+1) = fenderForce(w).RLat(i+1);
        end

    %Calculate Acceleration Step

    %vddot(:,i+1) = inv(M+deltaT*gamma*C)*(F(:,i+1)-R(:,i+1)-C*(vdot(:,i)+deltaT*(1-
gamma)*vddot(:,i)));
    Svddot(:,i+1) = inv(M)*(F(:,i+1)-R(:,i+1)+ RL(:,i+1));

    %Calculate Velocity Step
    Svdot(:,i+1) = Svdot(:,i) + deltaT*((1-gamma)*Svddot(:,i)+ gamma*Svddot(:,i+1));

    time(i+1) = i*deltaT;
    i = i+1;


end


figure('DefaultAxesFontSize',16);

subplot(3,1,1)

plot(time,f,'k', 'LineWidth',2);
title('Ground Acceleration','fontsize',16)
ylabel('Acceleration (in/sec^2)','fontsize',16)
xlabel('Time (sec)','fontsize',16)
```

```
axes('fontsize',16)
subplot(3,1,2)
plot(time,fdot,'k', 'LineWidth',2);
title('Ground Velocity','fontsize',16)
ylabel('Velocity (in/sec)','fontsize',16)
xlabel('Time (sec)','fontsize',16)

subplot(3,1,3)
plot(time,fpos,'k', 'LineWidth',2);
hold on
plot(time,Sv(1,:),'--r', 'LineWidth',2);
plot(time,Sv(2,:),'-.b', 'LineWidth',2);
title('Ground Displacement','fontsize',16)
ylabel('Displacement (in)','fontsize',16)
xlabel('Time (sec)','fontsize',16)
legend('Ground','Longitudinal','Transverse')


% to plot 0 axes lines
xline1 = (-35:35:35);
xline2(3) = (0);
yline1 = (-750:750:750);
yline2(3) = (0);

figure('DefaultAxesFontSize',16);

subplot(2,2,1)
plot (Sv(1,:),Fplot(1,:), 'b', 'LineWidth',2)
hold on

plot (Sv(1,:),Fplot(2,:), '--r', 'LineWidth',2)
plot (xline1, xline2,'k')
plot (yline2,yline1,'k')
axis([-35,35,-750,750])
set(gca,'XTick',-35:5:35)
set(gca,'YTick',-750:250:750)
title('Axial Fender Force vs. MHP Displacement (Longitudinal)','fontsize',16)
xlabel('Displacement (in)','fontsize',16)
ylabel('Force (kips)','fontsize',16)


subplot(2,2,3)
plot (Sv(2,:),LatPlot(1,:),'--r', 'LineWidth',2)
hold on
grid on
plot (Sv(2,:),LatPlot(2,:), 'b', 'LineWidth',2)

title('Lateral Fender Force vs. MHP Displacement (Longitudinal)','fontsize',16)
xlabel('Displacement (in)','fontsize',16)
ylabel('Force (kips)','fontsize',16)


subplot(2,2,2)
```

```
plot (Sv(2,:),Fplot(5,:)/2, 'b', 'LineWidth',2)
hold on

plot (Sv(2,:),Fplot(6,:)/2, '--r', 'LineWidth',2)

plot (xline1, xline2,'k')
plot (yline2,yline1,'k')
axis([-35,35,-750,750])
set(gca,'XTick',-35:5:35)
set(gca,'YTick',-750:250:750)
title('Axial Fender Force vs. MHP Displacement (Transverse)','fontsize',16)
xlabel('Displacement (in)','fontsize',16)
ylabel('Force (kips)','fontsize',16)

subplot(2,2,4)
plot (Sv(1,:),LatPlot(5,:), '--r', 'LineWidth',2)
hold on
grid on
plot (Sv(1,:),LatPlot(6,:), 'b', 'LineWidth',2)

title('Lateral Fender Force vs. MHP Displacement (Transverse)','fontsize',16)
xlabel('Displacement (in)','fontsize',16)
ylabel('Force (kips)','fontsize',16)


figure('DefaultAxesFontSize',16);

subplot(2,2,1)
plot (time,fenderDef(1).uD(1,:), 'b', 'LineWidth',2)
grid on
hold on
plot (time,fenderDef(2).uD(1,:), '--r', 'LineWidth',2)
title('Axial Fender Displacement (Longitudinal)','fontsize',16)
xlabel('Time (sec)','fontsize',16)
ylabel('Displacement (in)','fontsize',16)

subplot(2,2,2)
plot (time,fenderDef(3).uD(1,:), 'b', 'LineWidth',2)
grid on
hold on
plot (time,fenderDef(4).uD(1,:), '--r', 'LineWidth',2)
title('Axial Fender Displacement (Transverse)','fontsize',16)
xlabel('Time (sec)','fontsize',16)
ylabel('Displacement (in)','fontsize',16)

subplot(2,2,3)
plot (time,fenderDef(1).uD(2,:), 'b', 'LineWidth',2)
grid on
hold on
plot (time,fenderDef(2).uD(2,:), '--r', 'LineWidth',2)
title('Lateral Fender Displacement (Longitudinal)','fontsize',16)
xlabel('Time (sec)','fontsize',16)
ylabel('Displacement (in)','fontsize',16)
```

```
subplot(2,2,4)
plot (time,fenderDef(3).uD(2,:), 'b', 'LineWidth',2)
grid on
hold on
plot (time,fenderDef(4).uD(2,:), '--r', 'LineWidth',2)
title('Lateral Fender Displacement (Transverse)','fontsize',16)
xlabel('Time (sec)','fontsize',16)
ylabel('Displacement (in)','fontsize',16)

%title('1979 Imperial Valley - El Centro #5 (475 year)')
%title('1979 Imperial Valley - El Centro #5 (975 year)')
%title('1995 Kobe, Japan - KJMA (475 year)')
%title('1995 Kobe, Japan - KJMA (975 year)')
%title('1999 Koccaeli - Yarimca (475-year)')
%title('1999 Koccaeli - Yarimca (975-year)')
%title('1992 Landers - Lucerne (475 years)')
%title('1992 Landers - Lucerne (975 years)')
%title('1989 Loma Prieta - LGPC (475 year)')
%title('1989 Loma Prieta - LGPC (975 year)')

% figure
% plot (v(3,:),Fplot(5,:), 'b', 'LineWidth',2)
% hold on
% plot (v(3,:),Fplot(6,:), 'b', 'LineWidth',2)
% title('Force inparted to MHP from fenders')
% xlabel('Disp')
% ylabel('Force')


fprintf(1,'\nSeismic Analysis Successful\n');
fprintf(1,'\nSee Output\n');
fprintf(1,' \n');

end
```

```
%*****************************************************************
%***                                                           ***
%***          Seismic Non-Linear MHP Analysis                  ***
%***                                                           ***
%***  Programmer            :      Adam Bogage          ***
%***  Date                  :      Spring 2008          ***
%***  Version               :      3.0                  ***
%***  Advisor               :      Professor Shing      ***
%***  File Name             :      Final_MHP.m          ***
%***                                                           ***
%*****************************************************************
%*****************************************************************

function [] = Final_MHP()

close all
clear all
clc

fprintf(1,'\nSeismic Analysis of the Modular Hybrid Pier\n');
fprintf(1,' \n');
fprintf(1,'\n');

% Fenders
for i=1:6

% fenderProp(i).mass = 3.2/(32.2*12); % UHMW PE pad and 1/2 of fenders
% fenderProp(i).length = 35.43; % in inches (900 mm)
% fenderProp(i).height = 49.2; % in inches (1250 mm)
% fenderProp(i).width = 15.79; % in inches (401 mm)
% fenderProp(i).youngs =  1; %ksi
% fenderProp(i).gap= 0;  % in inches (each side of mooring column)
% fenderProp(i).NumAxial = 8; % Number of Axial fender elements
%
%
% if ( i==1 || i == 2)
%     fenderProp(i).NumAxial = 4; % Number of Axial fender elements
% end


   if ( i==1 || i == 2)
fenderProp(i).mass = 2.076/(32.2*12); % UHMW PE pad and 1/2 of fenders
fenderProp(i).length = 35.4; % in inches (900 mm)
fenderProp(i).height = 39.4; % in inches (1000 mm)
fenderProp(i).width = 12.7; % in inches (322 mm)
fenderProp(i).youngs =  1; %ksi
fenderProp(i).gap= 0.01;  % in inches (each side of mooring column)
fenderProp(i).NumAxial = 4; % Number of Axial fender elements

   else
fenderProp(i).mass = 2.469/(32.2*12); % UHMW PE pad and 1/2 of fenders
fenderProp(i).length = 43.3; % in inches (900 mm)
fenderProp(i).height = 39.2; % in inches (1000 mm)
```

```
fenderProp(i).width = 12.7; % in inches (322 mm)
fenderProp(i).youngs =  1; %ksi
fenderProp(i).gap= 0.01;  % in inches (each side of mooring column)
fenderProp(i).NumAxial = 8; % Number of Axial fender elements

  end

% Deformation (Axial, Lateral)
fenderDef(i).uD = zeros(2,1);  % Displacement (in inches)
fenderDef(i).uDdot = zeros(2,1);   % Velocity
fenderDef(i).uDddot = zeros(2,1);  % Acceleration
% Force
fenderForce(i).RLat(1) = 0;  % Lateral Force Tracking
fenderForce(i).RAxial = 0; % Axial Force Tracking
end

% Initial Constants
% MDOF for MHP
Sv = zeros(3,1);     % Displacement
Svdot = zeros(3,1);  % Velocity
Svddot = zeros(3,1);  % Acceleration

% Timestep
% see forcing function for EQ
dT = .001;        % Timestep for fender

M = Mass();    % Initialize Mass Matrix

% Newmark Constants
gamma = .5;

% Initialize Damping (MHP not Fender (Fluid/Structure)

% Damping Ratio chosen
% z = 0.00;
% w1 = 0.477;
% w2 = 0.954;

% Create Rayleigh Damping Matrix
%a0 = (z*2*w1*w2)/(w1+w2);
%a1 = z*2/(w1+w2);
%C = a0*M + a1*K

% Forcing Function (Time must be updated above)
fid = fopen('Kobe975.txt','r');
EQData = fscanf(fid,'%g');
fclose(fid);
deltaT = .02;    % Timestep for Pier (from EQ in seconds)

%
   f = EQData * 32.2*12; % % of EQ in in/s^2
```

```
   fdot = cumsum(f)*deltaT;  fdot = fdot - mean(fdot); % vel
   fpos = cumsum(fdot)*deltaT;  fpos = fpos - mean(fpos); %disp



   % Forcing Function
   forcing = f * ones(1,3);

   F = M * forcing';

length = size(f);

i = 1;

while (i < length(1))


   % MHP displacement step
   Sv(:,i+1) = Sv(:,i) + deltaT*Svdot(:,i) + (deltaT^2/2)*Svddot(:,i);

%%%%%%%%%%%%%%%%%%%%%%%%%%%%%%%%%%%%%%%%%%%%%%%%%%%%%%%%%%%%%%%%%%%%%%%%
%%%%%%%%%%%%%%%%%%%%%%%%%


   %%%%%%%%%%%%%%%%%%%%%%%%%%%%%%%%%
   % Force from non-linear fender %
   %%%%%%%%%%%%%%%%%%%%%%%%%%%%%%%%%

   % Total Disp vector

   changeDisp = (Sv(:,i+1) - Sv(:,i)); % change in MHP displacement (i step)
   steps = deltaT/dT; % Number of fender steps per MHP step
   stepsize = changeDisp / steps; % step for fender (j) iterations

   for p=1:3

      if stepsize(p) ~=0
         disp(p,:) = Sv(p,i):stepsize(p):Sv(p,i+1);
      else
        for w = 1:(steps+1)

         disp(p,w) = (Sv(p,i+1)) ; % Creates vectors of if no change

        end

       end

   end


      %fender loops
```

```
        for fnum = 1:6

        [newDef,newForce] =
Fender_1000_final(steps,disp,fenderProp(fnum),fenderDef(fnum).uD(:,i),fenderDef(fnum).uDdot(:,i),fe
nderDef(fnum).uDddot(:,i),fenderForce(fnum).RAxial,fenderForce(fnum).RLat(i),fnum);

        fenderDef(fnum).uD(1,i+1) = newDef.vD(1);
        fenderDef(fnum).uDdot(1,i+1) = newDef.vDdot(1);
        fenderDef(fnum).uDddot(1,i+1) = newDef.vDddot(1);
        fenderDef(fnum).uD(2,i+1) = newDef.vD(2);
        fenderDef(fnum).uDdot(2,i+1) = newDef.vDdot(2);
        fenderDef(fnum).uDddot(2,i+1) = newDef.vDddot(2);

        fenderForce(fnum).RAxial = newForce.RAxial;
        fenderForce(fnum).RLat(i+1) = newForce.RLat;

        end

        % Axial Force from Fenders in Global
        R(1, i+1) = (fenderForce(1).RAxial + fenderForce(2).RAxial );  % Force in Long. Direction
        R(2, i+1) = (fenderForce(3).RAxial + fenderForce(4).RAxial ); % Force in Transverse 1
        R(3, i+1) = (fenderForce(5).RAxial + fenderForce(6).RAxial ); % Force in Transverse 1

        % Lateral Force from Fenders in Global

        RL(1, i+1) = (fenderForce(3).RLat(i+1) + fenderForce(4).RLat(i+1) + fenderForce(5).RLat(i+1) +
fenderForce(6).RLat(i+1));
        RL(2, i+1) = (fenderForce(1).RLat(i+1) + fenderForce(2).RLat(i+1)); % Force in Transverse 1
        RL(3, i+1) = 0; % Force in Transverse 2


        % Vector of Forces for plotting

        for w=1:6
            Fplot(w,i+1) = fenderForce(w).RAxial;
            LatPlot(w,i+1) = fenderForce(w).RLat(i+1);
        end

    %Calculate Acceleration Step

    %vddot(:,i+1) = inv(M+deltaT*gamma*C)*(F(:,i+1)-R(:,i+1)-C*(vdot(:,i)+deltaT*(1-
gamma)*vddot(:,i)));
    Svddot(:,i+1) = inv(M)*(F(:,i+1)-R(:,i+1)+ RL(:,i+1));

    %Calculate Velocity Step
    Svdot(:,i+1) = Svdot(:,i) + deltaT*((1-gamma)*Svddot(:,i)+ gamma*Svddot(:,i+1));

    time(i+1) = i*deltaT;
    i = i+1;


end
```

```
figure('DefaultAxesFontSize',16);

subplot(3,1,1)

plot(time,f,'k', 'LineWidth',2);
title('Ground Acceleration','fontsize',16)
ylabel('Acceleration (in/sec^2)','fontsize',16)
xlabel('Time (sec)','fontsize',16)
axes('fontsize',16)
subplot(3,1,2)
plot(time,fdot,'k', 'LineWidth',2);
title('Ground Velocity','fontsize',16)
ylabel('Velocity (in/sec)','fontsize',16)
xlabel('Time (sec)','fontsize',16)

subplot(3,1,3)
plot(time,fpos,'k', 'LineWidth',2);
hold on
plot(time,Sv(1,:),'--r', 'LineWidth',2);
plot(time,Sv(2,:),'-.b', 'LineWidth',2);
title('Ground Displacement','fontsize',16)
ylabel('Displacement (in)','fontsize',16)
xlabel('Time (sec)','fontsize',16)
legend('Ground','Longitudinal','Transverse')


% to plot 0 axes lines
xline1 = (-35:35:35);
xline2(3) = (0);
yline1 = (-750:750:750);
yline2(3) = (0);

figure('DefaultAxesFontSize',16);

subplot(2,2,1)
plot (Sv(1,:),Fplot(1,:), 'b', 'LineWidth',2)
hold on

plot (Sv(1,:),Fplot(2,:), '--r', 'LineWidth',2)
plot (xline1, xline2,'k')
plot (yline2,yline1,'k')
axis([-35,35,-750,750])
set(gca,'XTick',-35:5:35)
set(gca,'YTick',-750:250:750)
title('Axial Fender Force vs. MHP Displacement (Longitudinal)','fontsize',16)
xlabel('Displacement (in)','fontsize',16)
ylabel('Force (kips)','fontsize',16)


subplot(2,2,3)
plot (Sv(2,:),LatPlot(1,:),'--r', 'LineWidth',2)
hold on
```

```
grid on
plot (Sv(2,:),LatPlot(2,:), 'b', 'LineWidth',2)

title('Lateral Fender Force vs. MHP Displacement (Longitudinal)','fontsize',16)
xlabel('Displacement (in)','fontsize',16)
ylabel('Force (kips)','fontsize',16)


subplot(2,2,2)
plot (Sv(2,:),Fplot(5,:)/2, 'b', 'LineWidth',2)
hold on

plot (Sv(2,:),Fplot(6,:)/2, '--r', 'LineWidth',2)

plot (xline1, xline2,'k')
plot (yline2,yline1,'k')
axis([-35,35,-750,750])
set(gca,'XTick',-35:5:35)
set(gca,'YTick',-750:250:750)
title('Axial Fender Force vs. MHP Displacement (Transverse)','fontsize',16)
xlabel('Displacement (in)','fontsize',16)
ylabel('Force (kips)','fontsize',16)

subplot(2,2,4)
plot (Sv(1,:),LatPlot(5,:), '--r', 'LineWidth',2)
hold on
grid on
plot (Sv(1,:),LatPlot(6,:), 'b', 'LineWidth',2)

title('Lateral Fender Force vs. MHP Displacement (Transverse)','fontsize',16)
xlabel('Displacement (in)','fontsize',16)
ylabel('Force (kips)','fontsize',16)


figure('DefaultAxesFontSize',16);

subplot(2,2,1)
plot (time,fenderDef(1).uD(1,:), 'b', 'LineWidth',2)
grid on
hold on
plot (time,fenderDef(2).uD(1,:), '--r', 'LineWidth',2)
title('Axial Fender Displacement (Longitudinal)','fontsize',16)
xlabel('Time (sec)','fontsize',16)
ylabel('Displacement (in)','fontsize',16)

subplot(2,2,2)
plot (time,fenderDef(3).uD(1,:), 'b', 'LineWidth',2)
grid on
hold on
plot (time,fenderDef(4).uD(1,:), '--r', 'LineWidth',2)
title('Axial Fender Displacement (Transverse)','fontsize',16)
xlabel('Time (sec)','fontsize',16)
ylabel('Displacement (in)','fontsize',16)
```

```
subplot(2,2,3)
plot (time,fenderDef(1).uD(2,:), 'b', 'LineWidth',2)
grid on
hold on
plot (time,fenderDef(2).uD(2,:), '--r', 'LineWidth',2)
title('Lateral Fender Displacement (Longitudinal)','fontsize',16)
xlabel('Time (sec)','fontsize',16)
ylabel('Displacement (in)','fontsize',16)

subplot(2,2,4)
plot (time,fenderDef(3).uD(2,:), 'b', 'LineWidth',2)
grid on
hold on
plot (time,fenderDef(4).uD(2,:), '--r', 'LineWidth',2)
title('Lateral Fender Displacement (Transverse)','fontsize',16)
xlabel('Time (sec)','fontsize',16)
ylabel('Displacement (in)','fontsize',16)

%title('1979 Imperial Valley - El Centro #5 (475 year)')
%title('1979 Imperial Valley - El Centro #5 (975 year)')
%title('1995 Kobe, Japan - KJMA (475 year)')
%title('1995 Kobe, Japan - KJMA (975 year)')
%title('1999 Koccaeli - Yarimca (475-year)')
%title('1999 Koccaeli - Yarimca (975-year)')
%title('1992 Landers - Lucerne (475 years)')
%title('1992 Landers - Lucerne (975 years)')
%title('1989 Loma Prieta - LGPC (475 year)')
%title('1989 Loma Prieta - LGPC (975 year)')

% figure
% plot (v(3,:),Fplot(5,:), 'b', 'LineWidth',2)
% hold on
% plot (v(3,:),Fplot(6,:), 'b', 'LineWidth',2)
% title('Force inparted to MHP from fenders')
% xlabel('Disp')
% ylabel('Force')

fprintf(1,'\nSeismic Analysis Successful\n');
fprintf(1,'\nSee Output\n');
fprintf(1,' \n');

end
```

```
%*****************************************************************
%***                                                           ***
%***          Fender Behavior - MHP Analysis                   ***
%***                                                           ***
%***  Programmer          :      Adam Bogage                   ***
%***  Date                :      Spring 2008                   ***
%***  Version             :      3.2                           ***
%***  Advisor             :      Professor Shing               ***
%***  File Name           :      Fender_final.m                ***
%***                                                           ***
%*****************************************************************
%*****************************************************************


function [newDef,newForce] =
Fender_final(steps,disp,fenderProp,uD,uDdot,uDddot,RAxial,RLat,fnum)


%%%%%%%%%%%%%%%%%%%%
% Initial Constants %
%%%%%%%%%%%%%%%%%%%%

% Timestep (from EQ in future)
dT = 0.001;  % in seconds

% Effective Mass - UHMW PE pad and 1/2 of fenders
%  Mass of Fender element
M = fenderProp.mass/4;

% Stiffness for Gap Simulation
% Assume initial stiffness of fender ~ 8 kips/in
Kbar = 160;  % kips/in

% Damping of fender
% damping non-linear (SEE DAMPING.M)
beta = -0.55;
alpha = 1.21;
length = fenderProp.length; % in inches
height = fenderProp.height; %in inches
width = fenderProp.width; % in inches
area = width * length;
delta = 0.001;

% Newmark Constants
gamma = .5;
% beta =

j=1;

% Axial Last-step write
vD(j) = uD(1);
vDdot(j) = uDdot(1);
vDddot(j) = uDddot(1);
```

```
% Lateral Last-step write
vLD(j) = uD(2);
vLDdot(j) = uDdot(2);
vLDddot(j) = uDddot(2);
% Force Last Step
fenderForce.RAxial = RAxial;
fenderForce.RLat(j) = RLat;

%%%%%%%%%%%%%%%%%%%%
%  Axial Direction  %
%%%%%%%%%%%%%%%%%%%%

while (j <= steps)
   % Compute v(j+1)
   if  ( fnum ==1 || fnum ==2) % Fenders in "positive" direction
      vA(j) = disp(1,j);
      vA(j+1) = disp(1,j+1);
   elseif  ( fnum ==3 || fnum ==4) % Fenders in "positive" direction
      vA(j) = disp(2,j);
      vA(j+1) = disp(2,j+1);
   elseif ( fnum ==5 || fnum ==6) % Fenders in "negative" direction
      vA(j) = disp(3,j);
      vA(j+1) = disp(3,j+1);
   end

   % Compute vD(i+1)
      vD(j+1) = vD(j) + dT*vDdot(j) + dT^2/2*vDddot(j);

   % Compute rD (% of 1000 mm fenders)
      rD(j+1) = length/39.4 * Force(vD(j+1));

  % Compute rD (% of 1250 x 900 mm fenders)
      %rD(j+1) = length / 35.433 * Force1250(vD(j+1));

   % Compute r

 if  ( fnum == 1 || fnum == 3 || fnum ==5) % Fenders in "positive" direction
      if (vA(j+1)+ fenderProp.gap) > vD(j+1)
          r(j+1) = 0; % Models the gap
      else
          r(j+1) = Kbar * (vA(j+1)+ fenderProp.gap - vD(j+1));
      end
   elseif ( fnum == 2 || fnum == 4 || fnum == 6) % Fenders in "negative" direction
      if (vA(j+1)- fenderProp.gap) < vD(j+1)
          r(j+1) = 0; % Models the gap
      else
          r(j+1) = Kbar * (vA(j+1)- fenderProp.gap - vD(j+1));
      end
 end

%%%%%%%%%%%%%%%%%%%%%%%%%%%%%%%%%%%%
% Iteration to converge on velocity
      vDdot(j+1) = vDdot(j); % velicity from last step
```

```
      check = 999;              % initialize residual

while (check >= 0.00001)  %(0.001*uDdot(i)))

  % Compute Phi (Known Values)
      Phi = - rD(j+1) + r(j+1) + M*(2/dT*vDdot(j) + vDddot(j));

  % Compute Damping Force
      dampA(j+1) = DampingNew(vDdot(j+1),rD(j+1),alpha,height);

  % Compute Residual
      R(j+1) = 2*M/dT*vDdot(j+1) + dampA(j+1) - Phi;

  % Compute Ct (Tangent Damping Coefficient)
      Ct(j+1) = (1+beta)*(alpha*abs(rD(j+1))/height^(1+beta)*(abs(vDdot(j+1))+delta)^beta);

  % Compute change in velocity
     deltaVel = -R(j+1) / (2*M/dT + Ct(j+1));

  % Modify velocity for next loop
     vDdot(j+1) = vDdot(j+1) + deltaVel;
     %fenderDef.uDdot(1,k+1) = vDdot(j+1);

  % To check for convergence
     check = abs(R);

end

  % Compute new acceleration
     vDddot(j+1) = 2/dT * (vDdot(j+1) - vDdot(j)) - vDddot(j);
     %fenderDef.uDddot(1,k+1) = vDddot(j+1);

%%%%%%%%%%%%%%%%%%%%%%
%  Lateral Direction  %
%%%%%%%%%%%%%%%%%%%%%%

  % Compute v(j+1)
      if (fnum == 1 || fnum == 2)

     vL(j) = disp(2,j);
     vL(j+1) = disp(2,j+1);

     elseif (fnum == 3 || fnum == 4  || fnum == 5 || fnum == 6)

     vL(j) = disp(1,j);
     vL(j+1) = disp(1,j+1);

     end

  % Compute vD(i+1)
     vLD(j+1) = vLD(j) + dT*vLDdot(j) + dT^2/2*vLDddot(j);
     %fenderDef.uD(2,k+1) = vLD(j+1);
```

```
   % Compute rD - spring force from lateral fender

   % Lateral Stiffness

      % Bending Stiffness (Assume Fixed / Fixed)
      % Young's Modulus
      E = fenderProp.youngs;
      %Moment of Inertia
      I = width *length^3 / 12;

      Kbend = 12*E*I/height^3;

      % Shear Stiffness
      % Shape Factor
      shape = (5/6);
      %  Shear Modulus (poisson's = 0.5)
      G = E/3; % in ksi

      Kshear = (shape * G * area ) / height;

      KLat = (Kshear*Kbend)/(Kshear + Kbend); % Lateral Stiffness

      KbarLat = 20 * KLat;     % Lateral Penalty Stiffness

      rLD(j+1) = KLat * vLD(j+1);

   % Compute r - contact force with mooring shaft
   mu = .15; % coefficient of friction

   if  r(j+1) == 0 % Not in Contact

      fenderForce.RLat(j+1) =  0;

   else             % In Contact
      % Incremental Force from change in displacement
      rL(j+1) = KbarLat * (( vL(j+1) - vLD(j+1) ) - ( vL(j) - vLD(j) ));
       % Total Force (old force + Incremental)
      fenderForce.RLat(j+1) = fenderForce.RLat(j) + rL(j+1);
      % Check to see if sliding (friction ~ 15% of axial)

       if abs(fenderForce.RLat(j+1)) > mu * abs(r(j+1))
          fenderForce.RLat(j+1) = mu * abs(r(j+1)) * sign(fenderForce.RLat(j+1));

       end
   end

%%%%%%%%%%%%%%%%%%%%%%%%%%%%%%%%%%%%
% Iteration to converge on velocity
      vLDdot(j+1) = vLDdot(j); % velicity from last step
      check = 999;                % initialize residual

 while (check >= 0.00001)  %(0.001*uDdot(i)))
```

```
    % Compute Phi (Known Values)
        Phi = - rLD(j+1) + fenderForce.RLat(j+1) + M*(2/dT*vLDdot(j) + vLDddot(j));

    % Compute Damping Force
        dampA(j+1) = DampingNew(vLDdot(j+1),rLD(j+1),alpha,height);

    % Compute Residual
        R(j+1) = 2*M/dT*vLDdot(j+1) + dampA(j+1) - Phi;

    % Compute Ct (Tangent Damping Coefficient)
        Ct(j+1) = (1+beta)*(alpha*abs(rLD(j+1))/height^0.45)*(abs(vLDdot(j+1))+delta)^beta;

    % Compute change in velocity
       deltaVel = -R(j+1) / (2*M/dT + Ct(j+1));

    % Modify velocity for next loop
       vLDdot(j+1) = vLDdot(j+1) + deltaVel;
       %fenderDef.uDdot(2,k+1) = vLDdot(j+1);

    % To check for convergence
       check = abs(R);

 end

    % Compute new acceleration
       vLDddot(j+1) = 2/dT * (vLDdot(j+1) - vLDdot(j)) - vLDddot(j);
        %fenderDef.uDddot(2,k+1) = vLDddot(j+1);

      % Iteration Counter
       j = j+1;
end

newDef.vD(1) = vD(j);
newDef.vDdot(1) = vDdot(j);
newDef.vDddot(1) = vDddot(j);
newDef.vD(2) = vLD(j);
newDef.vDdot(2) = vLDdot(j);
newDef.vDddot(2) = vLDddot(j);

% Four elements at each DOF
newForce.RAxial = fenderProp.NumAxial * r(j);

% Two elements at each DOF (i steps)
newForce.RLat = fenderProp.NumAxial/2 * fenderForce.RLat(j);

end
```

```
%*****************************************************************
%***                                                           ***
%***          Fender Behavior - MHP Analysis                   ***
%***                                                           ***
%***  Programmer          :      Adam Bogage                   ***
%***  Date                :      Spring 2008                   ***
%***  Version             :      3.2                           ***
%***  Advisor             :      Professor Shing               ***
%***  File Name           :      Fender_final.m                ***
%***                                                           ***
%*****************************************************************
%*****************************************************************


function [newDef,newForce] =
Fender_1250_final(steps,disp,fenderProp,uD,uDdot,uDddot,RAxial,RLat,fnum)


%%%%%%%%%%%%%%%%%%%%
% Initial Constants %
%%%%%%%%%%%%%%%%%%%%

% Timestep (from EQ in future)
dT = 0.001;  % in seconds

% Effective Mass - UHMW PE pad and 1/2 of fenders
%  Mass of Fender element
M = fenderProp.mass/4;

% Stiffness for Gap Simulation
% Assume initial stiffness of fender ~ 8 kips/in
Kbar = 160;  % kips/in

% Damping of fender
% damping non-linear (SEE DAMPING.M)
beta = -0.55;
alpha = 1.21;
length = fenderProp.length; % in inches
height = fenderProp.height; %in inches
width = fenderProp.width; % in inches
area = width * length;
delta = 0.001;

% Newmark Constants
gamma = .5;
% beta =

j=1;

% Axial Last-step write
vD(j) = uD(1);
vDdot(j) = uDdot(1);
vDddot(j) = uDddot(1);
```

```
% Lateral Last-step write
vLD(j) = uD(2);
vLDdot(j) = uDdot(2);
vLDddot(j) = uDddot(2);
% Force Last Step
fenderForce.RAxial = RAxial;
fenderForce.RLat(j) = RLat;

%%%%%%%%%%%%%%%%%%%%
%  Axial Direction  %
%%%%%%%%%%%%%%%%%%%%


while (j <= steps)
   % Compute v(j+1)
   if  ( fnum ==1 || fnum ==2) % Fenders in "positive" direction
      vA(j) = disp(1,j);
      vA(j+1) = disp(1,j+1);
   elseif  ( fnum ==3 || fnum ==4) % Fenders in "positive" direction
      vA(j) = disp(2,j);
      vA(j+1) = disp(2,j+1);
   elseif ( fnum ==5 || fnum ==6) % Fenders in "negative" direction
      vA(j) = disp(3,j);
      vA(j+1) = disp(3,j+1);
   end

   % Compute vD(i+1)
      vD(j+1) = vD(j) + dT*vDdot(j) + dT^2/2*vDddot(j);

   % Compute rD (% of 1000 mm fenders)
      %rD(j+1) = length/39.4 * Force(vD(j+1));

  % Compute rD (% of 1250 x 900 mm fenders)
      rD(j+1) = length / 35.433 * Force1250(vD(j+1));

   % Compute r

if  ( fnum == 1 || fnum == 3 || fnum ==5) % Fenders in "positive" direction
      if (vA(j+1)+ fenderProp.gap) > vD(j+1)
           r(j+1) = 0; % Models the gap
      else
           r(j+1) = Kbar * (vA(j+1)+ fenderProp.gap - vD(j+1));

      end
   elseif ( fnum == 2 || fnum == 4 || fnum == 6) % Fenders in "negative" direction
      if (vA(j+1)- fenderProp.gap) < vD(j+1)
           r(j+1) = 0; % Models the gap
      else
           r(j+1) = Kbar * (vA(j+1)- fenderProp.gap - vD(j+1));
      end
end

%%%%%%%%%%%%%%%%%%%%%%%%%%%%%%%%%%%%
```

```
% Iteration to converge on velocity
      vDdot(j+1) = vDdot(j); % velicity from last step
      check = 999;              % initialize residual

 while (check >= 0.00001)  %(0.001*uDdot(i)))

   % Compute Phi (Known Values)
       Phi = - rD(j+1) + r(j+1) + M*(2/dT*vDdot(j) + vDddot(j));

   % Compute Damping Force
       dampA(j+1) = DampingNew(vDdot(j+1),rD(j+1),alpha,height);

   % Compute Residual
       R(j+1) = 2*M/dT*vDdot(j+1) + dampA(j+1) - Phi;

   % Compute Ct (Tangent Damping Coefficient)
       Ct(j+1) = (1+beta)*(alpha*abs(rD(j+1))/height^(1+beta)*(abs(vDdot(j+1))+delta)^beta);

   % Compute change in velocity
      deltaVel = -R(j+1) / (2*M/dT + Ct(j+1));

   % Modify velocity for next loop
      vDdot(j+1) = vDdot(j+1) + deltaVel;
      %fenderDef.uDdot(1,k+1) = vDdot(j+1);

   % To check for convergence
      check = abs(R);
end

   % Compute new acceleration
      vDddot(j+1) = 2/dT * (vDdot(j+1) - vDdot(j)) - vDddot(j);
      %fenderDef.uDddot(1,k+1) = vDddot(j+1);

%%%%%%%%%%%%%%%%%%%%%
%  Lateral Direction  %
%%%%%%%%%%%%%%%%%%%%%

   % Compute v(j+1)
      if (fnum == 1 || fnum == 2)

      vL(j) = disp(2,j);
      vL(j+1) = disp(2,j+1);

      elseif (fnum == 3 || fnum == 4  || fnum == 5 || fnum == 6)

      vL(j) = disp(1,j);
      vL(j+1) = disp(1,j+1);

      end

   % Compute vLD(i+1)
      vLD(j+1) = vLD(j) + dT*vLDdot(j) + dT^2/2*vLDddot(j);
```

```
    % Compute rD - spring force from lateral fender

    % Lateral Stiffness

        % Bending Stiffness (Assume Fixed / Fixed)
        % Young's Modulus
        E = fenderProp.youngs;
        %Moment of Inertia
        I = width *length^3 / 12;

        Kbend = 12*E*I/height^3;

        % Shear Stiffness
        % Shape Factor
        shape = (5/6);
        %  Shear Modulus (poisson's = 0.5)
        G = E/3; % in ksi

        Kshear = (shape * G * area ) / height;

        KLat = (Kshear*Kbend)/(Kshear + Kbend); % Lateral Stiffness

        KbarLat = .10 * KLat;     % Lateral Penalty Stiffness

        rLD(j+1) = KLat * vLD(j+1);


    % Compute r - contact force with mooring shaft
    mu = .15; % coefficient of friction

    if  r(j+1) == 0 % Not in Contact

        fenderForce.RLat(j+1) =  0;

    else            % In Contact
        % Incremental Force from change in displacement
        rL(j+1) = KbarLat * (( vL(j+1) - vLD(j+1) ) - ( vL(j) - vLD(j) ));
         % Total Force (old force + Incremental)
        fenderForce.RLat(j+1) = fenderForce.RLat(j) + rL(j+1);
         % Check to see if sliding (friction ~ 15% of axial)

         if abs(fenderForce.RLat(j+1)) > mu * abs(r(j+1))
            fenderForce.RLat(j+1) = mu * abs(r(j+1)) * sign(fenderForce.RLat(j+1));

         end
    end

%%%%%%%%%%%%%%%%%%%%%%%%%%%%%%%%%%%%%%%%%%%%%%%%%%%%%%%%%%%%%%%%%%%%%%%%%%%%%%
% Iteration to converge on velocity
        vLDdot(j+1) = vLDdot(j); % velicity from last step
        check = 999;             % initialize residual

 while (check >= 0.00001)  %(0.001*uDdot(i)))
```

```
   % Compute Phi (Known Values)
       Phi = - rLD(j+1) + fenderForce.RLat(j+1) + M*(2/dT*vLDdot(j) + vLDddot(j));

   % Compute Damping Force
       dampA(j+1) = DampingNew(vLDdot(j+1),rLD(j+1),alpha,height);

   % Compute Residual
       R(j+1) = 2*M/dT*vLDdot(j+1) + dampA(j+1) - Phi;

   % Compute Ct (Tangent Damping Coefficient)
       Ct(j+1) = (1+beta)*(alpha*abs(rLD(j+1))/height^0.45)*(abs(vLDdot(j+1))+delta)^beta;

   % Compute change in velocity
      deltaVel = -R(j+1) / (2*M/dT + Ct(j+1));

   % Modify velocity for next loop
      vLDdot(j+1) = vLDdot(j+1) + deltaVel;
      %fenderDef.uDdot(2,k+1) = vLDdot(j+1);

   % To check for convergence
      check = abs(R);
end

   % Comp ute new acceleration
      vLDddot(j+1) = 2/dT * (vLDdot(j+1) - vLDdot(j)) - vLDddot(j);
       %fenderDef.uDddot(2,k+1) = vLDddot(j+1);

     % Iteration Counter
      j = j+1;
end

newDef.vD(1) = vD(j);
newDef.vDdot(1) = vDdot(j);
newDef.vDddot(1) = vDddot(j);
newDef.vD(2) = vLD(j);
newDef.vDdot(2) = vLDdot(j);
newDef.vDddot(2) = vLDddot(j);

% Four elements at each DOF
newForce.RAxial = fenderProp.NumAxial * r(j);

% Two elements at each DOF (i steps)
newForce.RLat = fenderProp.NumAxial/2 * fenderForce.RLat(j);

end
```

```
%*****************************************************************
%***                                                           ***
%***          Fender Behavior - MHP Analysis                   ***
%***                                                           ***
%***  Programmer            :      Adam Bogage          ***
%***  Date                  :      Spring 2008          ***
%***  Version               :      3.2                  ***
%***  Advisor               :      Professor Shing      ***
%***  File Name             :      Fender_final.m       ***
%***                                                           ***
%*****************************************************************
%*****************************************************************


function [newDef,newForce] =
Fender_final(steps,disp,fenderProp,uD,uDdot,uDddot,RAxial,RLat,fnum)


%%%%%%%%%%%%%%%%%%%%
% Initial Constants %
%%%%%%%%%%%%%%%%%%%%

% Timestep (from EQ in future)
dT = 0.001;  % in seconds

% Effective Mass - UHMW PE pad and 1/2 of fenders
%  Mass of Fender element
M = fenderProp.mass/4;

% Stiffness for Gap Simulation
% Assume initial stiffness of fender ~ 8 kips/in
Kbar = 160;  % kips/in

% Damping of fender
% damping non-linear (SEE DAMPING.M)
beta = -0.55;
alpha = 1.21;
length = fenderProp.length; % in inches
height = fenderProp.height; %in inches
width = fenderProp.width; % in inches
area = width * length;
delta = 0.001;

% Newmark Constants
gamma = .5;
% beta =

j=1;

% Axial Last-step write
vD(j) = uD(1);
vDdot(j) = uDdot(1);
vDddot(j) = uDddot(1);
```

```
% Lateral Last-step write
vLD(j) = uD(2);
vLDdot(j) = uDdot(2);
vLDddot(j) = uDddot(2);
% Force Last Step
fenderForce.RAxial = RAxial;
fenderForce.RLat(j) = RLat;

%%%%%%%%%%%%%%%%%%%%
%  Axial Direction  %
%%%%%%%%%%%%%%%%%%%%

while (j <= steps)
   % Compute v(j+1)
   if  ( fnum ==1 || fnum ==2) % Fenders in "positive" direction
      vA(j) = disp(1,j);
      vA(j+1) = disp(1,j+1);
   elseif  ( fnum ==3 || fnum ==4) % Fenders in "positive" direction
      vA(j) = disp(2,j);
      vA(j+1) = disp(2,j+1);
   elseif ( fnum ==5 || fnum ==6) % Fenders in "negative" direction
      vA(j) = disp(3,j);
      vA(j+1) = disp(3,j+1);
   end

   % Compute vD(i+1)
      vD(j+1) = vD(j) + dT*vDdot(j) + dT^2/2*vDddot(j);

   % Compute rD (% of 1000 mm fenders)
      rD(j+1) = length / 39.4 * Force(vD(j+1));

  % Compute rD (% of 1250 x 900 mm fenders)
      %rD(j+1) = length / 35.433 * Force1250(vD(j+1));

   % Compute r

if  ( fnum == 1 || fnum == 3 || fnum ==5) % Fenders in "positive" direction
      if (vA(j+1)+ fenderProp.gap) > vD(j+1)
         r(j+1) = 0; % Models the gap
      else
         r(j+1) = Kbar *  (vA(j+1)+ fenderProp.gap - vD(j+1));

      end
   elseif ( fnum == 2 || fnum == 4 || fnum == 6) % Fenders in "negative" direction
      if (vA(j+1)- fenderProp.gap) < vD(j+1)
         r(j+1) = 0; % Models the gap
      else
         r(j+1) = Kbar * (vA(j+1)- fenderProp.gap - vD(j+1));
      end
end

%%%%%%%%%%%%%%%%%%%%%%%%%%%%%%%%%%%%
% Iteration to converge on velocity
```

```
      vDdot(j+1) = vDdot(j); % velicity from last step
      check = 999;              % initialize residual

while (check >= 0.00001)  %(0.001*uDdot(i)))

  % Compute Phi (Known Values)
      Phi = - rD(j+1) + r(j+1) + M*(2/dT*vDdot(j) + vDddot(j));

  % Compute Damping Force
      dampA(j+1) = DampingNew(vDdot(j+1),rD(j+1),alpha,height);

  % Compute Residual
      R(j+1) = 2*M/dT*vDdot(j+1) + dampA(j+1) - Phi;


  % Compute Ct (Tangent Damping Coefficient)
      Ct(j+1) = (1+beta)*(alpha*abs(rD(j+1))/height^(1+beta)*(abs(vDdot(j+1))+delta)^beta);

  % Compute change in velocity
     deltaVel = -R(j+1) / (2*M/dT + Ct(j+1));

  % Modify velocity for next loop
     vDdot(j+1) = vDdot(j+1) + deltaVel;
     %fenderDef.uDdot(1,k+1) = vDdot(j+1);

  % To check for convergence
     check = abs(R);

end

  % Compute new acceleration
     vDddot(j+1) = 2/dT * (vDdot(j+1) - vDdot(j)) - vDddot(j);
     %fenderDef.uDddot(1,k+1) = vDddot(j+1);

%%%%%%%%%%%%%%%%%%%%%
%  Lateral Direction  %
%%%%%%%%%%%%%%%%%%%%%

  % Compute v(j+1)
      if (fnum == 1 || fnum == 2)

     vL(j) = disp(2,j);
     vL(j+1) = disp(2,j+1);

     elseif (fnum == 3 || fnum == 4  || fnum == 5 || fnum == 6)

     vL(j) = disp(1,j);
     vL(j+1) = disp(1,j+1);

     end

  % Compute vD(i+1)
     vLD(j+1) = vLD(j) + dT*vLDdot(j) + dT^2/2*vLDddot(j);
```

```
    %fenderDef.uD(2,k+1) = vLD(j+1);

  % Compute rD - spring force from lateral fender

  % Lateral Stiffness

    % Bending Stiffness (Assume Fixed / Fixed)
    % Young's Modulus
    E = fenderProp.youngs;
    %Moment of Inertia
    I = width *length^3 / 12;

    Kbend = 12*E*I/height^3;

    % Shear Stiffness
    % Shape Factor
    shape = (5/6);
    %  Shear Modulus (poisson's = 0.5)
    G = E/3; % in ksi

    Kshear = (shape * G * area ) / height;

    KLat = (Kshear*Kbend)/(Kshear + Kbend); % Lateral Stiffness

    KbarLat = 20 * KLat;     % Lateral Penalty Stiffness

    rLD(j+1) = KLat * vLD(j+1);

  % Compute r - contact force with mooring shaft
  mu = .15; % coefficient of friction

  if  r(j+1) == 0 % Not in Contact

    fenderForce.RLat(j+1) =  0;

  else            % In Contact
    % Incremental Force from change in displacement
    rL(j+1) = KbarLat * (( vL(j+1) - vLD(j+1) ) - ( vL(j) - vLD(j) ));
     % Total Force (old force + Incremental)
    fenderForce.RLat(j+1) = fenderForce.RLat(j) + rL(j+1);
     % Check to see if sliding (friction ~ 15% of axial)

     if abs(fenderForce.RLat(j+1)) > mu * abs(r(j+1))
        fenderForce.RLat(j+1) = mu * abs(r(j+1)) * sign(fenderForce.RLat(j+1));

     end
  end

%%%%%%%%%%%%%%%%%%%%%%%%%%%%%%%%%%%%
% Iteration to converge on velocity
    vLDdot(j+1) = vLDdot(j); % velicity from last step
    check = 999;             % initialize residual
```

```
 while (check >= 0.00001)  %(0.001*uDdot(i)))

    % Compute Phi (Known Values)
        Phi = - rLD(j+1) + fenderForce.RLat(j+1) + M*(2/dT*vLDdot(j) + vLDddot(j));

    % Compute Damping Force
        dampA(j+1) = DampingNew(vLDdot(j+1),rLD(j+1),alpha,height);

    % Compute Residual
        R(j+1) = 2*M/dT*vLDdot(j+1) + dampA(j+1) - Phi;

    % Compute Ct (Tangent Damping Coefficient)
        Ct(j+1) = (1+beta)*(alpha*abs(rLD(j+1))/height^0.45)*(abs(vLDdot(j+1))+delta)^beta;

    % Compute change in velocity
       deltaVel = -R(j+1) / (2*M/dT + Ct(j+1));

    % Modify velocity for next loop
       vLDdot(j+1) = vLDdot(j+1) + deltaVel;
       %fenderDef.uDdot(2,k+1) = vLDdot(j+1);

    % To check for convergence
       check = abs(R);
end

    % Compute new acceleration
       vLDddot(j+1) = 2/dT * (vLDdot(j+1) - vLDdot(j)) - vLDddot(j);
        %fenderDef.uDddot(2,k+1) = vLDddot(j+1);

     % Iteration Counter
       j = j+1;
end

newDef.vD(1) = vD(j);
newDef.vDdot(1) = vDdot(j);
newDef.vDddot(1) = vDddot(j);
newDef.vD(2) = vLD(j);
newDef.vDdot(2) = vLDdot(j);
newDef.vDddot(2) = vLDddot(j);

% Four elements at each DOF
newForce.RAxial = fenderProp.NumAxial * r(j);

% Two elements at each DOF (i steps)
newForce.RLat = fenderProp.NumAxial/2 * fenderForce.RLat(j);

end
```

```
%*****************************************************************
%***                                                           ***
%***          Axial Fender Curve - MHP Analysis                ***
%***                                                           ***
%***  Programmer              :       Adam Bogage          ***
%***  Date                    :       Spring 2008          ***
%***  Version                 :       1.0                  ***
%***  Advisor                 :       Professor Shing      ***
%***  File Name               :       Force.m              ***
%***                                                           ***
%*****************************************************************
%*****************************************************************



function[R] = Force1250 (x)
   % Returns force based on displacement


   y = abs(x);

   % MV1250 x 900 A Element (0.5 mm/sec)
      R = 0.0011*y^4 - 0.0408*y^3 + 0.0624*y^2 + 10.836*y;

      if (x < 0)
       R = -R; % to recover negative sign
      end

end
```

```
%*****************************************************************
%***                                                           ***
%***          Axial Fender Curve - MHP Analysis                ***
%***                                                           ***
%***  Programmer              :       Adam Bogage          ***
%***  Date                    :       Spring 2008          ***
%***  Version                 :       1.0                  ***
%***  Advisor                 :       Professor Shing      ***
%***  File Name               :       Force.m              ***
%***                                                           ***
%*****************************************************************
%*****************************************************************



function[R] = Force1000 (x)
   % Returns force based on displacement


   y = abs(x);

    % MV1000 x 1000 A Element (0.5 mm/sec)
       R = 0.0024*y^4 - 0.0735*y^3 + 0.0899*y^2 + 12.487*y;

       if (x < 0)
        R = -R; % to recover negative sign
       end

end
```

```
%*****************************************************************
%***                                                           ***
%***            Mass Matrix - MHP Analysis                     ***
%***                                                           ***
%***  Programmer            :      Adam Bogage          ***
%***  Date                  :      Spring 2008          ***
%***  Version               :      2.0                  ***
%***  Advisor               :      Professor Shing      ***
%***  File Name             :      Mass.m               ***
%***                                                           ***
%*****************************************************************
%*****************************************************************

function[M] = Mass()   % Returns Mass matrix

   % Mass Matrix at Center of Gravity (COG)
   Mcog = [176.061, 0,0;0,176.061,0;0,0,2.495*10^7];
   % Matrix Relating COG DOF and Desired DOF
   %O = [1,0,0;0,.5,.5;0,(-1/753.65),1/753.65];
   O = [1,0,0;0,.5,.5;0,(-1/650),1/650];
  % Desired Mass Matrix
   M = O'*Mcog*O; % in kips


end
```

```
%*****************************************************************
%***                                                           ***
%***          Fender Damping Curve - MHP Analysis          ***
%***                                                           ***
%***  Programmer              :       Adam Bogage        ***
%***  Date                    :       Spring 2008        ***
%***  Version                 :       1.3                ***
%***  Advisor                 :       Professor Shing    ***
%***  File Name               :       DampingNew.m       ***
%***                                                           ***
%*****************************************************************
%*****************************************************************


function[R] = DampingNew (x, fs, alpha, fendersize)
   % Returns force based on velocity, static force and size

   %x = current velocity
   %fs = static force
   %alpha = 1.21 currently
   %fendersize = in inches

   % Stores direction
   if x >= 0
      sign=1;
   else
      sign=-1;
   end

   y = abs(x); % Absolute Value of Velocity

   % Damping Force
   R = (alpha*abs(fs)/(fendersize^(0.45))) * (y + 0.0000001)^(1-0.55);

   % Recovers direction
   R = sign*R;

end
```